THE
PHYSICAL REVIEW
A Journal of Experimental and Theoretical Physics Established by E. L. Nichols in 1893
VOL. 51, NO. 9 MAY 1, 1937 SECOND SERIES

Gamma-Rays from Light Elements Due to Proton Bombardment

R. G. HERB, D. W. KERST AND J. L. MCKIBBEN
Department of Physics, University of Wisconsin, Madison, Wisconsin
(Received March 8, 1937)

With the high potential electrostatic generator recently constructed at this laboratory a survey of a number of elements has been made in a search for gamma-ray emission due to proton bombardment. Six of the elements examined gave gamma-rays of sufficient intensity to permit accurate measurement. These six elements are Li, Be, B, F, Na and Al. Their gamma-ray yield was studied as a function of proton energy, or generator voltage, starting with the minimum potential at which the yield was easily measurable. In the region of fairly low potentials the six elements studied gave evidence for resonance excitation of gamma-radiation and at high potentials each of the six elements gave a gamma-ray intensity which increased nearly exponentially with voltage up to the maximum voltage obtainable from the generator (approximately 2 Mev). The measurements were made using a Lauritsen electroscope, and therefore they give the intensity in arbitrary units which depend on the hardness of the radiation and the geometry of the apparatus. The other elements which were bombarded are C, O, Si, K, Ca, Ni, Cu, Zn, Mo, Pt, Pb. Gamma-radiation from these elements was weak and the observed intensities may have been largely due to contaminants.

INTRODUCTION

THE excitation of gamma-rays from the light elements due to high energy proton bombardment has been studied at several different laboratories. Lauritsen[1-3] and his colleagues observed gamma-radiation from Li, Be, B, and F using protons with energies up to about 0.9 Mev. Using 1.2 Mev protons McMillan[4] observed gamma-radiation from Li, Be, and F and obtained indications of a weak intensity from B. The work of Hafstad, Heydenburg and Tuve[5] on the voltage excitation curves of gamma-radiation from Li and F showed the advantages of a monochromatic beam of protons and accurately measured generator voltages. Their curves of gamma-ray intensity from thick targets of Li and F as a function of proton energy show a number of well-defined steps and demonstrate the importance of nuclear energy levels in the interaction of protons with nuclei.

Lithium was shown by these observers to give a sharp resonance emission of gamma-radiation for incident protons with an energy of 440 kv. This resonance is convenient for voltage calibration and upon completion of the electrostatic generator recently developed at this laboratory this lithium gamma-ray resonance was used to determine its voltage scale. Further work on proton bombardment of lithium using voltages up to a maximum of nearly 2 Mev gave results of such interest that it seemed advisable to extend the investigation to other elements. A fairly extended survey was therefore made which

[1] Crane, Delsasso, Fowler, Lauritsen, Phys. Rev. **46**, 531 (1934).
[2] Crane, Delsasso, Fowler, Lauritsen, Phys. Rev. **47**, 782 (1935).
[3] Crane, Delsasso, Fowler, Lauritsen, Phys. Rev. **48**, 102 (1935).
[4] Edwin McMillan, Phys. Rev. **46**, 868 (1934).
[5] Hafstad, Heydenburg and Tuve, Phys. Rev. **50**, 504 (1936).

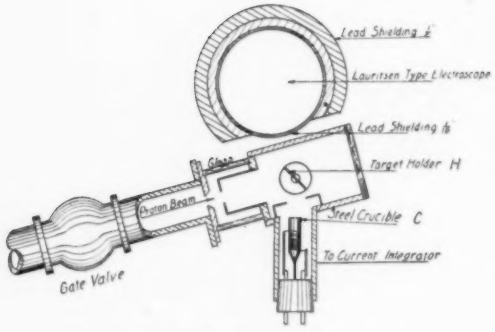

FIG. 1. Target chamber and electroscope.

included most of the light elements up to aluminum and also several heavy elements.

APPARATUS AND PROCEDURE

High energy protons for these experiments were obtained by means of a belt type electrostatic generator operating in a steel tank under high air pressure.[6] Fig. 1 shows the construction of the target chamber which was used for all of the work on gamma-ray emission. Several different targets were mounted on holder H which consisted of a sheet of nickel or molybdenum. By means of a threaded rod and a ground brass plug the holder could be moved so that the proton beam impinged on any desired target. Gamma-ray intensity was measured with a quartz fiber electroscope of the Lauritsen type placed as shown in Fig. 1 and provided with lead shielding to cut down the background intensity caused by x-rays from the generator. To obtain gamma-ray intensity from a weak emitter at any particular generator voltage, a run of several minutes was often necessary to give sufficient deflection of the electroscope fiber. As the proton current was often unsteady, the total charge incident on the target during a run was measured by means of a current integrator as shown in Fig. 2.

This circuit makes use of a thyratron tube to periodically discharge a condenser which is being charged by the proton current. As protons enter the Faraday cage in which the target is mounted, the potential of the condenser which furnishes the plate current for the thyratron rises until it reaches the critical discharge voltage associated with the bias used on the grid. The thyratron then discharges the condenser, and immediately becomes nonconducting so that the condenser may recharge. The number of discharges is recorded by a separate thyratron circuit the same in principle as the one described by Dunning.[7]

To prevent the plate condenser from completely discharging and thus causing the potential of the Faraday cage to fluctuate greatly, the condenser C_7 is put in series with a smaller condenser C_4, so that the discharge from C_7 goes into C_4. In this way the voltage of C_7 may drop only 7 volts while the voltage of C_4 changes by 35 volts and extinguishes the discharge. R_8 discharges C_4 before the thyratron becomes conducting again. This seven-volt fluctuation of the Faraday cage has not been sufficient to cause interference in an amplifier brought up near the target for alpha-particle counting.

The positive impulse for setting off the recording thyratron circuit is obtained from the rise in voltage across R_8 accompanying the discharge through the tube. Other resistances and condensers shown in the circuit are used for different sensitivities. Radio gang selector switches, S_1, S_2, S_3, and S_4, change the sensitivity by means of one control; but when the highest sensitivity is used, position 1, the grid bias must be changed

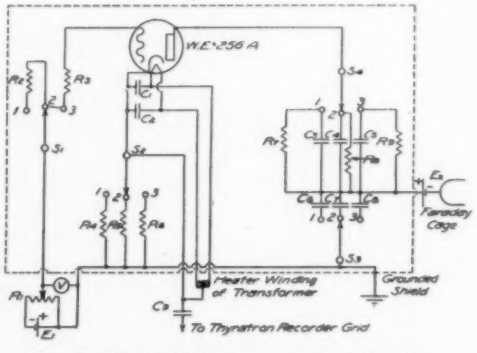

FIG. 2. Circuit of thyratron current integrator.

R_1—25,000 ohm potentiometer, w.w.
R_2, R_7—30 megohm grid leaks
R_4—7000 ohm w.w.
R_5—700 ohm w.w.
R_6—70 ohm w.w.
R_7—50 megohm grid leak
R_8—5 megohm grid leak
R_9—500,000 ohm grid leak
E_1—3 volts
C_1, C_2—0.004 mf condensers
C_3—0.0002 mf mica
C_4—0.002 mf mica
C_5—0.02 mf mica
C_6—0.001 mf
C_7—0.01 mf
C_8—0.1 mf
well-insulated condensers
C_9—0.002 mf
E_2—45 volts

[6] The construction and operation of the generator are described in Phys. Rev. **51**, 75 (1937).

[7] John R. Dunning, Rev. Sci. Inst. **5**, 387 (1934).

from its normal −2.0 volts to −2.5 volts. Switch points with the same numbers are used simultaneously.

A shield, represented by the dotted line, keeps the time constant of the grid circuit fixed and provides a chamber which can be dried to prevent surface leakage of charge. However, in spite of the elimination of surface leakage, the two high sensitivity calibration curves of counts per minute as a function of current to the Faraday cage show an apparent leakage. The error is negligible for the low sensitivity, 1 to 10 microamperes; but in the cases of 0.1 to 1.0 and 0.02 to 0.1 microampere sensitivities a small number of counts per minute must be added to the observed number. The Western Electric type 256 A thyratron was selected because tube leakage, which seems to be the cause of the error, is known to be very small.

In the seven months of operation the calibration has shifted toward slightly less sensitivity and less tube leakage. Consequently if absolute data are wanted the calibration should be checked periodically.*

Results

Lithium

For the preparation of lithium targets metallic lithium in crucible *C* of Fig. 1 was evaporated onto target holder *H*, which was perpendicular to the stream of lithium vapor during evaporation and was then turned into position for proton bombardment. Work with a small electrostatic generator at this laboratory had shown that gamma-ray emission from lithium has a sharp resonance for protons at about 440 kv which agrees with the results of Hafstad, Heydenburg and Tuve. This 440 kv resonance was carefully studied with the large generator using lithium films of several different thicknesses and the resonance position was used to determine the sensitivity of the generating voltmeter with which the large generator is equipped. Details of the calibration experiments are given in the paper which describes the large generator.

After the low voltage calibration work several runs were taken on lithium targets over the entire voltage range of the generator. Curve *A* of Fig. 3 shows the yield from a target having an absorption thickness of about 30 kv for 440 kv protons. The resonance peak at 440 kv is much broader from this film than from several of the thinner films used for voltage calibration. An accurate determination of the width of the 440 kv level is being made with the small generator and will be given in a later publication. Above the 440 kv resonance, curve *A* drops to a level which is only slightly above the x-ray background (background intensity is not subtracted) and at 900 kv shows another comparatively gradual rise with a broad maximum at about 1000 kv. Above 1200 kv the yield curve has a smooth rise which is approximately exponential up to the maximum generator potential. For curve *B* the lithium film used for curve *A* was moved about 5/16 inch so that the proton beam hit at a different place. Results of this run, which was taken to check the resonance peak at 1000 kv, show good agreement with curve *A*.

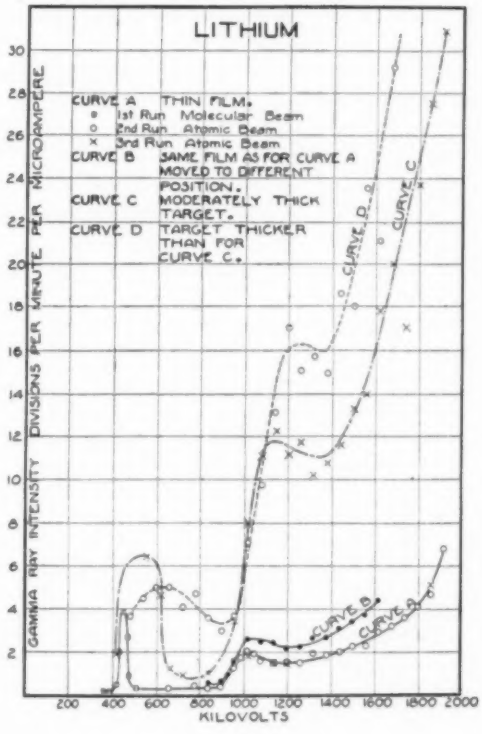
LITHIUM
CURVE A THIN FILM.
1st Run Molecular Beam
2nd Run Atomic Beam
3rd Run Atomic Beam
CURVE B SAME FILM AS FOR CURVE A MOVED TO DIFFERENT POSITION.
CURVE C MODERATELY THICK TARGET.
CURVE D TARGET THICKER THAN FOR CURVE C.
GAMMA RAY INTENSITY DIVISIONS PER MINUTE PER MICROAMPERE
KILOVOLTS
CURVE A
CURVE B
CURVE C
CURVE D

FIG. 3.

* For precision work it is necessary to keep the thyratron heater current constant. A 5 percent drop in the heater current decreases the count 3 percent.

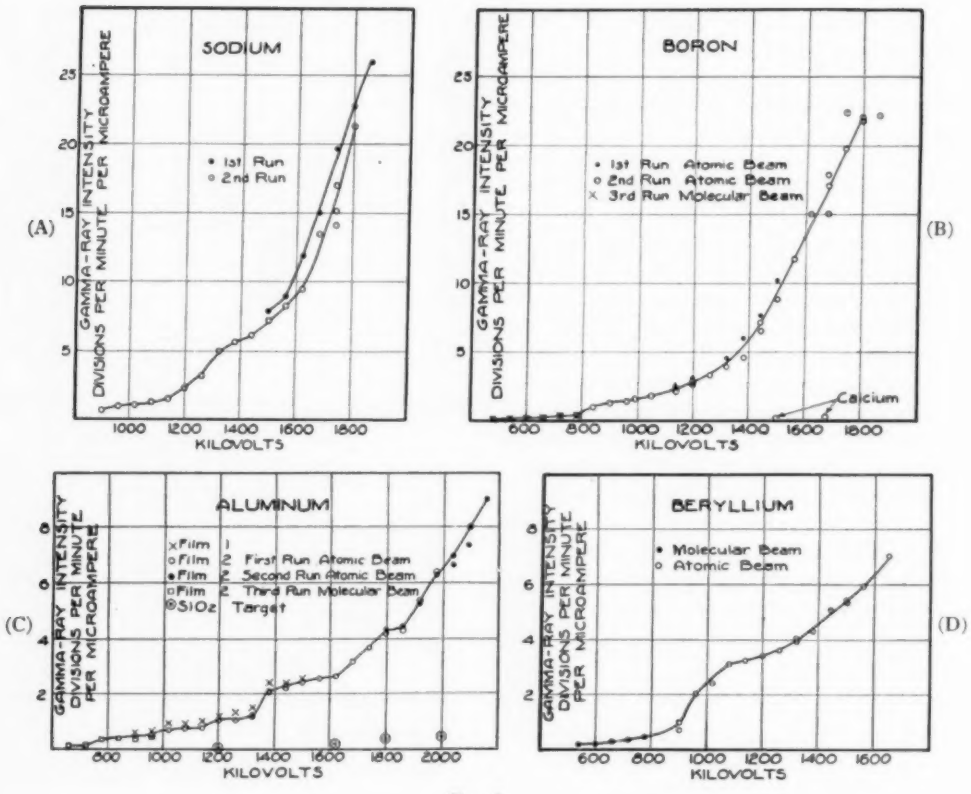

FIG. 4.

Curves *C* and *D* show the results obtained from two comparatively thick lithium films. During these runs the charging belts of the generator were in poor condition and caused considerable voltage fluctuation so that the data are not very reliable, but in both curves the effect of the 1000 kv resonance is quite clearly shown. It was expected that the lithium film used for curve *D* would completely stop the most energetic protons and would thus give a thick target yield curve, but the form of the curve shows that the film was not sufficiently thick.

The lithium gamma-ray resonance at 440 kv is known to be due to the Li^7 isotope and recent work of Rumbaugh and Hafstad,[8] using voltages up to 1100 kv showed that the 1000 kv resonance is also due to Li^7. It therefore seems quite likely that all of the observed gamma-radiation from lithium is from Li^7. Recent work of Delsasso, Fowler, and Lauritsen[9] indicates that the energy spectrum of lithium gamma-radiation from the 440 kv resonance consists of a strong line at 17.5 Mev and a weaker line at about 14.0 Mev. Gaerttner and Crane,[10] however, find indications of a number of low energy components in the gamma-ray spectrum.

The reaction responsible for gamma-ray emission from lithium is still not definitely established. The product is probably stable Be^8 with all available energy emitted as gamma-radiation but there seems to be a possibility that the gamma-radiation carries away most, but not all, of the available energy and that two short range alpha-particles are emitted.[11]

[8] Rumbaugh and Hafstad, Phys. Rev. **50**, 681 (1936).

[9] Delsasso, Fowler, and Lauritsen, Pasadena meeting, Am. Phys. Soc. (1936).

[10] Gaerttner and Crane, Phys. Rev. **51**, 49 (1937).

[11] A thorough discussion of the process of gamma-ray emission from lithium is given by Professor G. Breit in a paper by L. R. Hafstad, N. P. Heydenburg and M. A. Tuve, Phys. Rev. **50**, 504, 510–514 (1936).

Beryllium

The target used for this work was a thick piece of beryllium metal obtained from the Belmont Smelting and Refining Company, who guaranteed the metal to have a purity of 98 percent or better. As the shape of the yield curve (Fig. 4D) is considerably different from the yield curves given by other elements it seems improbable that much of the observed gamma-radiation could have been due to contaminants.

The curve of Fig. 4D indicates that beryllium has a broad resonance level for gamma-ray excitation at approximately 990 kv. In other regions the curve shows a smooth increase of gamma-ray yield with voltage.

Gamma-radiation due to bombardment of beryllium by protons was first observed by Crane, Delsasso, Fowler and Lauritsen[2] and was later observed by Hafstad and Tuve.[12] From cloud chamber measurements of the gamma-ray energy Lauritsen concluded that the gamma-ray spectrum consists of a number of lines of which the hardest component has an energy of about 6 Mev. From these results he concluded that the reaction is probably as given by the equation ${}_4Be^9+{}_1H^1={}_5B^{10}+\gamma$. To account for low energy components of the gamma-ray spectrum Lauritsen assumed that the radiation may be emitted in a number of steps. Low energy gamma-radiation might, however, be due to an excited product nucleus in the reaction ${}_4Be^9+{}_1H^1={}_3Li^6+{}_2He^4$ or in the reaction ${}_4Be^9+{}_1H^1={}_4Be^8+{}_1H^2$.[13]

Boron

A target of metallic boron was prepared in the following way. Granulated boron metal was spread onto a molybdenum sheet to form a layer about 1 mm thick. This was wetted with distilled water and after the water evaporated the granules were found to be firmly enough bound so that the target could be inverted and still remain intact. The boron used in this work was of unknown purity but the observed gamma-ray intensity as shown by Fig. 4B is of such magnitude that only fluorine and possibly lithium would be serious as contaminants. As yield curves from lithium and fluorine are considerably different in shape from the boron yield curve it seems unlikely that either of these materials could have contributed appreciably to the intensity observed from the boron target. The yield curve for boron as shown in Fig. 4B gives a smooth rise of intensity with voltage except for a weak resonance at approximately 820 kv.

Crane, Delsasso, Fowler and Lauritsen[3] have reported the discovery of gamma-radiation from boron due to proton bombardment and from cloud chamber measurements of the gamma-ray energies they concluded that some, and perhaps all, of the radiation is due to the reaction ${}_5B^{11}+{}_1H^1=C^{12}+\gamma$. Calculations of Breit and Wigner indicate, however, that the process involving emission of an alpha-particle leaving Be^8 in an excited state may also take place with an appreciable probability.

Fluorine

For the investigation of gamma-radiation from fluorine two different targets were used. The first target was a thick layer of CaF_2 powder which adhered satisfactorily to a molybdenum plate after being wetted with distilled water and then permitted to dry. For the preparation of the

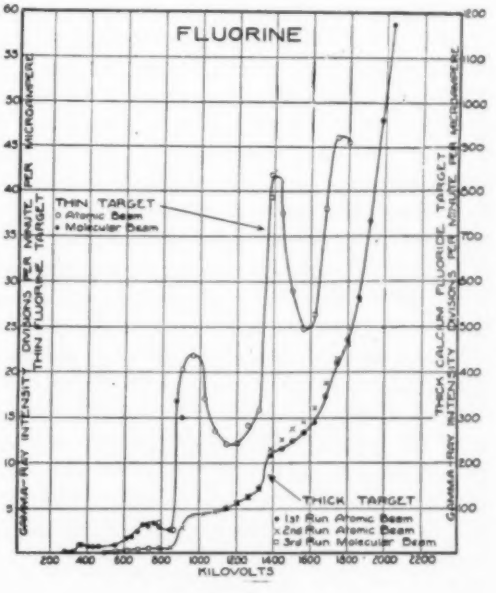

FIG. 5.

[12] Hafstad and Tuve, Phys. Rev. **48**, 306 (1935).

[13] The probability of gamma-ray emission in these reactions is discussed in a paper by Breit and Wigner which will be published soon in the Physical Review.

second target, which was to be thin, an iron sheet was immersed in a weak solution of hydrofluoric acid and the resulting thin layer of combined fluorine was found to be satisfactory as a target.

The gamma-ray yield from fluorine as shown by the curves of Fig. 5 is outstanding because of the number and prominence of resonance levels and because of the great intensity of the yield. Two separate runs on the CaF_2 target show good agreement and peaks in the thin target yield curve correspond closely to steps in the thick target curve. The contribution of Ca to the gamma-ray intensity from CaF_2 is negligible since the yield at 1680 kv from a target of metallic calcium was less than 0.1 percent of the yield from CaF_2 at the same voltage. Because of an oversight iron was not investigated for gamma-ray emission, but the great intensity of the fluorine radiation and the correspondence of the thick and thin target yield curves indicate that the iron background did not contribute appreciably to the thin target yield.

Hafstad, Heydenburg, and Tuve[5] made a careful investigation of gamma-ray emission from a thick CaF_2 target using protons with energies up to about 1050 kv. They observed sharp resonances at 328, 892, and 942 kv and a broad resonance between 600 kv and 700 kv. Because of lack of time the experimental points in the yield curves of Fig. 5 were not taken at closely enough spaced voltages to resolve the 892, 942 kv doublet. A comparison of the curves of Fig. 5 with results obtained at Washington shows, however, that the voltage scales at the two laboratories agree to within a few percent over the voltage range from 328 kv to 900 kv.

In addition to the low voltage resonance peaks which check the results of Hafstad, Heydenburg, and Tuve, the curves of Fig. 5 show a prominent resonance at approximately 1400 kv and give indications of another resonance at 1760 kv.

From their calculations Breit and Wigner find that for fluorine the most probable reaction giving gamma-radiation is ${}_9F^{19}+{}_1H^1={}_8O^{16}+{}_2He^4$ with formation of O^{16} nuclei in an excited state and subsequent emission of radiation. This conclusion is supported by the work of Crane, Delsasso, Fowler, and Lauritsen who made cloud chamber measurements of the energy of gamma-radiation from fluorine bombarded by 0.9 Mev protons. They concluded that the radiation is probably monochromatic with an energy of 5.4 Mev. If the reaction is assumed to be one of radiative capture with formation of stable Ne^{20} the total energy available would be 13.9 Mev. The absence of radiation harder than 5.4 Mev supports the conclusion of Breit and Wigner that the reaction involving radiative capture is much less probable than the reaction leading to formation of excited ${}_8O^{16}$ nuclei.

Sodium

A thick sheet of sodium metal obtained from Mallinckrodt gave the yield curve shown in Fig. 4A. Although the purity of the sodium is not known an examination of the shape of the yield curve and the yield intensity shows that the results could hardly be due to contaminants. As a further check on these results gamma-ray intensities have been measured recently from targets of sodium metal, analytical reagent, obtained from Mallinckrodt. The impurities listed in the analysis of this metal could not possibly contribute appreciably to the gamma-ray yield. Although fluorine was not listed in the analysis we were assured by correspondence with the Mallinckrodt Company that the fluorine content is almost certainly less than 0.0015 percent and is therefore negligible.

Gamma-ray yields from sodium were found to be considerably affected by the layer of sodium oxide and sodium hydroxide which formed on the targets when they were being mounted. Two targets of sodium metal analytical reagent were studied, and of these two the first was exposed to air much longer than the second. At 1800 kv the gamma-ray yield from the first was 0.75 of the yield shown in Fig. 4A and from the second the yield was 1.2 of the value given by Fig. 4A. Since oxygen has been found to be inactive these results indicate that the yields of Fig. 4A are not due to contaminants but that the intensities are somewhat lower than would be obtained from pure sodium.

The yield curve of Fig. 4A shows one broad resonance between about 1150 kv and 1320 kv.

Gamma-radiation from sodium is probably due

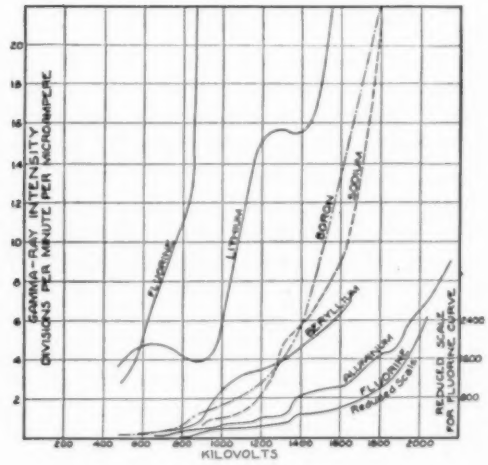

FIG. 6. Comparison of yield curves.

to one of the two following reactions:

$$_{11}Na^{23}+{}_{1}H^{1}={}_{12}Mg^{24}+\gamma, \quad (1)$$

$$_{11}Na^{23}+{}_{1}H^{1}={}_{10}Ne^{*20}+{}_{2}He^{4}, \quad (2)$$
$$_{10}Ne^{*20}={}_{10}Ne^{20}+\gamma,$$

or possibly both reactions may occur.

Using the new mass values of Aston and Pollard and assuming an energy of 1.8 Mev for the incident protons we find 11.5 Mev for the available energy in reaction (1) and 4.4 Mev in reaction (2). In reaction (2) part of the energy will go into kinetic energy of the alpha-particle.

Because of the great difference between the energy changes in these two reactions a determination of gamma-ray hardness should give information regarding the relative probability of the reactions. An attempt has been made to measure the hardness of the radiation by a determination of its absorption coefficients in lead and copper. The values obtained were 0.52 cm^{-1} for lead and 0.35 cm^{-1} for copper.

In the book *Quantum Theory of Radiation* Heitler gives calculated absorption coefficients for hard gamma-radiation, but from his absorption curves our experimental absorption coefficients for lead and copper do not give consistent values for the gamma-ray energy.

Lauritsen[14] has recently shown that the energy of hard gamma-radiation cannot be determined by ordinary measurement of absorption coefficients and it therefore seems that from our data no conclusion may be drawn regarding the hardness of sodium radiation.

[14] Delsasso, Fowler and Lauritsen, Phys. Rev. **51**, 391 (1937).

Aluminum

Alcoa aluminum foil of sufficient thickness to stop the most energetic protons was used to investigate aluminum radiation. Two different foils were tried, giving the results shown in Fig. 4C. As the data on film 1 were taken before adequate shielding was provided for the electroscope, x-ray background from the generator gave a considerable contribution to the observed intensity. Before taking data on film 2 the shielding arrangement as shown in Fig. 1 was adopted and the x-ray background was then considerably less than 0.1 of the aluminum intensity over all regions of the yield curve above 1200 kv.

Taking into account the difference in background intensity for the two aluminum foils studied their yield curves show good agreement and check runs on film 2 also agree well. The yield curve shows a very prominent resonance at approximately 1370 kv. Weak resonances are also indicated at approximately 750 kv, 990 kv, and 1160 kv, but more work must be done using thin aluminum targets before these can be definitely established. At higher voltages the yield curve gives indications of two broad resonances, one at 1620 and the second at 1850 kv.

A comparison of the yield curve from aluminum with the fluorine yield curve (see Fig. 6) shows that the two are quite similar in general shape and that each has a prominent resonance at approximately 1.37 Mev. It was therefore suspected that the radiation observed from aluminum might be due to a small amount of fluorine present in the aluminum as an impurity. By correspondence with Dr. F. C. Frary, Aluminum Research Laboratory, Aluminum Company of America, we were assured, however, that the fluorine content of this aluminum is of the order of 0.001 percent or less and that there is no possibility of a 0.25 percent fluorine content which is the amount necessary to account for the observed intensity from aluminum.

Breit and Wigner find that the most probable reaction giving gamma-ray emission from alumi-

num is $_{13}Al^{27}+_1H^1=_{14}Si^{28}+\gamma$ where the total energy available for radiation is 13.6 Mev with an incident proton energy of 1.5 Mev.

Other elements

Table I shows the results of a few measurements of gamma-ray intensity from targets giving low yields. To serve as a comparison the yield values from aluminum are included. SiO_2 gave a very low yield and it was at first believed that the observed intensity was entirely due to x-ray background from the generator. Later work showed, however, that a Pt target gave still lower yields and that some of the observed intensity from SiO_2 was actually due to gamma-radiation from the target. It is quite probable, however, that part or all of the observed intensity was due to contaminants, either on the surface or present in the compound as impurities. Intensities from targets of Mo, Ca, Ni, C, brass, and Pb_2O_3 were all above the Pt intensity and therefore above the x-ray background of the generator but as in the case of SiO_2 the effects may have been due to contaminants.

Radiation from targets of K_2CO_3 and $CaCl_2$ were fairly intense but the yield values given are not very reliable because of a possible surface contamination of sodium. These materials were placed on the target holder together with a sheet of sodium which had absorbed a considerable amount of water vapor. When the target chamber was pumped down sputtering occurred from the sodium and probably caused contamination of the K_2CO_3 and $CaCl_2$ targets.

TABLE I. *Gamma-ray intensity in divisions per minute per microampere.*

Kilovolts	1200	1440	1500	1620	1680	1740	1800	1980
Al	1.0	2.3	2.4	2.7	3.1	3.7	4.3	6.4
SiO_2	0.084			0.19			0.37	.50
Pt					0.052		0.25	
Mo						0.38		
Ca		0.18			0.31			
Ni							0.58	
C							0.39	
Brass							0.70	
Pb_2O_3				0.98				
K_2CO_3							1.5	
$CaCl_2$			1.1					

Discussion of Yield Curves

In order to show the relative intensities of gamma-radiation from the six elements studied and to compare the shapes of their yield curves the thick target yields are all plotted to the same scale in Fig. 6. CaF_2 yield values from Fig. 4 were multiplied by a factor of 2.11 to convert them to yields from pure fluorine. Because of the high intensity of the fluorine radiation very little of the yield curve can be shown when plotted to the same scale as that used for weak emitters, and a curve plotted to a reduced scale is therefore included. The lithium yield curve shown is not entirely satisfactory for comparison since the target used was not sufficiently thick to completely stop incident protons of high energy.

The curves of Fig. 6 show that the relative intensities of gamma-radiation from the elements bears no simple relationship to the atomic number of the elements or to the energies released in the reactions. Fluorine, for example, is of higher atomic number than boron, has less reaction energy, and yet gives an intensity, at 1800 kv, 45.5 times as great as the intensity from boron. To explain the observed intensities of gamma-radiation from the elements studied and to explain the shapes of their yield curves, Breit and Wigner in their paper show that it is necessary to take into consideration the nuclear energy level systems of elements involved in the reactions.

The work reported in this paper was intended to be only a preliminary survey and further studies will be made using thin targets and closely spaced voltages in order to determine the widths and positions of nuclear energy levels more accurately.

We are indebted to Professor G. Breit, Professor H. B. Wahlin, and Professor L. R. Ingersoll for advice and support, and to D. B. Parkinson, E. Bernet, and C. Hudson for valuable help. This work has been greatly facilitated by generous grants from the Wisconsin Alumni Research Foundation and from the Bowman Cancer Foundation.

The Construction and Operation of a Cyclotron to Produce One Million Volt Deuterons

P. GERALD KRUGER AND G. K. GREEN
Department of Physics, University of Illinois, Urbana, Illinois

(Received February 15, 1937)

A cyclotron for producing one million volt deuterons is described. The general magnetic field characteristics, and the effect of shims on the magnetic field have been examined. The production of ions for acceleration with and without filaments is discussed. The operation with a continuous glow discharge in the vacuum chamber is possible only because a transmission line is used to feed power to the dees. Various construction and operation details are given. The cyclotron has been found very reliable in operation and a maximum ion beam of 11 microamperes has been maintained for long periods of time. The beam has been removed in vacuum to a point about four feet from the vacuum chamber and partially focused. This allows bombardment work to be done with little interference from background radiation and high intensity fields.

VARIOUS methods[1-4] for accelerating heavy particles for nuclear disintegration work have been devised. A consideration of them led the authors to choose the cyclotron, or magnetic resonance accelerator. Two of its chief advantages are that a cyclotron yielding 2 Mev deuterons and 4 Mev protons or α-particles can be housed easily in a room approximately 15 feet by 20 feet and 15 feet high, and that voltages no larger than 50,000 volts need be applied to obtain the above effective potentials. The latter condition greatly reduces, as compared to other methods, the insulation problems which must be solved.

At the time the present installation was commenced, the high velocity beam of particles from the cyclotron could not be removed from the vacuum chamber and on this account the utility of the apparatus was limited. It seemed to the authors that this apparent disadvantage could be removed, an opinion which has been substantiated by Lawrence and his co-workers, and by the experience described below.[5]

Several descriptions of the cyclotron, its operation and fundamental characteristics have been discussed by other authors[4, 6, 7] so that it is unnecessary to give here an account of the general ideas involved. However, during the construction and operation of our small cyclotron (1 Mev deuterons) several new features have been introduced and since a number of investigators have requested information on these points, it is the chief purpose of this paper to discuss these new features in detail.

The size of the cyclotron is essentially the same as that designed by Livingston,[7] and from whom several important points on design were obtained prior to publication. The length of the Armco iron magnet is approximately 88 inches, the height 48 inches, and the pole face diameter 16 inches. A view of the whole unit is shown in Fig. 1.

The energizing coils of the magnet have 1248 turns of $\frac{1}{4}$-inch copper tubing and take a current of 100 amperes so that the magnetomotive force is 124,800 ampere turns. The magnet coils are cooled by a 12 gallon per minute flow of distilled water. The distilled water is cooled by tap water flowing through a copper radiator in a heat exchanger.

The intensity of the magnetic field in the accelerating chamber is 12,400 gauss at a current of 100 amperes and is essentially uniform over a radius of 16 cm as is shown in Fig. 2. Fig. 2 also depicts the effect of placing ring shims of various widths above and below the vacuum chamber. With no shims the field is flat and uniform except for a hump just inside the point where the field falls off rapidly. This hump may be due to the fact that the lid and bottom of the vacuum chamber are $\frac{1}{4}$-inch larger in diameter than the poles of the magnet. A ring shim ($\frac{1}{16}$ in. thick,

[1] Cockcroft and Walton, Proc. Roy. Soc. **A129**, 477 (1930).
[2] Van de Graaff, Compton and Van Atta, Phys. Rev. **43**, 149 (1933).
[3] Crane, Lauritsen and Soltan, Phys. Rev. **45**, 507 (1934).
[4] Lawrence and Livingston, Phys. Rev. **40**, 19 (1932); Phys. Rev. **45**, 608 (1934).
[5] Kruger and Green, Phys. Rev. **51**, 57 (1937).
[6] Lawrence and Cooksey, Phys. Rev. **49**, 866 (1936); Phys. Rev. **50**, 1131 (1936).
[7] Livingston, Rev. Sci. Inst. **7**, 55 (1936).

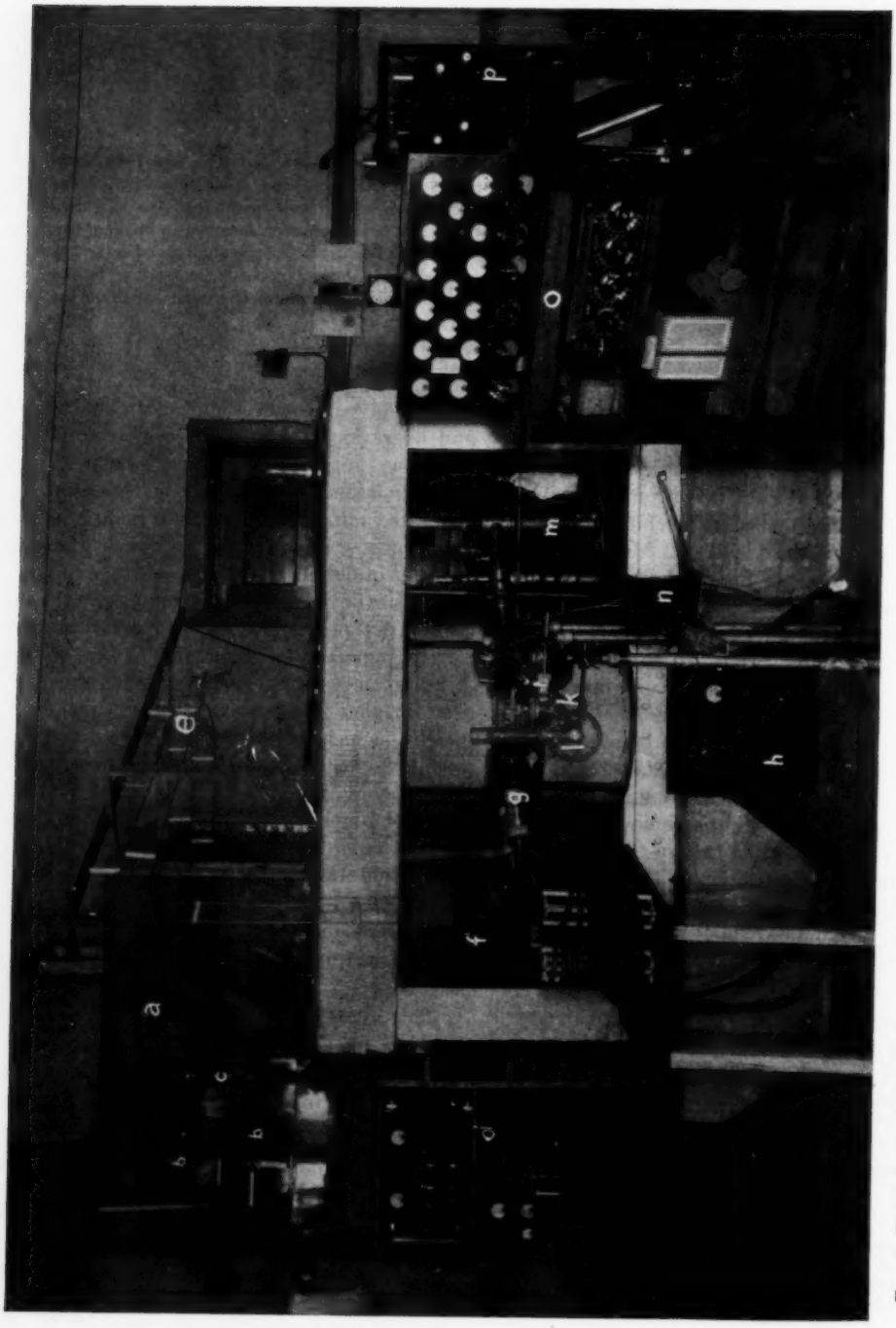

FIG. 1. General view of the cyclotron. (a) Oscillator house; (b) grid condensers; (c) 207 tube and water jacket; (d) oscillator-rectifier control panel; (e) transmission line; (f) dee coil; (g) dee insulators; (h) filament panel; (i) beam exit tube and focusing magnets; (k) stopcock to segregate exposure chamber; (l) exposure chamber; (m) Apiezon oil pump; (n) beam meter box; (o) movable control desk; (p) rack with auxiliary units and controls.

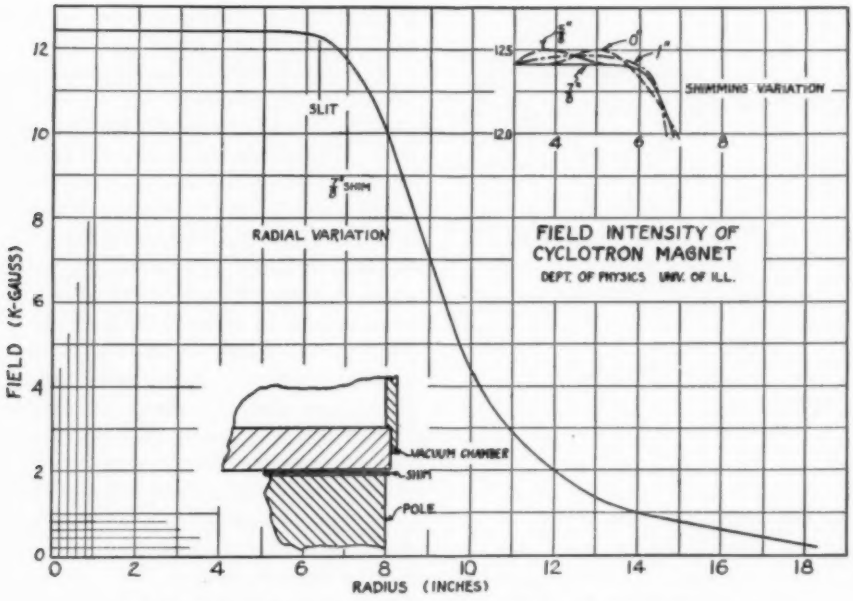

FIG. 2. Magnetic field intensity curve. Insert shows relative position of vacuum chamber and pole edges.

$\frac{7}{8}$ in. wide, 16 in. o.d. $14\frac{1}{4}$ in. i.d.) removes this hump (others do not, see Fig. 2), and gives a uniform field over an area almost 16 cm in radius. For that reason the exit slit in the dee is placed 16 cm from the center of the vacuum chamber. The large field gradient at greater radii makes it easy to remove the beam from the cyclotron chamber.

Fig. 3 shows schematically the vacuum chamber, the dees, deflection electrodes, and exit for removing the ion beam from the region between the poles of the magnet. The dees are one inch deep inside and are essentially the same as the design of Lawrence and Livingston. The vacuum chamber lid and bottom are made of Armco iron and are one inch thick. There is a space of three inches between top and bottom of the vacuum chamber.

During the first months of operation, 10-mil tungsten filaments were used, and a maximum ion beam current of three microamperes obtained at the collector cup (see Fig. 3). Recently a new filament assembly using 40-mil tungsten wire, and similar to the design of Lawrence and Cooksey,[6] has been installed. With this a steady beam current of 11 microamperes has been maintained during continuous operation of several hours. All of our results indicate that the ion beam current is nearly proportional to the filament emission, provided the gas pressure in the vacuum chamber is of the order of 10^{-5} mm Hg or less. At pressures slightly above 10^{-5} mm Hg, space charge limitations occur so that it is necessary to reduce the filament heating current to an optimum value which gives maximum beam current. At still higher pressures a glow discharge occurs between the dees and then the filaments can be turned off and a beam of 5 microamperes obtained.[8] Fig. 4 shows the relation between the ion beam current and the pressure in the vacuum chamber. Two independent sets of data taken under different conditions are represented by the dots and crosses. In taking these data the pressure was increased to about 10^{-4} mm Hg by letting in a burst of heavy hydrogen. Then readings of pressure and beam current were recorded while the pumps reduced the pressure. The right half of the curve represents a condition of gaseous discharge and cold filaments. The use of filaments in this pressure region does not

[8] Kruger, Green and Stallmann, Phys. Rev. **51**, 291 (1937).

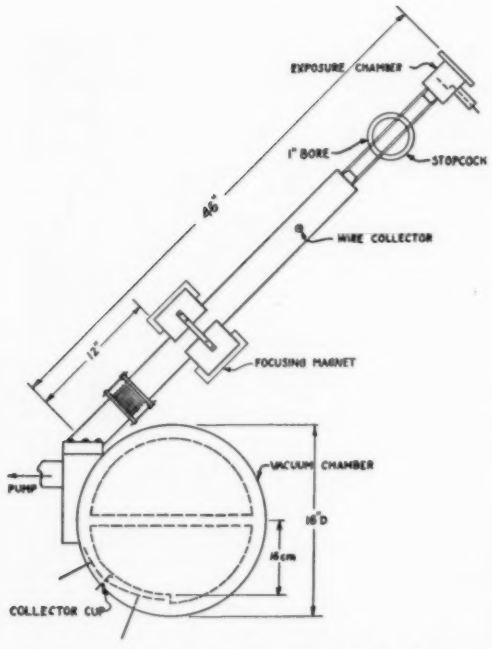

FIG. 3. Schematic diagram of vacuum chamber and beam exit appurtenance.

increase the beam current. The left half of the curve represents a pressure condition so low that no glow discharge occurs and filaments must be used. It will be noticed that the maximum beam current is obtained over a rather limited pressure region.

The electrons from the filament are accelerated by a 0–1800 volt potential applied between the filament and a surrounding shield. The optimum potential[9] is dependent on operating conditions and is set by watching the effect on the beam current. As the accelerating potential is increased the beam current increases up to the optimum value of the accelerating potential and then decreases with any further increase in accelerating potential. At first the electrons were accelerated through a round hole in the filament shield but later a three wire 10-mil tungsten grid was placed over the hole. With this grid the beam current was 2.5 times the current without a grid. We are planning to use six or eight wire grids in the future. This should increase the efficiency of the filaments even more.

The details of the construction of the dee insulators are shown in Fig. 5. Molded Pyrex glass tubing has internal cones ground on both ends. These cones are fitted with brass end cones which are machined to fit the vacuum chamber on one end and the dee support tube on the other, and are cemented to the glass with litharge cement (mixture of PbO and glycerin). This makes a joint which is so stable that a hammer must be used to separate the cones. However, the joint is not strictly vacuum tight and must be painted with shellac or glyptol under vacuum. Aluminum rings, as shown in the figure, are spaced along the glass wall to shield the glass and at the same time provide a sufficiently long glass path for insulation. These rings are split with the ends tapered and overlapping so that the ring is not continuous, and so that the copper dee supporting rod cannot "see" the glass at any point. This prevents sputtering of the glass with copper. The rings also serve two other purposes. They prevent any cold cathode emission from striking the glass and act as a high frequency shield to prevent the glass from heating. One such pair of insulators gave several hundred hours of service between March and November, 1936, without heating or puncture. The second pair has been in service since then.

Removing the beam from the region between the poles of the magnet is very important, because it enables the performance of bombardment and disintegration experiments in a region comparatively free from the disturbing influence of background radiation from the walls of the vacuum chamber. Moreover, detecting devices such as a Wilson cloud chamber or electrical

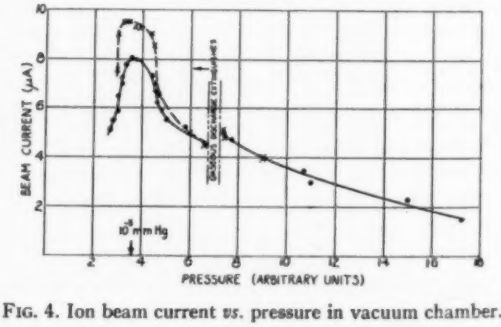

FIG. 4. Ion beam current *vs.* pressure in vacuum chamber.

[9] This potential varies from zero to 1500 volts under different operating conditions but normally is about 800 volts.

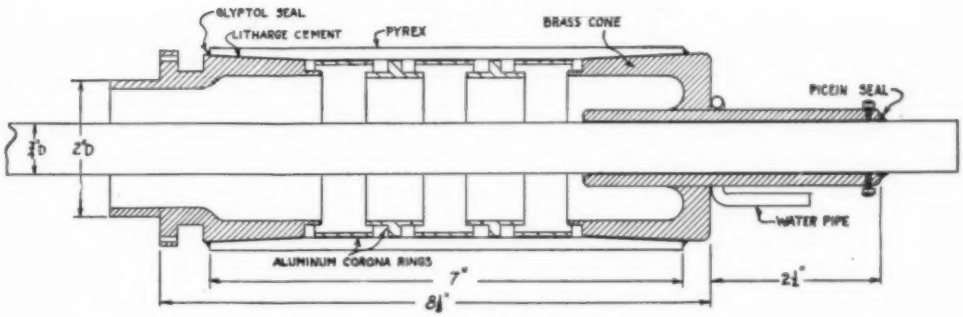

FIG. 5. Dee insulator.

counters can be operated with less influence from intense electric, magnetic and high frequency fields. It is comparatively simple to remove the beam if advantage is taken of the sharp decrease in the magnetic field at the edge of the pole, i.e., if the slit in the dee is placed at the edge of the plateau in the magnetic field curve as shown in Fig. 2. When this is done the ions move in a rapidly decreasing field and consequently a path of increasing radius of curvature as soon as they are pulled a small distance out from their last circle by the deflecting field. The size of the beam was examined at the point where it passed the edge of the vacuum chamber and was found to be 50 mm long by 5 mm high. Thus to remove the beam several feet from the cyclotron, as has been done, it was necessary to prevent further divergence of the beam and focus it. Partial focusing has been accomplished with a pair of small electromagnets.

The high frequency power for accelerating ions is supplied by two PR 207 tubes and is transferred to the cyclotron vacuum chamber by an untuned transmission line (Fig. 6). This method was selected for several reasons: limited space makes it impractical to set the oscillators next to the vacuum chamber; the small output of our rectifier (10 kw) requires the highest possible efficiency; the vacuum chamber can be rotated or removed without disturbing the oscillator system; and during operation the oscillators are not thrown out of oscillation by bursts of gas in the vacuum chamber. Thus the cyclotron can be run with a glow discharge in the chamber in order to outgas the metal surfaces rapidly, and, as described above, can produce a beam without the use of filamentary ion sources.

Greatest efficiency is realized with the oscillator tubes working into a circuit with a high L–C ratio. For this reason the plate tank circuit is made "low C," i.e., high impedance, and matched by the transmission line to the dee tank circuit. This latter resonant circuit may have a relatively low impedance, especially with a glow discharge, which is equivalent to shorting the dees with a resistance. The dee coil is wound with $\frac{5}{16}$ in. copper tubing on a 4 in. form and has ten turns. The transmission line[10] is made with two lengths of $\frac{1}{4}$-in. copper tubing which are supported on 4 in. Isolantite feeder spreaders. (See Fig. 1.) The length of an untuned line does not affect its characteristics and is fixed to accommodate the arrangement of the apparatus. The line tubes, at the terminal end, are clipped across 1.1 turns of the dee coil which matches the line to the dee tank impedance. At the input end the line is coupled to the plate tank by $\frac{1}{2}$ turn of $\frac{1}{4}$ in. tubing wound on a 6 in. form and placed around the center of the plate coil. This plate coil has eleven turns of $\frac{5}{16}$-in. copper tubing wound on a 4 in. form.

The cooling water exhausts from the oscillator tube jackets into the plate coil ends and leaves the coil through its center tap. This arrangement

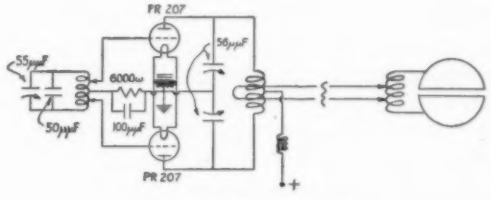

FIG. 6. Oscillator circuit.

[10] Green, Kruger, Phys. Rev. **51**, 57 (1937).

saves three hose reels, which in our installation contain 16 feet of hose, each. The tank coil is tuned by double concentric cylindrical condensers whose stationary elements are 6.5 in. i.d. by 12 in. long, and have cylindrical corona rings around bottom and top. The movable elements are 4.75 in. o.d.×15 in. long, with copper hemispheres over their tops, and their positions controlled by racks and ganged pinions. The grid tank consists of a seven turn, water-cooled coil of $\frac{1}{4}$ in. tubing wound 2.5 in. i.d. and a conventional type variable condenser built in our shop. The condenser has five $3\frac{1}{2}$ in. radius rotor plates, and four stator plates, spaced one inch apart and is paralleled by a fixed air condenser having three 11 in.×11 in. plates spaced 1 in. (see Fig. 1). All condensers are supported on Isolantite pillars. The grid coil center tap connects to a grid condenser made of glass plates and sheet copper, and a grid leak consisting of three 200 watt 2000 ohm vitreous enameled resistors in series. The oscillator tubes have a low grid plate impedance so that it is necessary to tap the grid leads about a turn in from the coil ends to keep the excitation and d.c. grid current low enough. This tapping gives a transformer action causing a high peak voltage across the grid condenser, which arcs between plates occasionally. It may be necessary to introduce a small amount of cross neutralization to prevent arcing when using higher power. The filaments of the two tubes are connected in parallel with copper rods which conduct the circulating current. This eliminates by-pass condensers, and reduces parasitic oscillations.

The high frequency system is supplied with power by a three-phase full wave rectifier having a high voltage transformer rated at 10 kva. Rectification is provided by six FG 19A (same as 872A) carbon anode mercury vapor tubes. A small filter is connected in the rectifier output, mostly for high frequency and surge protection.

When making either the initial or subsequent adjustments, the dee circuit is tuned to the desired frequency by varying the number and spacing of turns, of the tank coil. The resonant frequency is determined by finding the point at which a small, calibrated, oscillator delivers load to the tank when coupled loosely to it. The power oscillators are then tuned to this frequency and the transmission line connected at both ends with turn ratios determined by a rough impedance calculation. Operating with reduced input energy, the plate condenser is varied over the region in which the plate current peak occurs, and the characteristics of this current peak observed. This operation is repeated for a series of grid condenser positions and the grid and plate condensers adjusted to give the best peak obtainable. The coupling at the dee end of the line is then varied to find the best plate current peak. Finally the coupling at the tank end is adjusted to give the desired power transfer. When the tuning is correct, varying the plate condenser will give a smooth plate current peak and a neon lamp touched to the line will glow with an intensity independent of the point touched. (Such tests may be made with a neon glow lamp fixed to the end of a clean glass tube about a meter long. This sort of indicator should never be put in contact with any part of a circuit at very high radiofrequency potentials.) The potential developed across the dees is directly proportional to the square root of the high frequency power they absorb. In normal operation the oscillators are supplied with 10 kw of d.c. power at 9600 volts, of which about 60 percent appears as high frequency power in the dee tank. This produces a peak voltage of 50±5 kv across the dees, as measured with a cathode-ray oscilloscope and capacity voltage divider. The relation between beam current and peak voltage across the dees is shown in Fig. 7.

Ion beam current is measured with a vacuum tube voltmeter indicating the potential drop

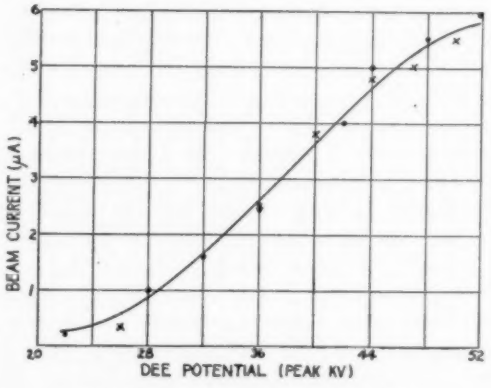

FIG. 7. Beam current *vs.* dee potential.

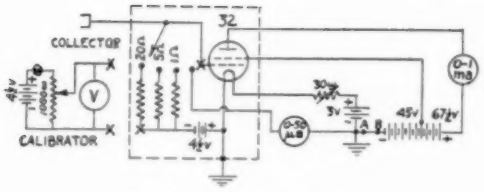

FIG. 8. Beam meter circuit.

across a high resistance. The meter, Fig. 8, is cheap and rugged, and holds calibration for long periods. A permanent calibrator is built to clip on at points X so that a calibration requires less than five minutes. The type 32 tube obtains filament current from two No. 6 dry cells and its plate and screen grid current from batteries which also supply the grid and plate potentials for the ionization vacuum gauge. The insulated metalized type resistors are calibrated and will hold their value for a long period. With 20 megohms, 10^{-8} amperes gives one scale division deflection on the 0–1 ma plate current meter. This has been found to be adequate sensitivity. The above milliameter is mounted on the movable control panel with about 60 feet of shielded cable to the tube and resistors, which are in a shield box near the beam collectors. Shielded rubber covered hookup wire makes a satisfactory grid lead. Several feet of lead wire can be used if the shield is carefully grounded.

A 0.25 megohm resistor has been inserted at AB and a cathode-ray oscillograph connected across it to photograph the wave form of the ion beam. When doing this it is best to increase the plate battery voltage to 90 volts. An oscillogram taken in this manner shows about 10 percent beam current ripple caused by the 360 cycle ripple in the input to the oscillators.

All operating controls and meters are built into a desk (see Fig. 1) mounted on castors and connected by a long cable to a terminal box into which all control and indicating leads are run. This has been especially convenient for developmental and adjustment work when the controls need to be moved to any desired region. Two keys, on the panel, control motor driven resistors in the magnet generator field. One resistor has a low value and gives a fine adjustment, which can be controlled by a balanced-galvanometer and photo-cell system (similar to that of Wynn-Williams[11]) so that the magnet current is held constant. The other resistor has a higher value, for coarse adjustment, and is controlled by a push button so that the generator shunt field circuit is broken when the resistance is all in. The relatively low inductance of the magnet and generator allows these resistors to function with small lag in the generator field circuit, whereas the 200 ampere magnet current makes control in the magnet coil circuit impractical. Both resistors have auxiliary contacts which energize neon bulbs on the panel to indicate their positions.

In operation, the cyclotron has been very reliable. Outgassing is easy because one can let the oscillators run with gas in the vacuum chamber and pump until the gas cleans up. Then a beam can be obtained in a few minutes. When the vacuum chamber is clean, a small amount of air introduced and immediately pumped out does not impede operation. For instance, by closing the big glass stopcock in the beam exit line (Fig. 1) one can change the target in the exposure chamber and within ten minutes be in operation bombarding the new target.

Some rectangular shims are used in addition to the ring shims described above. However, with magnetic field deviations of the order of one percent, such as are present over the area of the dees, very little empirical shimming is necessary.

The authors wish to express thanks to their laboratory colleague, Mr. F. W. Stallmann, for his cooperation and help in the assembly of the cyclotron. The senior author also wishes to acknowledge a grant-in-aid from the National Research Council and generous support from the Graduate School Research Board of the University of Illinois.

[11] Wynn-Williams, Proc. Roy. Soc. **145**, 250 (1934).

Collision of Neutron and Proton. II

PHILIP M. MORSE, J. B. FISK* AND L. I. SCHIFF
Massachusetts Institute of Technology and Harvard University, Cambridge, Massachusetts

(Received February 11, 1937)

A neutron-proton potential field of the form discussed in an earlier paper has been chosen, of radius $r_0=2.7\times10^{-13}$ cm, with a triplet depth of 36.04 Mev, corresponding to a binding energy of 2.2 Mev for the deuteron. Two different singlet depths are used, 14.64 Mev and 16.36 Mev, corresponding to cross sections for neutron-proton scattering of 12 and 40×10^{-24} cm², respectively, having no stable singlet state. Using these potentials, the elastic and inelastic collision of neutron and proton have been computed for a range of energies of the incoming neutron from 0 to 40 Mev. The angular distribution of elastic scattering shows decided departure from the spherical symmetry predicted by the use of a "square hole" potential; and is in fair agreement with available experimental data. Agreement is also obtained with experimental data on elastic cross section and capture cross section for fast neutrons. Curves for cross section for deuteron disintegration by gamma-rays are also computed. Experimental confirmation of these will provide a test of the correctness of our choice of form of potential. In all these cases, the results for the two different singlet potentials are practically identical for energies larger than 1 Mev.

SINCE the publication of our earlier paper[1] new data have been made available on neutron-proton scattering cross sections[2] and on the angular distribution of recoil protons from such collisions.[3] We have accordingly modified and extended our previous calculations.

It is found that the potential

$$V=71.23(e^{-2x}-2e^{-x})\times[(1-g)P^M+gP^H] \text{ nuclear units} \quad (1)$$

corresponds to a value of 4.35 nuclear units ($m_e c^2$) for the binding energy of H^2. In this formula P^M and P^H are the usual Majorana and Heisenberg permutation operators. In the notation of I, $x=r/0.15$, which corresponds to a value $r_0=0.3$ ($=2.7\times10^{-13}$ cm) for the mean radius of the potential hole.

The value of g depends on the value of the cross section $Q(0)$ for elastic scattering of slow neutrons from protons. This dependence is given in Table I. The most recent value[2] of $Q(0)$ is 15 nuclear units, $(h/2\pi c)^2(1/m_e m_p)$, corresponding to $g=0.297$, or a depth of singlet potential of 28.94 nuclear units, for a field with no stable singlet bound state. This corresponds fairly closely to the conclusions of other workers[4] as to the width and depth of the potential hole. However, in order to show the effect of the change in g on the magnitudes computed, and to provide for a possible redecision as to the value of $Q(0)$, we have also made calculations for $Q(0)=50$ nuclear units, corresponding to $D_s=32.34$. As will be shown below, the results for the two choices differ so little that a linear interpolation suffices to obtain results for intermediate values of $Q(0)$. All succeeding tables and curves are for no bound singlet state.

Using the methods discussed in I, wave functions have been computed for the bound state of the deuteron, and for the continuous dissociated states for $l=0$ and 1, and for energies from $W=0$ to $W=40$. When these were tabulated, it was found that they could be approximately expressed in terms of simple analytic forms, better suited for further calculation:

Bound triplet state ($l=0$)

$$\psi_n=0.9679e^{-0.3129x}(1-1.825e^{-x}+0.825e^{-2x})/r, \quad (2)$$

$$\int\int\int\psi_n^2 dv=1.$$

* Junior Fellow, Harvard University.

[1] Morse, Fisk and Schiff, Phys. Rev. **50**, 748 (1936), hereinafter called I. See also Fisk and Morse, Phys. Rev. **51**, 54 (1937).

[2] Amaldi and Fermi, Phys. Rev. **50**, 899 (1936).

[3] Harkins, Kamen, Newson and Gans, Phys. Rev. **50**, 980 (1936). See also Kurie, Phys. Rev. **44**, 461 (1933).

[4] Breit and Feenberg, Phys. Rev. **50**, 850 (1936); Cassen and Condon, Phys. Rev. **50**, 846 (1936). It may be that the radius r_0 should be chosen to be less than 0.3 in order to check binding energy data, though this is by no means certain. However, if r_0 were chosen to be 0.25, the energy scale shown in the present paper would be changed, each curve being for an energy about 3/2 the energy shown here. Other changes would be minor ones. *Note added in proof:* Copy of recent work by Ochiai, kindly sent to the authors and to be published soon, shows that a check for the binding energies of H^2, H^3, He^3 and He^4 can be obtained for a radius of interaction $r_0=2.65\times10^{-13}$ cm. This result, together with the results of this paper, indicate that nearly all of the experimental data on light nuclei can be satisfactorily accounted for by the potential given in Eq. (1).

TABLE I. *Dependence of g on $Q(0)$. $r_0=0.3$, $k_t=1.266$, $\Delta_t=-4.652$, $D_t=71.23$.*

		No Bound Singlet State			Bound Singlet State		
$Q(0)$	$\lvert\Delta_s\rvert$	k_s	D_s	g	k_s'	D_s'	g'
15	11.75	0.807	28.94	0.2969	1.022	46.42	0.1742
25	16.62	.831	30.69	.2846	.983	42.94	.1986
35	20.36	.843	31.58	.2783	.967	41.56	.2083
45	23.91	.850	32.12	.2745	.962	41.13	.2113
55	26.71	.855	32.49	.2719	.950	40.11	.2184

TABLE II. *Parameters for the dissociated triplet state. $b=0$.*

k	W	δ_0 degrees	a	δ_1 degrees	c	d
0	0	180.0	0.4942	0	0	0
0.5	0.25	160.7	.4667	− 0.1	0.012	−0.001
1.0	1.00	142.9	.4396	− 0.8	.045	− .004
1.5	2.25	127.0	.4128	− 2.5	.090	− .008
2.0	4.00	113.4	.3860	− 5.2	.100	− .010
2.5	6.25	101.9	.3591	− 8.6	.074	− .007
3.0	9.00	92.7	.3318	−12.3	+ .027	+ .001
3.5	12.25	85.4	.3039	−15.9	− .033	.010
4.0	16.00	79.8	.2753	−19.2	− .100	.020
4.5	20.25	74.4	.2457	−22.2	− .172	.031
5.0	25.00	69.6	.2149	−24.9	− .247	.043
5.5	30.25	65.2	.1828	−26.9	− .323	.056
6.0	36.00	60.8	.1490	−27.9	− .400	.070

Dissociated states

$$\psi_l=(1/r)P_l(\cos\vartheta)R_l(r),$$

$$R_0=\cos(\delta_0)\sin(\mu x)+(1-e^{-x})\sin(\delta_0)\cos(\mu x)+a\mu x^2e^{-x}+b\mu xe^{-x},\quad \int\psi_nR_{0l}rdr=0, \tag{3}$$

$$R_1=(\pi\mu x/2)^{\frac{1}{2}}\{\cos(\delta_1)J_{3/2}(\mu x)-\sin(\delta_1)[1-e^{-x}(1+x+\tfrac{1}{2}x^2)]N_{3/2}(\mu x)\}+cx^2e^{-2x}+dx^3e^{-x},$$

where $x=(r/0.15)$, $\mu=0.15k$, $(\mu x)=(kr)$, and $k^2=W$. These analytic forms differ from the exact solutions by never more than two percent over the entire range of r. Tables II, III and IV give best values of the parameters used in Eq. (3) for different values of the energy W and for the different choices of $Q(0)$. From these tables the properties of the neutron-proton collision can be computed.

RESULTS

The total cross section for elastic scattering is given by the formula

$$Q(W)=(\pi/W)[(\sin^2\delta_{0s}+3\sin^2\delta_{1s})+3(\sin^2\delta_{0t}+3\sin^2\delta_{1t})]. \tag{4}$$

TABLE III. *Parameters for the singlet state corresponding to $Q(0)=15$.*

k	δ_0	a	b	δ_1	c	d
0	0	0.663	−5.386	0	0	0
0.1	9.3	.632	−4.985	—	—	—
0.2	17.0	.603	−4.551	0.0	0.001	0.0000
0.5	32.1	.523	−3.558	− 0.1	.006	− .0002
1.0	42.5	.404	−2.328	− 0.4	.019	− .0010
1.5	45.8	.319	−1.592	− 1.4	.034	− .0016
2.0	46.2	.260	−1.109	− 3.0	.040	− .0022
2.5	44.7	.218	− .850	− 4.6	.039	− .0024
3.0	42.0	.190	− .653	− 6.2	+ .027	− .0020
3.5	38.2	.171	− .512	− 7.8	.000	− .0007
4.0	34.4	.155	− .415	− 9.1	− .035	+ .0016
4.5	31.1	.141	− .347	−10.3	− .074	.0060
5.0	28.8	.129	− .294	−11.4	− .118	.0121
5.5	27.5	.118	− .256	−12.4	− .167	.0210
6.0	26.8	.109	− .228	−13.3	− .219	.0330

TABLE IV. *Parameters for the singlet state corresponding to $Q(0)=50$.*

k	δ_0	a	b	δ_1	c	d
0	0	1.820	−10.560	0	0	0
0.1	18.6	1.371	− 7.825	—	—	—
0.2	31.0	1.066	− 5.969	0.0	0.001	0.0000
0.5	48.7	.618	− 2.126	− 0.1	.006	− .0002
1.0	55.1	.412	− 1.777	− 0.4	.019	− .0010
1.5	55.2	.345	− 1.464	− 1.5	.034	− .0016
2.0	53.7	.300	− 1.184	− 3.2	.040	− .0022
2.5	51.1	.262	− .942	− 5.0	.039	− .0024
3.0	47.5	.228	− .732	− 6.7	+ .027	− .0020
3.5	43.0	.198	− .554	− 8.4	.000	− .0007
4.0	38.6	.171	− .417	− 9.9	− .035	+ .0015
4.5	34.9	.149	− .320	−11.2	− .074	.0057
5.0	32.3	.130	− .255	−12.3	− .118	.0117
5.5	30.8	.116	− .218	−13.4	− .167	.0200
6.0	30.0	.105	− .207	−14.4	− .219	.0310

Here Q is given in square nuclear units ($=0.8\times10^{-24}$ cm^2) and W is also in nuclear units ($=0.506$ Mev for the center of gravity at rest). Since the energy of the incoming neutron with respect to the observer is $2W$, the parameter W is approximately equal to the initial neutron energy in Mev.

The cross section Q is plotted in Fig. 1 as a function of W, and is compared with the experimental data recently obtained.[5] The correspondence is satisfactory, except for the rectangle marked G, representing the value obtained by

[5] See, for instance, Booth and Hurst, Nature **138**, 1011 (1936); Tuve and Hafstad, Phys. Rev. **50**, 490 (1936); Dunning, Pegram, Fink and Mitchell, Phys. Rev. **48**, 265 (1935).

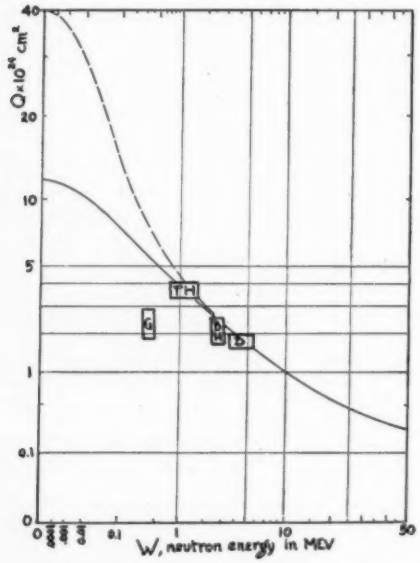

FIG. 1. Elastic cross section $Q(W)$ of protons for neutrons. The two curves are for two different singlet potentials, chosen to give $Q(0)=12\times10^{-24}$ and 40×10^{-24} cm², respectively. The rectangles represent the experimental data of Goldhaber, Booth and Hurst, Tuve and Hafstad, and of Dunning *et al.*

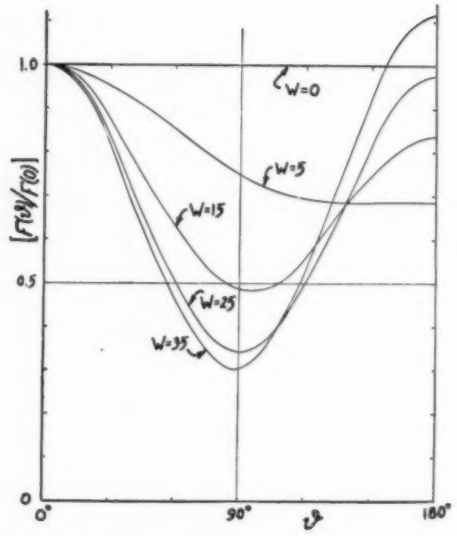

FIG. 2. Angular distribution of elastically scattered neutrons in system with center of gravity at rest.

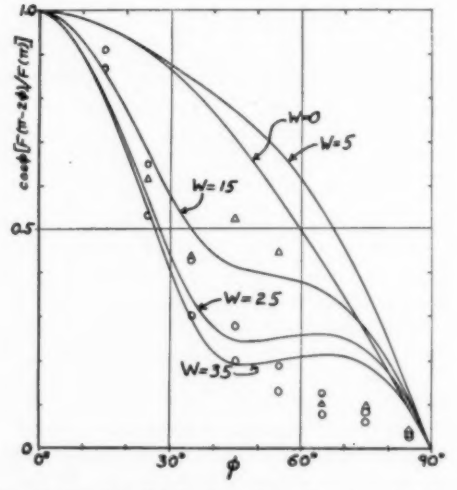

FIG. 3. Angular distribution of recoil protons in laboratory coordinate system. W is total neutron energy in Mev. Triangles show experimental data of Kurie, circles those of Harkins, *et al.*

Goldhaber. The dotted line represents the Q for $Q(0)=50$. The difference between the two curves is only marked below $W=0.5$.

The differential cross section, the number of neutrons per unit solid angle scattered at an angle ϑ (c.g. at rest) is given by the formulas

$$F(\vartheta)=(1/4)(F_s+3F_t), \quad Q=\int F d\Omega,$$

$$F_t=(1/W)[\sin^2\delta_{0t}+6\sin\delta_{0t}\sin\delta_{1t} \times\cos(\delta_{0t}-\delta_{1t})\cos\vartheta+9\sin^2\delta_{1t}\cos^2\vartheta],$$

with a similar formula for F_s, involving δ_{0s} and δ_{1s}. Curves of $[F(\vartheta)/F(0)]$ are given in Fig. 2 for different values of W. In this case, only the curves for $Q(0)=15$ are given, because, for the energies shown, the corresponding curves for $Q(0)=50$ are so similar as to be indistinguishable. For neutron energies below one Mev, the scattering is nearly spherically symmetrical. Above this energy, however, the distribution becomes unsymmetrical, with first a preponderance in the forward direction, and later a slight preponderance backward. This unsymmetry is chiefly due to the triplet function F_t, which is determined by the same field which is responsible for the stable deuteron. Therefore, the shape of the differential cross section curves is fixed primarily by the value of the deuteron binding energy. A change in the depth of the singlet potential to correspond to another value of Q for slow neutrons produces very little change in the magnitude of F for energies above $W=2$, or in the shape of F for any energy.

The presence of unsymmetric scattering for energies as small as $W=4$ is due to the choice of shape of the potential function V. Calculations[6] show that the "square hole" potential, with V exactly zero for $r>r_0$, does not give scattering asymmetry until W is larger than 10. The form of V used in this paper has small but finite values beyond $r=r_0$. This has little influence on the total scattering cross section, but has a marked effect on the angular distribution.

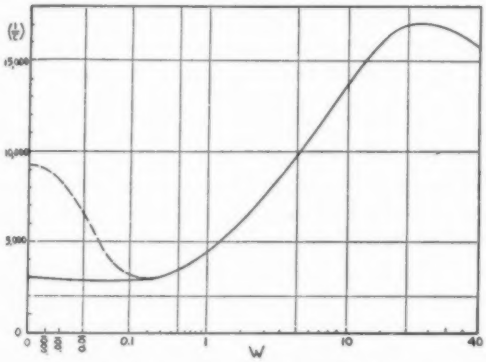

FIG. 4. Rate of recombination of neutron in paraffin in sec.$^{-1}$ as function of initial neutron energy in Mev. Solid line corresponds to $Q(0)=12\times10^{-24}$ cm^2 and dotted line to $Q(0)=40\times10^{-24}$ cm^2, respectively.

The angular distribution of recoil protons, in the coordinates of the proton initially at rest $[F(\pi-2\varphi)\cos\varphi/F(\pi)]$, is given in Fig. 3. It is seen that, for neutron energies between 10 and 20 Mev, the distribution is far from the simple cosine function required by the "square hole" potential. Considerably more protons are knocked forward in proportion to those knocked sideward. That this is in accord with experiment is shown by Fig. 3. The experimental data, on an arbitrary scale, are given by the circles and triangles. The check is not conclusive, for the data are not accurate, nor are the absolute magnitudes known. However, the correspondence shown in Fig. 3 may safely be taken to indicate that a neutron-proton potential of the form given in Eq. (1) is more likely to be correct than is a "square hole."

The probability of transition from the normal state of the deuteron to one of the dissociated states, either by electric or magnetic dipole radiation, has also been calculated. From this can be computed the probability of dissociation of the deuteron, and of the inverse process, the recombination of proton and neutron. The formulas for these quantities are given in I.

The inverse mean life before capture of a neutron in paraffin, $(1/\tau)=nq v$, is plotted in Fig. 4 as a function of the neutron energy W (solid line for $Q(0)=15$ and dotted for $Q(0)=50$). The rise for low energies is due to the magnetic dipole type of capture which predominates at low energies, but is negligible for energies above $W=1$. It is only this magnetic type which depends on the value of $Q(0)$. The data of Amaldi and Fermi[2] indicate a value of $(1/\tau)$ for very slow neutrons of about 5000 sec.$^{-1}$. This seems to check best for the solid line, for $Q(0)=15$.

The total cross section for disintegration of the deuteron by photon impact is given in Fig. 5. In this case, the magnetic dipole transition is

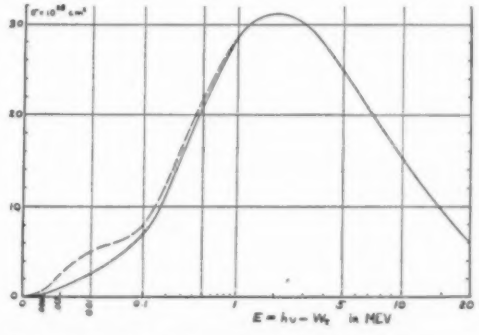

FIG. 5. Photoelectric cross section for deuteron disintegration as function of the excess of photon energy over the threshold energy. Energy scale is chosen to bring out details of the curves near the threshold. Solid line is for $Q(0)=12\times10^{-24}$ cm^2 and dotted curve for $Q(0)=40\times10^{-24}$ cm^2.

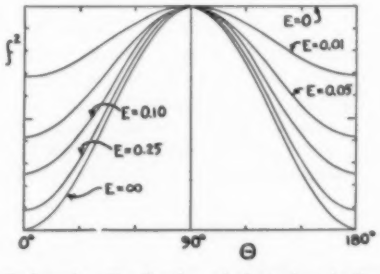

FIG. 6. Angular distribution of photoelectrically ejected protons from deuterons, for different values of E, the excess of photon energy over the threshold energy. θ is the angle between the ejected proton and the incident photon directions. Curves are for $Q(0)=12\times10^{-24}$ cm^2.

[6] Bethe and Bacher, Rev. Mod. Phys. **8**, 121 (1936).

negligible except just above the threshold energy. It is interesting to notice that the curve is similar to the one calculated by Breit and Condon[7] for the "square hole" and ordinary force, rather than their curve for Majorana force. The difference can again be ascribed to the effect on the $l=1$ wave function of the presence or absence of a small amount of V beyond $r=r_0$.

In addition to the total cross section for disintegration, we have computed the differential cross section

$$f^2(\theta)=\frac{1}{4\pi}\sigma_m+\frac{3}{4\pi}\sigma_e\cos^2\theta,$$

the distribution in angle of the protons produced in the disintegration, where θ is the angle between the direction of the incident photon and that of the ejected proton. This distribution is plotted in Fig. 6 for different values of E, the difference between $h\nu$ and the threshold energy. Only the curves for $h\nu$ just above the threshold energy show any great departure from the simple $\cos^2\theta$ behavior.

A measurement of the absolute magnitudes of this disintegration cross section for photon energies between 2 and 6 Mev will be of great use in determining more precisely the form of the neutron-proton binding force. For the higher energies, this cross section is due predominantly to the electric dipole transition, involving a transition to a triplet p state of the outgoing wave from the normal triplet s state. Therefore, it depends on the $l=1$ wave function, which is more sensitive to the shape of the triplet potential hole than is the s function. The absolute magnitude of the cross section depends on the width of the hole, reduction in r_0 causing a reduction in σ. The position of the maximum in the curve, however, depends on the details of the shape of the potential; the more sharply V falls to zero beyond $r=r_0$, the higher will be the energy for maximum σ.

The angular dependence of ejected protons for photon energies close to the threshold gives information as to the form of the singlet potential, since this measures the ratio of magnetic to electric dipole transition, and the magnetic cross section depends on the singlet state. In general, the deeper or wider this singlet potential, the larger will be the range of photon energy over which this angle dependence differs markedly from the simple $\cos^2\theta$ law.

[7] Breit and Condon, Phys. Rev. **49**, 904 (1936). The correspondence is also close with the curves calculated by Way, Phys. Rev. **51**, 552 (1937).

MAY 1, 1937 PHYSICAL REVIEW VOLUME 51

The Distribution in Time of Counts Due to a Constant Source and Its Daughter in Equilibrium

LEE DEVOL
University of Pittsburgh, Pittsburgh, Pennsylvania
AND
ARTHUR RUARK
University of North Carolina, Chapel Hill, North Carolina

(Received January 26, 1937)

An expression is obtained for the size distribution function of the time intervals between counts caused by a constant source and its daughter substance in equilibrium. The efficiency of the detector and its finite recovery time are taken into account. The results apply also to counts caused by bombarding particles and artificially radioactive atoms which they produce.

I. INTRODUCTION

EXPERIMENTS in which the time distribution of rays or particles from a radioactive source is used to obtain information about the source require for their interpretation a theory of the distribution to be expected. We have recently discussed[1] the fluctuations in the stocks of substances present in a complex source, and

[1] Ruark and Devol, Phys. Rev. **49**, 355 (1936); see also Peierls, Proc. Roy. Soc. **A149**, 467 (1935); Adams, Phys. Rev. **44**, 651 (1933); and Schiff, Phys. Rev. **50**, 88 (1936).

fluctuations in the disintegration of its atoms; but the distribution of disintegration times is not the same as that of the counts they produce in a detecting device of efficiency less than unity, and of limited time resolving power. Here we shall present a formula describing the distribution of counts produced by a long-lived substance and its short-lived daughter, of decay constant λ, in equilibrium. The formula applies also to any experiment in which a detector receives bombarding particles from a constant source and particles from a short-lived artificial radioactive source produced by that bombardment. For convenience, our discussion will be so worded as to apply to this situation. The word "rays" will be used to denote discrete entitities of any kind.

Consider a counter which is struck by F primary rays per second, on the average. Background rays are included in this category, as are also secondaries of any origin, *except* those due to the breakdown of activated atoms. A ray is included even if it does not enter the active space of the counter, provided it produces an activated atom which may later cause a count, by ejecting an ionizing particle into the active space. The chance that n primaries arrive in any interval t is given by Bateman's formula $(Ft)^n e^{-Ft}/n!$

Suppose that on the average, in one second, F_1 primaries arrive and do not produce activated atoms, while F_2 primaries do produce them. We refer to these two classes of primaries as class I and class II, respectively. Each class is distributed in time according to Bateman's formula, because a random selection from a Bateman distribution is itself a Bateman distribution. Similarly, the counts produced by each class form a Bateman distribution; for example, the chance that n class I primaries produce counts in time t is

$$(F_1 h_1 t)^n e^{-F_1 h_1 t}/n! \tag{1}$$

Here h_1 means the probability that a particular class I primary will produce a count; h_2 and h_3 will denote similar probabilities for class II primaries and activated atoms, respectively. These quantities include the influence of solid-angle factors and of detector efficiency. The recovery time of the detector will be neglected for the present. We shall need two formulas from our previous paper.[1]

(1) The chance of having a stock of j activated atoms is

$$S_j = x^j e^{-x}/j! \tag{2}$$

where x is the expected stock, F_2/λ.

(2) The chance that r activated atoms decay in time t is the same as the chance that r are produced, or that r class II primaries arrive.

$$(F_2 t)^r e^{-F_2 t}/r! \tag{3}$$

Now, we desire the probability that no count occurs in an interval of length t, and two functions of this kind must be considered. The first, p, is the probability that the interval *from an arbitrary instant to the next count* will exceed t; the second, P, is the probability that the *interval between two counts* will exceed t. These two functions are the same for a simple source obeying Bateman's formula, but in the present problem they are distinct. P is the function usually needed for interpretation of experiments, but we first obtain p, because it is useful in getting P.

II. Chance that the Interval from an Arbitrary Instant to the Next Count Will Exceed t

During an interval $(0, t)$, counts are in general produced in several ways which may be classified as follows. (1) Class I primaries arrive; (2) activated atoms present at time zero disintegrate; (3) class II primaries produce activated atoms, some of which disintegrate before time t, and, of course, some class II primaries produce counts directly. Thus p contains three factors:

(1) *The chance p_1 that no class I primary causes a count;*

$$p_1 = \exp(-F_1 h_1 t). \tag{4}$$

(2) *The chance p_2 that no activated atom present at time zero causes a count.* The chance that the stock of activated atoms is j at time zero, and that no atom of this stock causes a count in the interval $(0, t)$ is

$$S_j e^{-j\lambda t}[1+(1-h_3)(e^{\lambda t}-1)]^j, \tag{5}$$

by Eq. (16) of our earlier paper. Summing over all values of j, we get

$$p_2 = \exp[-F_2 h_3(1-e^{-\lambda t})/\lambda]. \tag{6}$$

(3) *The chance p_3 that no count is caused by class II primaries, or by the atoms which they*

activate. We first work out the chance that (a) r activated atoms are produced, that (b) none of the r primaries produce counts directly, and that (c) none of the r activated atoms produce counts. Summing the product of these three chances over all values of r, we shall get p_3. Using Eq. (3), the product in question is

$$[(F_2t)^r e^{-F_2t}/r!]\cdot(1-h_2)^r\cdot u^r, \tag{7}$$

where u is the chance that a given atom activated during the interval in question does not produce a count before time t. Let us consider this given atom. Since we have specified that it is activated during the interval $(0, t)$, the chance it is activated in a particular time element, t_1 to t_1+dt_1, is dt_1/t.

If it is produced in this time element, the probability it will *not* cause a count before time t is $1-[1-e^{-\lambda(t-t_1)}]h_3$. Averaging this over all positions of the time of activation we have

$$u=1-h_3+h_3(1-e^{-\lambda t})/\lambda t. \tag{8}$$

Putting this in Eq. (7) and summing the result over r we obtain

$$p_3=\exp\,[-F_2t(h_2+h_3-h_2h_3) + F_2(1-h_2)h_3(1-e^{-\lambda t})/\lambda]. \tag{9}$$

Finally, by Eqs. (4), (6) and (9),

$$p=\exp\,[-At-B(1-e^{-\lambda t})/\lambda], \tag{10}$$

where $A\equiv F_1h_1+F_2(h_2+h_3-h_2h_3)$; and
$B\equiv F_2h_3(2-h_2)$.

III. The Distribution of Intervals Between Counts

We now seek the probability P that no count will occur in an interval t, following an initial count at time zero. The initial count may be caused by a class I primary, a class II primary, or an activated atom. The probabilities of these three causes are F_1h_1/D, F_2h_2/D, and F_2h_3/D, where D is the sum of the numerators of these fractions. Let P_A, P_B, P_C denote the probabilities of no count in time t when the initial count is due to a class I primary, a class II primary, or an activated atom, respectively. Then

$$P=(F_1h_1P_A+F_2h_2P_B+F_2h_3P_C)/D. \tag{11}$$

P_A is identical with p, for the occurrence of a class I primary at time zero does not affect the probability that others will arrive in the interval $(0, t)$, or the stock of metastable atoms. P_B is computed in the same way as p, with one exception; the production of an activated atom at time zero changes the probability that no count will be produced by the activated atoms present just after time zero; therefore, to get P_B the factor p_2 occurring in p must be replaced by another, p_{B2}. The chance that the stock of activated atoms is j just after the initial count is the same as the chance that the stock is $j-1$ just before it. Therefore, in expression (5) we must replace S_j by S_{j-1}; summing over j from 1 to infinity, we find that

$$p_{B2}=[1-h_3(1-e^{-\lambda t})]p_2 \tag{12}$$

and

$$P_B=[1-h_3(1-e^{-\lambda t})]p. \tag{13}$$

Furthermore, the computation of P_C differs from that of p in only one way. Our knowledge that in the case before us the initial count was produced by decay of an activated atom alters the chance that there were j activated atoms *before* the initial count.

To obtain this chance, $S(j)_c$, we proceed as follows. Let $U_j(c)$ be the chance of a count due to an activated atom in the time element $(0, dt)$ when it is known that the stock of activated atoms was j *before* the count; and let $U(c)$ be the unconditional chance of a count due to an activated atom in this time element. Now $U(c)=\Sigma_jS_jU_j(c)$, and according to Bayes' theorem

$$S_jU_j(c)=U(c)S(j)_c. \tag{14}$$

Also $U_j(c)=h_3j\lambda dt$, and using Eq. (2) we finally get

$$S(j)_c=S_{j-1}. \tag{15}$$

That is, S_{j-1} is the chance that the stock was j *before* the initial count, so it is also the chance that the stock is $j-1$ just after the count. Therefore the computation of P_C is *identical* with that of p, and substituting the values of P_A, P_B and P_C into (11) we obtain

$$P=p[1-F_2h_2h_3(1-e^{-\lambda t})]/D. \tag{16}$$

By somewhat similar methods it is possible to deal with a detector which has a constant recovery time τ. If $t\gg\tau$, and $f\ll 1/\tau$,

$$P'=\{\exp\,[-A(t-\tau)-B(1-e^{-\lambda(t-\tau)})/\lambda]\} \times[1-F_2h_2h_3(e^{-\lambda\tau}-e^{-\lambda t})]/D. \tag{17}$$

Shape of the Beta-Ray Distribution Curve of Radium E at High Energies

LAWRENCE M. LANGER AND MARTIN D. WHITAKER
Department of Physics, New York University, University Heights, New York, N. Y.

(Received March 15, 1937)

The beta-ray spectrum of radium E was measured by means of a magnetic spectrometer and coincident counters with special emphasis on the shape of the curve in the neighborhood of the end-point. Because of the strong source available, and the low background of the detecting mechanism, it was possible to obtain significant data much closer to the end-point than has been done heretofore. The distribution was found to end, without a tail, at $H\rho = 5330$ oersted-cm, or 1.17×10^6 electron volts. The Fermi and K-U plots of the experimental data do not give straight lines as predicted by the theory. Extrapolation of the straight part of the K-U plot gives an end-point 17 percent higher than that observed.

INTRODUCTION

SINCE the maximum energy of the beta-ray spectrum is considered, in the absence of gamma-radiation, to give the total energy of disintegration, it is of great importance to know how to determine this end-point. Experimental difficulties arise because the distribution curve approaches the energy axis gradually and, if the number of beta-particles near the end-point is not sufficiently great, the true effect may be masked by the natural background inherent in all detecting devices. Moreover, if suitable precautions are not taken, the distribution curve will have a spurious tail, due to scattered electrons, which approaches the axis asymptotically to much higher energies than the true end-point. In order to obviate these difficulties in detecting the maximum energy, it has been the practice of many experimenters to make use of the Konopinski and Uhlenbeck[1] modification of the Fermi[2] theory of beta-ray decay. In applying this theory, one extrapolates a straight line obtained from experimental data at lower energies, and gets the end-point from the intercept on the energy axis. This procedure involves the assumption that the application of the theory will give a linear relation all the way to the end-point. Recent work of Lyman[3] and Paxton[4] on the energy distribution of the electrons from Ra E and P^{32} has raised doubts as to the validity of this procedure and, indeed, raises the question as to whether the K-U theory gives a reliable description of the beta-ray process. Paxton, measuring the energy of beta-ray tracks in a cloud chamber, found an end-point for the spectrum of P^{32} at 6950 $H\rho$, which is considerably lower than the limit of 8200 $H\rho$ obtained by extrapolating the K-U curve. Lyman used a beta-ray spectrograph with single counter and obtained results on both Ra E and P^{32}. In both cases, the observed end-point was found to be less than that obtained by extrapolation of the K-U curve. The natural counting rate of the single counter used by Lyman was of the same order of magnitude as that due to beta-particles for points near the end-point. In fact, at the last measured point the natural rate was over twenty times as great as that due to the beta-particles, so that the points are considerably scattered. Since coincidence counting methods can be made to give a very low natural rate, it was thought worthwhile to try this method with the purpose of obtaining more accurate data near the end-point. Furthermore, previous work of Scott[5] had indicated an end-point at considerably higher energies than that given by Lyman. With the availability of a very strong source of Ra E, it seemed desirable to repeat the experiment.

APPARATUS

The magnetic spectrometer, with source and counter boxes in position, is shown in Fig. 1. All parts, except the lead gamma-ray absorber, are made of aluminum. The source and Geiger-

[1] E. J. Konopinski and G. E. Uhlenbeck, Phys. Rev. **48**, 7 (1935).
[2] E. Fermi, Zeits. f. Physik **88**, 161 (1934).
[3] E. M. Lyman, Phys. Rev. **51**, 1 (1937).
[4] H. C. Paxton, Phys. Rev. **51**, 170 (1937).
[5] F. A. Scott, Phys. Rev. **48**, 391 (1935).

Müller counters are contained in separate boxes, which fit into fixed positions in the spectrometer.

The radium E was deposited on the upper surface of a piece of thin sheet nickel 0.2 cm wide and 1.5 cm long. The source was placed in the position S and tilted so that its projection on the plane AB was 0.10 cm. The defining slit, AB, was 0.3 cm wide and 1.0 cm long. The perpendicular distance from the middle of the source to the plane AB was 1.50 cm. The radius of curvature of the instrument as measured from the center of the source to the center of the slit, CD, was 9.99 cm.

The beta-particles, bent by the magnetic field, pass through the openings in the scattering baffles, EF and GH, and enter the counter box through the slit, CD (0.05 cm wide), which is in the focal plane of the beam. The beta-particle beam, as defined by the slit, AB, is of the same width at the baffle positions as the openings EF and GH. The space between the side plates of the spectrometer is 2.54 cm; the length of all slits and baffles is 1.0 cm.

The spectrometer was placed between the cylindrical pole pieces of an electromagnet capable of supplying 1500 oersteds in the 3.5 cm gap. The radius of the pole faces was 15 cm and the spectrometer was mounted in such a way that the line between the slits AB and CD was on the diameter of the pole face. The magnetic field was measured by means of a flip coil and ballistic galvanometer which were calibrated with the help of a standard mutual inductance. The primary current in the inductance was measured by means of a precision potentiometer and standard resistance, and a curve plotted showing H as a function of the current in the magnet. The entire region of the magnetic field traversed by the electrons was found to be uniform to within 0.5 percent. Field readings were taken with the flip coil in position M and checked against values obtained from measurement of the magnet current taken simultaneously. Readings of both types, taken at the beginning and end of each observation, were found to agree to better than 1 percent. A further check was obtained by measuring the $H\rho$ value of the strong line of the radium B spectrum. The "head" of the line was observed at $H\rho = 1930$ in good agreement with the results of Ellis,[6] Scott,[7] and Rogers.[8]

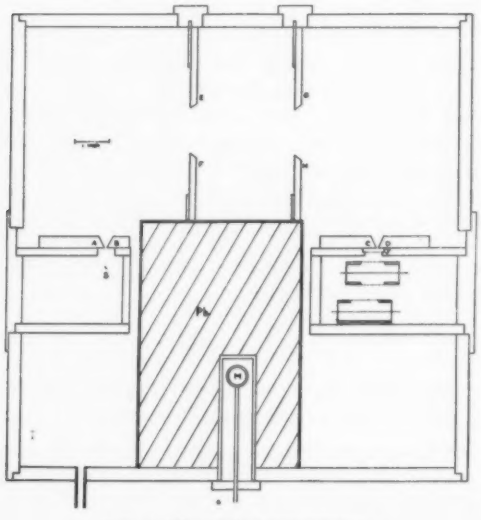

FIG. 1. Magnetic spectrometer.

The spectrometer is exhausted by a Cenco Hyvac pump which is kept in operation during an experiment. Thus, there is no material in the path of the electron beam until it reaches the (0.001") aluminum window "J" on the counter box. This box and the G-M tubes are shown to scale in Fig. 1. The entire box is filled with argon to a pressure of 6 cm of mercury. The aluminum counters are cut away and covered by thin aluminum foil (0.00025" thick) as shown by the dotted lines in the figure. The G-M tubes are rigidly mounted on the end of the box by means of hard rubber rods. Separate high potential leads and leads from the central wires are brought out of the box through hard rubber insulators.

The pulses from the two G-M tubes are amplified and coincidences selected by the circuit arrangement shown in Fig. 2. The amplifier was built for general utility and consequently was arranged so that it could be used as two separate amplifiers having the same or different outputs or as a coincidence selecting apparatus. The RC values of the several grid circuits are quickly adjustable for various types of work by replacing coupling condensers mounted so as to be readily

[6] C. D. Ellis, Proc. Roy. Soc. **143**, 352 (1934).
[7] F. A. Scott, Phys. Rev. **46**, 633 (1934).
[8] F. T. Rogers, Phys. Rev. **50**, 515 (1936).

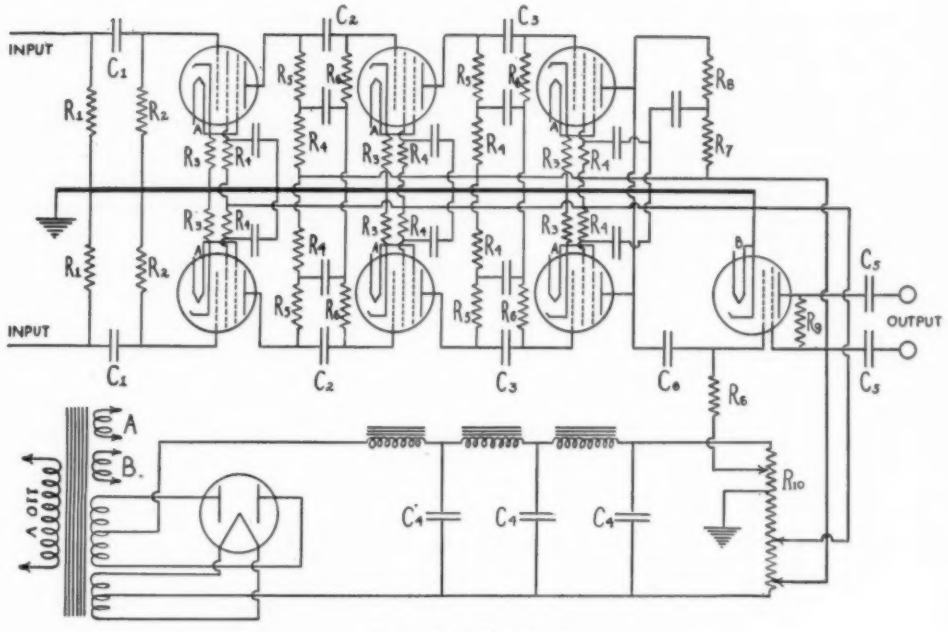

FIG. 2. Amplifier circuit.

$R_1 = 3.4 \times 10^{10}$ ohms
$R_2 = 10^7$
$R_3 = 2500$ ohms
$R_4 = 50{,}000$ ohms
$R_5 = 250{,}000$ ohms
$R_6 = 100{,}000$ ohms
$R_7 = 25{,}000$ ohms
$R_8 = 125{,}000$ ohms
$R_9 = 7000$ ohms
$R_{10} = 20{,}000$ ohms
$C_1 = 5 \times 10^{-11}$ farad
$C_2 = 3 \times 10^{-9}$ farad
$C_3 = 1.25 \times 10^{-10}$ farad
$C_4 = 8 \times 10^{-6}$ farad
$C_5 = 10^{-7}$ farad
$C_6 = 4.5 \times 10^{-10}$ farad

accessible. With the circuit constants used in this work and shown with Fig. 2, the amplification is great enough so that large pulses saturate the plate current in the second stage tubes and *all* the pulses up to counting rates of several thousand per minute produce plate current cut-off in the third stages. Therefore, the pulses fed to the grid of the selector tube are always of the same size so there is no chance of recording a large sized pulse from a single counter as a coincidence or of missing the coincidence of two small pulses. At the same time, the duration of the pulses on the selector tube grid is short enough so that chance coincidences are rare even at high single tube counting rates. A voltage stabilizer of the type designed by Evans[9] supplied the high potential for the G-M tubes. The apparatus was monitored, at all times, by a cathode-ray oscillograph. The counts were recorded on a thyratron "scale of four" counter.

[9] R. D. Evans, Rev. Sci. Inst. **5**, 371 (1934).

PROCEDURE AND RESULTS

1. High energy particles

In some preliminary experiments it was found that there were some counts for $H\rho$ values as high as 6500. In view of the fact that these counts might be due to particles scattered into the counters from lower energy regions we performed two sets of experiments designed to test this possibility. In the first set, certain adjustments were made on the baffles, *EF* and *GH*. It was found that, when the baffle, *EF*, was adjusted so as to pass a beam of electrons defined by the slit, *AB*, and having the desired energy, the high energy tail practically disappeared. On the other hand, if the baffle, *EF*, was adjusted to be wider than this beam, the high energy tail was much more pronounced. With proper adjustment of *EF*, it was found that the adjustment of *GH* produced no significant effect. This experiment lends weight to the view that the high energy tail is due to scattering.

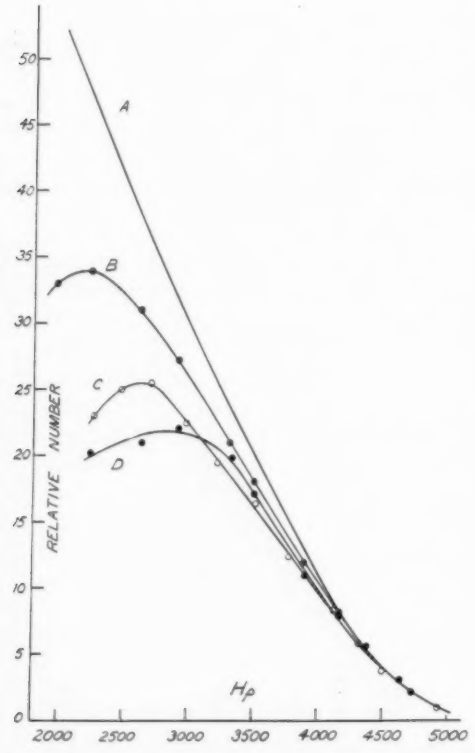

FIG. 3. Beta-ray spectrum of radium E. Curves *B* and *D* were obtained with an Al window 0.001″ thick; curve *C* with an additional Al; foil 0.001″ thick. Curves *B* and *C* are for data taken with a single counter; curve *D* is for coincident counter data. Curve *A* shows the distribution corrected to zero window thickness.

In order to test this possibility further, a special counter box was constructed in which the wall of the second counter had a thickness of 0.0625″ of aluminum. The combined thickness of the foils (0.439 g/cm²) should, according to the data of Varder,[10] stop all particles of energy less than $H\rho = 5025$. These counters had an unusually low coincident background of 0.17 count per minute, so that, with the strong source used, a rather weak effect should have been detectable. The data in Table I shows that no counts above the background were obtained for values of $H\rho$ greater than 5330. The decrease in the counting rate below $H\rho = 5200$ is due to the presence of the thick counter wall.

It would appear, therefore, from these experiments, that the high energy particles reported by Scott[5] and others are probably due to scattering.

[10] Varder, Phil. Mag. **29**, 726 (1915).

2. Shape of the distribution curve

The investigation of the distribution curve near the end-point was carried out using the thin wall counter system described in an earlier section of this paper. The data was taken starting at the high energy end of the spectrum and working toward lower energies. In order to preclude the possibility that the recording mechanism might not follow at high counting rates, no points were taken for which the rate was greater than 1000 per minute. The data was then checked by taking points, between those already taken, for increasing energies. This procedure was repeated from time to time relying on the decay of the source for extension of the data toward lower energies. A sufficient overlapping of the energy regions was obtained to rule out long time fluctuations.

Both single counter and coincident counter data were used in determining the complete shape of the curve (to 1900 $H\rho$). The coincident observations and those with the single counter were taken for each setting of $H\rho$. The single counter used was the one nearest the slit, *CD*. By introducing an extra thickness of 0.001″ of aluminum, data was obtained from which the curves could be corrected to zero window thickness. The results are shown in Fig. 3. All ordinates are expressed in relative number divided by H.

The high energy end of the spectrum is shown drawn to a larger scale in Fig. 4. An idea of the accuracy of the ordinates in the neighborhood of the end-point is best obtained from a sample of the uncorrected data from one set of observations. At $H\rho = 5085$, 1840 particles were counted at a rate of 46.0 per minute; at $H\rho = 5265$, 424 particles at 6.1 per minute; at $H\rho = 5295$, 278 particles

TABLE I. *Counts for beta-particles near the high energy limit.*

$H\rho$	Counts/min.
5160	2.0 ±0.45
5200	3.1 ±0.32
5270	0.80±0.12
5310	0.66±0.07
5330	0.23±0.09
5370	0.17±0.04
5430	0.14±0.04
7810	0.17±0.05
8230	0.15±0.05

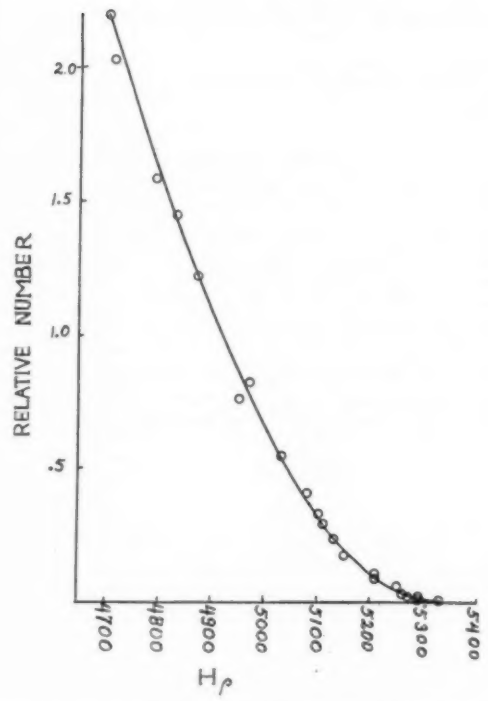

FIG. 4. Ra E spectrum showing distribution near the end-point.

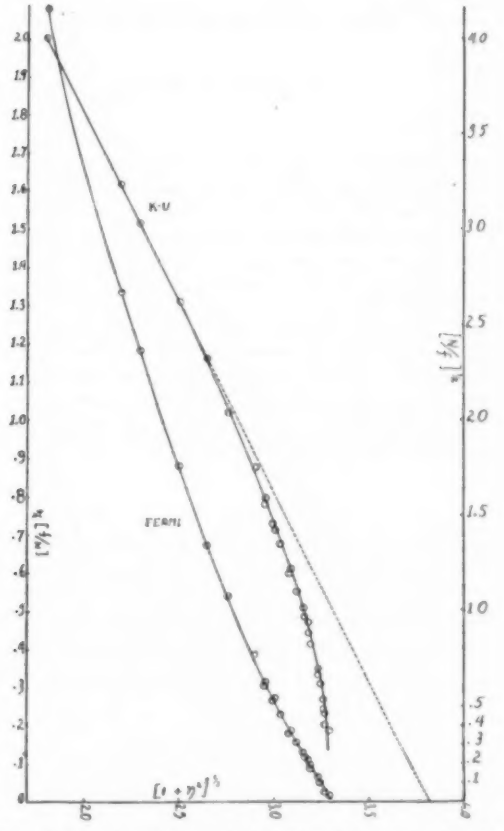

FIG. 5. Fermi and Konopinski-Uhlenbeck curves for the Ra E spectrum.

at a rate of 4.6 per minute. The background was 2.5 counts per minute. The value obtained for the end-point of the radium E spectrum is $H\rho = 5330 \pm 70$ oersteds$-$cm, or 1.17 Mev. This agrees with the value recently obtained by Lyman.[3]

Fermi and K-U plots of the experimental data near the end-point are shown in Fig. 5 in which $(N/f)^{1/\alpha}$ is plotted against $(1+\eta^2)^{\frac{1}{2}}$ where $f=(\eta+0.355\eta^2)$, $\eta = H\rho/1700$, $\alpha = 2, 4$ for Fermi or K-U, respectively. The extrapolated K-U end-point comes at 6250 $H\rho$ whereas the observed end-point is 5330 $H\rho$. The K-U plot was made without considering the fact that radium E is a forbidden transition. A correction to the theory has been worked out by Lamb[3] and Pollard[11] from which it appears that the extrapolated end-point is brought into somewhat better although not complete accord with the experimental value.

We are indebted to Dr. L. R. Hafstad, Professor J. A. Bearden, and Dr. R. W. Kanne for preparing the radium E source. We also desire to express our thanks to Professor A. C. G. Mitchell for many helpful suggestions and his interest in the work.

[11] W. G. Pollard, Bull. Am. Phys. Soc. February meeting, Abs. 1.

Effect of Galactic Rotation Upon the Intensity of Cosmic Radiation

W. F. G. SWANN
Bartol Research Foundation of the Franklin Institute, Swarthmore, Pennsylvania

(Received March 10, 1937)

The paper presents a mathematical theory of dependence of cosmic-ray intensity upon galactic rotation, discussed by A. H. Compton and I. A. Getting. The formulae obtained by Compton and Getting for neutral particles are deduced by processes closely analogous to the processes used by those authors. It is shown, however, that the extension to charged particles may be formulated in a manner which makes use of the modified form of Liouville's dynamical theorem which has been found successful in other cosmic-ray problems, and the result is that the intensity at any point on the earth's surface is expressed in simple manner in terms of the direction of the orbit of the charged particle when traced back to infinity. Attention is called to the modification demanded by the theory of relativity in the intuitive picture of the phenomenon. The simple naïve picture of what happens visions a stream of charged particles with the earth moving, for example, towards them. In this picture there is the alteration of relative velocity produced by the earth's motion, which is responsible for the change of intensity. The theory of relativity demands, however, a picture in which there is no alteration of relative velocity by the earth's motion, but where there is a change of particle density which conspires to produce a result the equivalent of that produced by change of relative velocity in the simple picture.

THE earth's rapid motion in space, resulting from the rotation of our galaxy, results in variations in cosmic-ray intensity fore and aft of the earth's motion. This effect has been discussed, and calculations of its magnitude have been made by A. H. Compton and I. A. Getting[1] and by A. H. Compton.[2]

The theory of the matter assumes a different form for neutral particles than for charged particles; and the calculation in the latter case is recognized as complicated and is not given explicitly. The purpose of the present paper is to formulate the solution for charged particles in a manner which is precise and general, although it is true that the actual calculation of the effect involves knowledge of the orbits concerned. A secondary purpose of the paper is to call attention to certain features which may have a simplifying effect upon the picture of the whole problem. We shall not concern ourselves here with the effect of the atmosphere, which effect has been discussed in detail by A. H. Compton. We shall confine ourselves to the intensity of the primary particles entering the atmosphere.

Our problem is the determination at a point O on the surface of the earth, of the cosmic-ray intensity in a direction towards O, parallel to a radius vector inclined at an angle θ to the velocity v of the point O, which velocity v shall be taken in the positive direction of the axis of x. The intensity may, of course, also be a function of the azimuth φ, and, in the direction concerned is defined as I, where

$$dN = I \sin\theta d\theta d\varphi ds, \tag{1}$$

where dN is the number of particles falling per second within the limits of the solid angle $\sin\theta d\theta d\varphi$ upon the element of area ds drawn perpendicular to the radius vector. We shall use dashed letters to denote measurements made in the system moving with velocity v; and, it will, therefore, be in terms of dashed letters that the quantity we desire will in general be expressed.

Now, in the case of a charged particle moving in a pure magnetic field (i.e., without electric field) it follows from a theorem analogous to Liouville's dynamical theorem, that the intensity in the above-defined sense is constant along a dynamical path when measured, of course, in the direction of that path, or rather in the opposite direction.[3] This result is true in a system of axes fixed to the moving earth on account of the invariance of the Hamiltonian equations which

[1] A. H. Compton and I. A. Getting, Phys. Rev. **47**, 817 (1935).
[2] A. H. Compton, Phys. Rev. **50**, 1119 (1936).
[3] This result was first stated by G. Lemaitre and M. S. Vallarta, Phys. Rev. **43**, 87 (1933). Their proof suffered from certain logical imperfections which really restricted it to a case where the magnetic field was absent. The proof developed subsequently by the present writer (W. F. G. Swann, Phys. Rev. **44**, 224 (1933)) removed these defects, and established, in place of Liouville's theorem, a sort of corollary of the general form of that theorem, but with the noncanonical variables required by the cosmic-ray problem.

control the dynamics of the problem.[4] Thus, in seeking the intensity in a given direction at a point on the earth's surface, we must trace the orbit back to infinity. The intensity we desire will be the intensity along this orbit at infinity estimated in the moving system; but we must obtain it through the relativity transformation as applied to a condition in which, in the fixed set of axes, the intensity is constant for all positions and directions at infinity. The conclusion reached is true for charged or uncharged particles, the only difference being that, for uncharged particles the direction of the orbit at the point O is the same as at infinity, so that the intensity at O is determined by the direction at O, while for charged particles it is determined by the different direction which the orbit assumes at infinity.

Let us then discuss the intensity in the direction defined by θ', φ', at infinity in the moving system S'.

The number of particles dN, in addition to being given by (1) is also given by

$$dN = u\delta\rho ds, \tag{2}$$

where u is the velocity in S of the particles which are moving parallel to the direction defined by θ, φ, and $\delta\rho$ is the contribution to the density in S by those particles which travel within the limits $d\theta d\varphi$. Thus, from (1) and (2)

$$I = u\delta\rho/\sin\theta d\theta d\varphi\text{; and, of course,}$$
$$I' = u'\delta\rho'/\sin\theta' d\theta' d\varphi'. \tag{3}$$

Now if $\epsilon \equiv (1-v^2/c^2)^{-\frac{1}{2}}$; $k \equiv (1-u^2/c^2)^{-\frac{1}{2}}$; $\beta = v/c$ and if $E(=m_0 k)$ refers to the total energy of the particle, we have, as 4−vectors, (ku_x, ku_y, ku_z, kic) and $(u_x\delta\rho, u_y\delta\rho, u_z\delta\rho, ic\delta\rho)$.

From the above relations, combined with the fact that $\sin^2\theta = (u_y^2+u_z^2)/(u_x^2+u_y^2+u_z^2)$, and with the assumption that $|u|$ is nearly equal to c, the velocity of light, and that quantities involving β^2 and higher powers are negligible, it readily follows that

$$\sin\theta' d\theta' = (1-\beta\cos\theta')^2 \sin\theta d\theta; \quad d\varphi' = d\varphi;$$
$$u'\delta\rho' = u\delta\rho/(1-\beta\cos\theta').$$

Hence, as given by Compton and Getting,

$$I' = I/(1-\beta\cos\theta')^3. \tag{4}$$

In accordance with the above remarks, therefore, if we desire the intensity in a certain direction at the point O, just outside the atmosphere, we must trace the trajectory which ends in that direction back to infinity, and there find the angle θ', which it makes with the direction of the earth's motion. With this value of θ', the intensity I' is given by (4) in terms of the standard uniform intensity I applicable for all directions at infinity in a stationary system. This statement is true for uncharged particles as well as for charged particles. For the former, however, the trajectories are straight and θ' is the same for the trajectory at infinity as it is at the earth's surface.

A further matter operative in the case of charged particles concerns the alteration of the numbers of particles which can reach the earth in opposition to the earth's magnetic influence. From the relativistic transformation for the energy we have $E' = \epsilon E(1-vu_x/c)$, or, neglecting v^2/c^2, and recognizing that $|u|$ and θ are very nearly equal to c, and θ' respectively, we have

$$E' = E(1+\beta\cos\theta'). \tag{5}$$

Now if $F(E)dE$ is the fraction of the rays which have energies between E and $E+dE$ at infinity in the resting system, the entering intensity involves an integral of $F(E)dE$ to infinity from a lower limit E_θ, characteristic of the magnetic latitude. In the moving system, the integral will be from $E' = E_\theta$ to infinity, and therefore, from $E_\theta/(1+\beta\cos\theta')$ to infinity. Thus, the range of integration is increased by $\beta E_\theta \cos\theta'$ (or, of course, reduced if $\cos\theta'$ is negative), and the intensity is altered by the fraction $\beta E_\theta F(E_\theta)\cos\theta'$ of its value.

Here E is characterized by the angle between v and the reversed path of the trajectory at O, while θ' is characterized by the angle between v and the reversed path of the same trajectory at infinity. In the case where $F(E)$ is of the form A/E^n, the above fraction becomes $(n-1)\beta\cos\theta'$, and for n of the order 2 or 3,[5] becomes comparable with the effects of the other kinds already discussed.

[4] As a matter of fact, the result would not be true for charged particles in a stationary set of axes for the case of a moving earth, since, in that set of axes, the moving magnetized earth would produce an electric field which was the equivalent of an electric doublet. This electric field would result in changes of energy along the dynamical path. In fact, while the energy is constant along a dynamical path when measured in one set of axes, it is not constant along that path when measured in another relatively moving set of axes.

[5] See W. F. G. Swann, Phys. Rev. **50**, 1103 (1936).

Reverting to the more obvious of the foregoing effects, that concerned with the impact of noncharged particles upon a moving earth, it is perhaps worthwhile to clarify one point which may cause difficulty if not appreciated, although it is, of course, properly taken care of in the foregoing discussion, and applies to charged particles as well. Suppose we confine our attention to the simple case where a plane perpendicular to the direction of the axis of x is moving along the positive direction of that axis with velocity v, and where parallel rays of velocity u are falling vertically upon it. The most naïve view of the phenomenon represents a picture in which the number of rays received per second per square centimeter of the plane is $\rho(u-v)$, when the plane is moving with velocity v, and ρu when it is stationary, so that the ratio is $(u-v)/u$. In this naïve picture, the relative velocity is altered by the motion from u to $u-v$, and ρ is unaltered. However, when u is nearly equal to c, the velocity of light, it follows from the theory of relativity that the relative velocity is not appreciably altered by the translatory velocity v of the system. In fact, observers in all systems specified by constant velocities v measure the same value for the velocity of a particle when in any one of them that velocity is equal to c. This is true whether the particle is an ordinary particle or a light particle. Our naïve expression $\rho(u-v)$ is now replaced by $\rho' u$; but, ρ' is no longer equal to ρ, but to $\epsilon\rho(1-uv/c^2)$ which, for u nearly equal to c is $\rho(1-v/c)=\rho(1-v/u)$. Hence $\rho' u=\rho(u-v)$ as for the naïve case, and the ratio of this quantity to that for a stationary plane is, as before, $(u-v)/u$. Now, however, the alteration is entirely due to a change in the apparent density resulting from the motion, whereas in the naïve picture it was caused by a change in relative velocity without change of density.

MAY 1, 1937 PHYSICAL REVIEW VOLUME 51

The Auger Effect in Germanium

MICHAEL FERENCE, JR.
Ryerson Physical Laboratory, University of Chicago, Chicago, Illinois
(Received February 27, 1937)

Auger electrons ejected from the L and M levels of germanium are studied by means of a magnetic spectrograph in which the ordinary photographic plate is replaced by a small Geiger-Müller electron counter. The maximum energy of the Auger electrons arising from the $K-L^2$ transition is found to be 8590 ± 15 volts. The kinetic energies of ejected Auger electrons are computed from theoretical considerations and shown to agree well with those observed. An attempt is made to separate the band of electrons from the L shell into three groups and compare their intensities with theory, but is not entirely reliable because of too low resolving power of the spectrograph. A reliable estimate of the relative probability of transitions $K\rightarrow L^2$ and $K\rightarrow LM$ is made and found to be 100 : 31, which is to be compared with 100 : 58 calculated from the theory.

INTRODUCTION

IT has been known for some time that an atom ionized in the K shell may, on reorganization to the normal state, either emit fluorescence radiation or eject an Auger electron of definite energy.[1,2] Robinson and Cassie[3] in their determination of x-ray levels from electron spectra measured the energies of a number of these "fluorescence" or Auger electrons. They found the energies to be considerably lower than would be expected for electrons extracted from normal atoms. These investigators, however, made no particular attempt to study the structure of the Auger lines. This paper is a report on some studies of the Auger electrons ejected from germanium; the electrons were recorded by a Geiger-Müller ion counter of the design described by Van den Akker and Watson.[4]

[1] P. Auger, Comptes rendus **180**, 65 (1925); J. de phys. et rad. **6**, 205 (1926); Ann. de physique, Paris **6**, 183 (1926); Comptes rendus **182**, 773: 1215 (1926).
[2] M. de Broglie and J. Thibaud, Comptus rendus **180**, 179 (1925).
[3] H. Robinson and Cassie, Proc. Roy. Soc. **A113**, 282 (1928).
[4] Van den Akker and Watson, Phys. Rev. **31**, 1631 (1931).

Apparatus

In Fig. 1 is shown the horizontal section through the slits of the magnetic spectrograph used in this research. The spectrograph together with the solenoid for deflecting the photoelectrons is the one designed by Kretschmar[5] for his precision determination of e/m. The only modification made in the present work was the introduction of the Geiger-Müller tube in place of a photographic plate.

The defining slit S_1, through which the electrons passed, was 0.2 mm wide. The lead shield P served to keep any scattered x-rays from affecting the counter, while the aluminum baffles A prevented scattered electrons from entering the counter. The heavy lead well L absorbed the main x-ray beam after it had passed through the thin film F of germanium deposited on a strip of Cellophane. The entrance window to the counter W was a disk with a set of 14 holes, each 0.25 mm in diameter and arranged in a vertical line. A thin film of celluloid about 10^{-6} cm thick covered the holes of the small disk. It was necessary that this film be as thin as possible and still strong enough to withstand a difference in pressure of about 6 cm of mercury. A detailed description of the specialized form of Geiger tube used in this research and of its operation is given by Van den Akker.[6] The tube itself was earthed, while the anode was connected to a source of high potential.[7] The amplifying circuit was that described by Locher,[8] modified slightly by the introduction of a power tube between the thyratrons and the Cenco impulse counter.

The electron spectra studied in this paper were obtained when the primary x-rays of silver passing through a palladium filter were allowed to strike a barely visible film of germanium. One can obtain an indication of the amount of germanium on this Cellophane strip from the way in which the metal was deposited. A sheet of Cellophane 10 cm square was folded in two and placed about 20 cm above a tungsten coil containing the germanium. The direct beam of

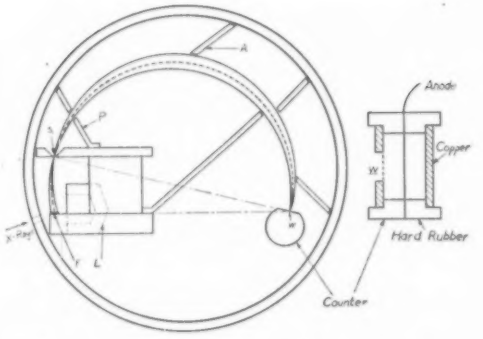

FIG. 1. Diagram of spectrograph with counter.

germanium was deposited on the bottom layer of Cellophane which was discarded. The top layer containing only the trace of germanium that had diffused around the Cellophane sheet was used in this experiment.

The x-rays were produced by a shielded filament, metal x-ray tube operated at 48 kilovolts and 20 milliamperes. By carefully aligning and adjusting the target of the x-ray tube it was possible to obtain counts as high as 320 per minute.

Experimental Procedure

The final data represented by the curves of Fig. 2 were obtained in the following manner. After the apparatus had reached temperature equilibrium, the magnetic field was adjusted for a point on the low velocity side of the L^2 curve and two-minute readings taken for every five milliampere increment in the field current until a point on the high velocity end of the LM curve was reached. This was repeated, starting, however, from a high velocity point of the LM curve. Each point thus represents the average of two trials. The vertical lines to the left of the L^2 curve show the deviation from the mean of the two sets of readings. The crosses below the L^2 curve represent counts obtained under approximately the same operating conditions as those on the curve except that the germanium film was replaced by a blank Cellophane strip.

In order to plot the readings on a linear volt scale as is done in Fig. 2, it is necessary to calibrate the spectrometer. This was done by calculating the energy of the Ag$K\alpha_1 \rightarrow K$(Ge) photo-

[5] G. G. Kretschmar, Phys. Rev. **43**, 417 (1933).
[6] Van den Akker, Rev. Sci. Inst. **1**, 672 (1930).
[7] T. H. Johnson and J. C. Street, J. Frank. Inst. **214**, 155 (1932).
[8] G. L. Locher, J. Frank. Inst. **216**, 553 (1933).

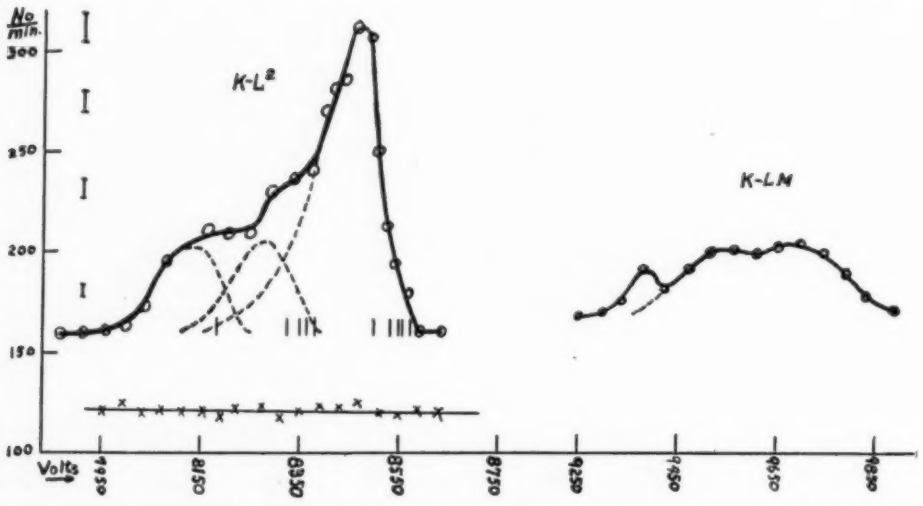

FIG. 2. Showing the Auger electrons due to the $K-L^2$ and $K—LM$ transitions. The vertical lines under the curve represent the position of the electrons of various kinetic energies as calculated from theory.

electrons with the following atomic constants. (Fig. 3.)

$$e/m = 1.769\times10^{7} \text{ e.m.u./g}$$
$$h = 6.545\times10^{-27} \text{ erg sec.}$$
$$c = 3\times10^{10} \text{ cm/sec.}$$
$$e = 4.774\times10^{-10} \text{ e.s.u.}$$
$$R = 109737 \text{ cm}^{-1}.$$

These are the same constants that were used by Robinson and Cassie.[8] The term values of germanium listed in Table I are taken directly from Siegbahn's book.[9] The constant of the solenoid, 11.434 oersteds per ampere, was that determined by Kretschmar.[5]

Discussion of Results

To facilitate the discussion of the results and the interpretation of the above curves recourse will be had to the purely qualitative x-ray energy diagram shown in Fig. 4. The L^2 levels (designated here as Auger levels) arise from the configurations

$$1s^2\left\{\begin{matrix}2s^0 2p^6\\ 2s^1 2p^5\\ 2s^2 2p^4\end{matrix}\right\}3s^2 3p^6 3d^{10} 4s^2 4p^2,$$

while the very large number of LM levels arise from the many configurations possible when an L and M electron are missing.

When an atom is ionized in the K shell, it may find itself in the state $1sK$ with a definite probability proportional to the fourth power of the atomic number[10] for a radiative transition to the $L_{II}L_{III}$ levels, giving rise to the $K\alpha_{12}$ lines of germanium. On the other hand because of the coupling between the discrete level $1sK$ and the continuum of the same energy, say $1s^2 2s^0 Es$

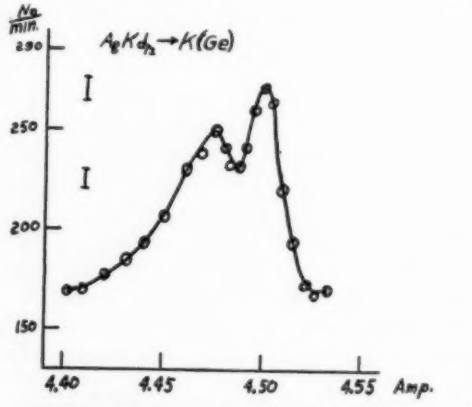

FIG. 3. Showing the two peaks of the K photoelectrons of germanium due to the silver $K\alpha_{12}$

[8] Siegbahn, *Specktroskopie der Röntgenstrahlen* (Julius Springer, 1931).

[10] G. Wentzel, Zeits. f. Physik **43**, 524 (1927).

where $E=K-L^2$, there is a probability that the ionized atom will undergo a radiationless or Auger transition to the level in the continuum, with the expulsion of an electron of energy $K-L^2$.

The electrons arising from the $K-L^2$ and $K-LM$ transitions are the ones represented by the two curves of Fig. 2. A measurement of the high velocity edge of the L^2 band thus fixes the lower limit of the L^2 Auger levels. The maximum energy of the electrons ejected from these levels was found to be 8590 ± 15 volts.

Any attempt to predict from theoretical considerations the kinetic energies of Auger electrons involves the estimation of the energy levels of an atom which has lost two electrons from inner shells. Accurate estimates of such levels in sodium have been made by Kennard and Ramberg[11] because of the connection of these levels with the satellites of the x-ray diagram lines. Because of the low resolving power of the β-ray spectrograph used in the present work, an estimate of the accuracy of that of Kennard and Ramberg seems unnecessary, and a comparatively rough method, with the use of Slater's[12] system of screening constants, has been used. By this means the *excess* energy required to remove an L electron when one L electron is already missing has been obtained. In Table II are summarized the numerical details of the calculation of the energy of the normal germanium atom. Table III gives the energies of the germanium atom in different states of excitation.

If E_1 is the energy of the normal atom, E_2 the energy of the atom with one L electron missing, and E_3 with two L electrons missing, then $E_L=E_1-E_2$ is the energy required to remove one L electron and $E_L'=E_1-E_3-E_L$ is the energy

TABLE I. *Germanium term values.*

TERM	ν/R	VOLTS
K	817.6	11066
L_{I}	103.9	1406
L_{II}	91.6	1240
L_{III}	89.3	1209
M_{I}	12.9	175
$M_{\text{II, III}}$	8.8	119
$M_{\text{IV, V}}$	1.8	24

[11] Kennard and Ramberg, Phys. Rev. **46**, 1034, 1040 (1934).
[12] J. C. Slater, Phys. Rev. **36**, 57 (1930).

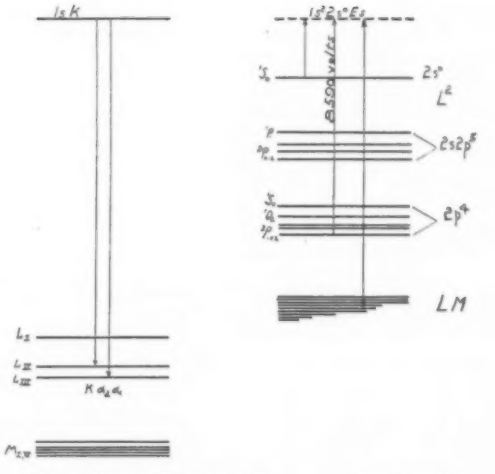

Normal x-ray levels Ge (32) Auger levels

FIG. 4. Some of the more important Auger levels in germanium.

required to remove the second L electron. The *excess* energy, therefore, required to pull out an L electron when one L electron is already missing is $(E_L'-E_L)=2E_2-E_1-E_3=5.3$ Rydberg units or 72 volts. From the empirical x-ray data of Table I, one finds the energy of the lowest L^2 level to be $2(1209)+72=2490$ volts, and the maximum energy of the electrons, given by $K-L^2$, to be $11066-2490=8576$ volts. The agreement with the observed value is satisfactory.

If we confine our attention to the levels arising from a doubly ionized L shell, their locations and relative energies can be predicted with some confidence. From ordinary spectroscopic theory, the following J values (total angular momenta) are known to arise from a doubly ionized L shell.

Configuration	J's
$2s^02p^6$	0
$2s^12p^5$	0, 1, 1, 2
$2s^22p^4$	0, 0, 1, 2, 2

The relative spacings of these levels will depend on the coupling, or ratio of the exchange energy to the spin-orbit energy in the various configurations.

It is convenient to locate the levels which would arise from extreme *jj* coupling, and then to discuss the deviations from these hypothetical

TABLE II. *Showing the details of the calculation of the energy in Rydberg units of the normal germanium atom.*

ELECTRON SHELLS	Z_{eff}	$\left(\frac{Z_{eff}}{n}\right)^2$
$1s^2$	31.70	2009.8
$2s^22p^6$	27.85	1551.3
$3s^23p^6$	20.85	382.7
$3d^{10}$	10.85	130.8
$4s^24p^2$	5.65	9.3
	$E_1=\sum_i (Z_{eff}/n_i)^2=-4083.9$	

TABLE III. *The energies of the germanium atom under various states of excitation.*

ELECTRON CONFIGURATIONS	ENERGIES IN RYDBERG UNITS	DESIGNATION
$1s^2\ 2s^22p^6\ 3s^23p^63d^{10}\ 4s^24p^2$	-4083.9	E_1
$1s^2\ 2s^22p^5\ 3s^23p^63d^{10}\ 4s^24p^2$	-3985.1	E_2
$1s^2\ 2s^22p^4\ 3s^23p^63d^{10}\ 4s^24p^2$	-3881.0	E_3

positions. In extreme *jj* coupling the six equivalent $2p$ electrons are subdivided into two groups, one of two electrons with $j=\frac{1}{2}$, and one of four electrons with $j=\frac{3}{2}$. The vacancies in this case may be shown in terms of vacancies in these Stoner[13] subgroups. Table IV shows how the positions of the extreme *jj* coupled levels may be estimated. The J values in column 2 of the table are those which would arise from the two equivalent, *jj* coupled, missing electrons, i.e., the $J=1,\ 2$ arising in the level whose energy is $L_{II}+L_{III}'$ are obtained from two equivalent p electrons one with $j=\frac{1}{2}$ and one with $j=\frac{3}{2}$. The primed symbols in column 3 of the table mean

$$L_I'=L_I+72, \text{ etc.}$$

It is assumed that this 72 volt excess applies to all the primed levels. The calculated levels in column 4 of the table are obtained from Table I.

If the coupling were Russell-Saunders, the levels would be ^3P, ^1D and ^1S arising from $2s^22p^4$, ^1P and ^3P from $2s^12p^5$, and ^1S from $2s^02p^6$. Kennard and Ramberg[11] have pointed out that the equations of Goudsmit[14] and Laporte and Inglis[15] may be used to locate these levels in Russell-Saunders or any intermediate coupling. They have also computed the ratio of the exchange energy to the spin-orbit energy in these configurations in Na(11), Cl(17), K(19) and Cu(29). The coupling type for Ge(32) has been estimated by extrapolation of their results. Thus the coupling factor X, which they found to be 3.052 Rydberg units for $2s^12p^5$ and 0.505 for $2s^22p^4$ in Cu(29), is estimated to be 3.22 and 0.564 for the analogous levels in germanium.

If we consider the J values arising from $2s^12p^5$, we find that the $J=0$ and $J=2$ of the ^3P are unique, that is, occur only once. Hence the total triplet width in the Russell-Saunders case is the width $(L_I+L_{II}')-(L_I+L_{III}')$ of the hypothetical *jj* coupled case. To the approximation in which we are working, this is merely the spin doublet separation of the singly ionized L shell. If we write the inverted triplet separations in the conventional form

$$\Gamma(J)=-\tfrac{1}{2}A\{J(J+1)-L(L+1)-S(S+1)\}$$

$\Gamma(J)$ represents the shift of a member of the triplet from the centroid of the triplet. From this equation we deduce that A, a convenient measure of the spin-orbit energy, is 1/3 of the total triplet width, and that the centroid lies below the $J=0$ level of the triplet at a distance $2A$. From the values of Tables I and IV we then deduce the following. For the case in discussion A is 10.3 volts. The centroid of the triplet arising from $1s^22p^4$ lies at 2511 volts. The centroid of the triplet arising from $1s^12p^5$ lies at 2697 volts.

The separations of the levels from these centroid positions are given by the following expressions:

$2s^12p^5$ $\quad \Gamma(2)=-A$

$\quad\quad\quad\ \Gamma(1)=A[(R+1)/2\pm((R-1)^2+8)^{\frac{1}{2}}]$

$\quad\quad\quad\ \Gamma(0)=2A$

$2s^22p^4$ $\quad \Gamma(1)=A$

$\quad\quad\quad\ \Gamma(0)=A[1+\frac{5}{2}R\pm\frac{1}{2}(25R^2-4(5R-9))^{\frac{1}{2}}]$

$\quad\quad\quad\ \Gamma(2)=A[R-\frac{1}{2}\pm\frac{1}{2}((2R-3)^2+16R)^{\frac{1}{2}}]$.

TABLE IV. *Levels in germanium arising from doubly ionized L shells, assuming extreme jj coupling.*

CONFIGURATION	J's	ENERGY	VOLTS
$(2s^0)_{1/2}\ (2p^2)_{1/2}\ (2p^4)_{3/2}$	0	$L_I\ +L_I'$	2884
$(2s^1)_{1/2}\ (2p^1)_{1/2}\ (2p^4)_{3/2}$	0, 1	$L_I\ +L_{II}'$	2718
$(2s^1)_{1/2}\ (2p^2)_{1/2}\ (2p^3)_{3/2}$	1, 2	$L_I\ +L_{III}'$	2687
$(2s^2)_{1/2}\ (2p^0)_{1/2}\ (2p^4)_{3/2}$	0	$L_{II}+L_{II}'$	2552
$(2s^2)_{1/2}\ (2p^1)_{1/2}\ (2p^3)_{3/2}$	1, 2	$L_{II}+L_{III}'$	2521
$(2s^2)_{1/2}\ (2p^2)_{1/2}\ (2p^2)_{3/2}$	0, 2	$L_{III}+L_{III}'$	2490

[13] E. C. Stoner, Phil. Mag. **48**, 718 (1924); also J. D. Main-Smith, *Chemistry and Atomic Structure* (D. Van Nostrand, New York, 1924).

[14] S. Goudsmit, Phys. Rev. **35**, 1325 (1929).

[15] O. Laporte and D. R. Inglis, Phys. Rev. **35**, 1337 (1930).

In these expressions $R=X/A$. The A for germanium is 0.757 Rydberg units, hence the R's are 4.25 and 0.745. The results are shown in Table V. The Auger electron energies of column 4 of this table are obtained by subtracting the values of column (3) from 11,066, which is the energy of the K state in volts.

The positions of the lines computed in Table V are indicated in Fig. 2 which shows the experimental curve. It is seen that the calculated lines fall well within the region of the experimental curve.

TABLE V. *Estimated energies of L^2 levels and corresponding Auger electrons in germanium.*

CONFIGURATION	LEVEL	ENERGY	AUGER ELECTRON ENERGY
$2s^02p^6$	$^1S_0$	2884 volts	8182 volts
$2s^12p^5$	$^1P_1$	2746	8320
	$^3P_0$	2718	8348
	$^3P_1$	2702	8364
	$^3P_2$	2687	8379
$2s^22p^4$	$^1S_0$	2571	8495
	$^1D_2$	2543	8523
	$^3P_1$	2521	8545
	$^3P_0$	2512	8554
	$^3P_2$	2494	8572

RELATIVE INTENSITIES IN THE L^2 GROUP

The relative intensities of the Auger electron beams ejected from the L shell have been theoretically investigated by Burhop,[16] Massey and Burhop,[17] and Pincherle.[18] The computations of Massey and Burhop take into account the relativistic wave functions which are important for heavy elements. The calculations of Burhop and of Pincherle may be compared, since they are both nonrelativistic. Their results are as follows:

	$2s^02p^6$	$2s^12p^5$	$2s^22p^4$
Burhop	15	51	100
Pincherle	10	36	100

The headings of the columns are the final atomic states after the ejection of an Auger electron. It is seen that the theoretical predictions do not agree to better than 30 percent.

Any attempt to test these predictions from the experimental curve involves resolving it into component curves. In view of the small energy differences between the L^2 levels and the asymmetry of the electron line due to the geometry of the spectrometer[19] and the straggling of the electrons on the low velocity end of the spectrum, an unambiguous resolution into components was not possible with the present resolving power of the apparatus. However, one can effect a reasonable resolution by studying the low velocity side of the spectrum of the K photoelectrons of germanium ejected by the silver $K\alpha_{12}$ lines and arrive at an estimate of the shape of the various groups. The dotted curves of Fig. 2 are such an estimate. The ratios of the areas under the three curves are 100 : 26 : 26. Due to the lack of uniqueness in the treatment of the unresolved experimental curve it is doubtful if much confidence can be placed in these ratios. In order to study in more detail these lines, a new spectrograph of higher resolving power is being built.

RELATIVE INTENSITIES OF THE L^2 AND LM BANDS

In the work of Pincherle previously mentioned, the relative probabilities of $K\rightarrow L^2$ and $K\rightarrow LM$ transitions is computed, a value of 100 : 58 being obtained. This ratio should be given quite accurately by the experimental curves of Fig. 2. The ratio of the areas under the two curves is 100 : 31. The hump on the low velocity edge of the LM band was not included in this area because it was impossible to correlate it with any $K\rightarrow LM$ transition. If, however, it is included, the above experimental ratio becomes 100 : 34. Any possible correction for differences in scattering and absorption of the electrons would tend to increase the discrepancy between theory and experiment. It should be noted that in view of the extraordinary thinness of the germanium film any difference in absorption between the L^2 and LM electrons would be negligible.

In conclusion, the author wishes to express his appreciation to Professor S. K. Allison who suggested this problem and gave valuable advice during its completion.

[16] E. H. S. Burhop, Proc. Roy. Soc. Lond. **A148**, 272 (1935).
[17] H. S. W. Massey and E. H. S. Burhop, Proc. Roy. Soc. Lond. **A153**, 661 (1936).
[18] L. Pincherle, Nuovo Cimento **12**, 81 (1935).
[19] W. A. Wooster, Proc. Roy. Soc. Lond. **A114**, 729 (1927).

The Spectra of Phosphorus

Part II: The Spectra of Doubly, Triply and Quadruply Ionized Phosphorus (P III, P IV, P V). Additions and Corrections to P II

HOWARD A. ROBINSON
Mendenhall Laboratory of Physics, Ohio State University, Columbus, Ohio

(Received March 10, 1937)

Data taken from spectrograms using a vacuum spark containing red phosphorus supplemented by spectrograms previously described have enabled a complete revision and extension of the spectra of P III, P IV, and P V. Certain quintet terms in P II have also been located. In P III nineteen new terms have been found which classify fifty-nine lines. Six of these terms replace previous terms which have proved erroneous. The ionization potential is found to be 30.012 ± 0.003 volts. Tentative intercombinations between the doublet and quartet systems are given. In P IV twenty-three new terms have been found which classify fifty-one lines. Several intercombinations have been located between the singlet and triplet systems. The various series are badly perturbed. The ionization potential is 51.106 ± 0.013 volts. In P V fourteen new terms have been located which classify twenty lines. The series are very regular and give an ionization potential of 64.698 ± 0.003 volts. The previous data have been entirely revised in view of new measurements and complete term tables as well as complete lists of lines now classified in the Schumann region are given.

IN Part I[1] of this paper data obtained from spectrograms taken at the Massachusetts Institute of Technology on the two meter vacuum spectrograph designed by Compton and Boyce[2] and built with funds obtained from the Carnegie Institute of Washington were described. Those spectra were obtained by means of a Geissler tube discharge in phosphorus vapor. Since that time additional spectrograms using a hot spark discharge between Be electrodes containing red phosphorus have been obtained with a one-meter grazing incidence vacuum spectrograph located in Professor Siegbahn's laboratory in the Physical Institute at Uppsala, Sweden. In the region where the new and old spectrograms overlap further information has been obtained concerning the segregation of the various lines into the stage of ionization to which they belong. The Uppsala hot spark equipment gives virtually no lines due to P II and none which may be attributed to P I. P III is generally weak but P IV and P V are much enhanced while the optical spectra of the L shell have now been traced as far as the Li I spectrum, P XIII.[3] These higher spectra will be described in detail in the future. The new spectrograms have shown that several of the lines previously used to fix the tentative term designated as $1_2{}^\circ$ in P II are in reality P III or P IV. This term which was listed tentatively is therefore not real and should be deleted from the P II term table. The tentative $3d^3F$ and ^1F terms must likewise be withdrawn as several lines which gave rise to them have now been found to fit other assignments. The line 4814.2A was included in the P II classification through an error and should also be deleted.

It is furthermore possible to classify three lines to give four new quintet terms in P II listed in Table I. The $3s3p^3\ {}^5S - 3s3p^2 4s\ {}^5P$ transitions apparently are partially blended with other lines and will not be added at this time. The absolute value of the $3s3p^3\ {}^5S$ may be estimated at 106,100 cm^{-1} by assuming a Rydberg denominator of 2.80 for the $3s3p^2 3d\ {}^5P_{5/2}$ (the limit is

TABLE I. *Ultraviolet quintet transitions in P II.*

INT.	λ (vac.)	ν (cm^{-1})	CLASSIFICATION	
1	927.771	107,785.2	$3s3p^2\ {}^5S^\circ - 3s3p^2 \cdot 3d\ {}^5P_{1/2}$	
1	928.550	107,694.7	${}^5S^\circ -$	${}^5P_{3/2}$
1	929.642	107,568.2	${}^5S^\circ -$	${}^5P_{5/2}$
$3s3p^3\ {}^5S^\circ_{3/2}$	106,100.0	$3s3p^2 \cdot 3d\ {}^5P_{1/2} - 1,685.2$		
				-90.5
		${}^5P_{3/2} - 1,594.7$		
				-126.5
		${}^5P_{5/2} - 1,468.2$		

[1] H. A. Robinson, Phys. Rev. **49**, 297 (1935).
[2] K. T. Compton and J. C. Boyce, Rev. Sci. Inst. **5**, 218 (1934).
[3] These data were briefly presented to the American Physical society at Atlantic City in December, 1936 by the author.

$sp^2\ ^4P_{5/2}$ of P III). The separation of these terms is calculated to be -89.1 cm^{-1} and -125.1 cm^{-1} if we use the Goudsmit and Humphreys' equations.[4]

Doubly Ionized Phosphorus P III

The spectrum of P III has been treated by Bowen and Millikan[5-7] and Saltmarsh[8] in the Schumann and visible regions, respectively. The classifications due to Bowen have been confirmed and extended; several of the terms due to Miss Saltmarsh must be rejected. These terms are the s^26s and $s^27s\ ^2S$, the $s^25p\ ^2P$ and the s^25d and $s^26d\ ^2D$. These terms were found by estimation from the quantum defects and were tied to the lower terms by two lines purporting to be the $s^24p\ ^2P-s^25d\ ^2D$ transitions. On the basis of the new measurements the $4p\ ^2P$ separation as given by this pair of lines was incorrect by 10 cm^{-1} an error very much greater than the accuracy of the present measurements. The $s^25p\ ^2P-s^26s\ ^2S$ transitions are furthermore necessarily P II lines[9] and were so classified in Part I (λ6043.45 and 6024.14). Certain other of the transitions involve lines which are coincident with lines in the argon spectrum. Since this element is an impurity in Geuter's[10] list these other transitions may likewise be open to question. It has furthermore been possible to extend these two series using only lines which may definitely be attributed to P III in both the visible and Schumann regions and to completely tie them in with the rest of the terms without the ambiguities arising from the previous classification.

While most of the new terms found in this analysis are doublets certain additions have been possible in the quartet system. These terms arise from the $3s3p4f$ configuration. It has not been possible to find the complete triad of ^4DFG terms predicted by the Hund theory mainly because of the inability to completely determine several of the quartets arising from the $sp\cdot p$ and $sp\cdot d$ configurations.

Extra terms can be found which arise mainly from the displaced doublet system coming from configurations of the $sp\cdot x$ type. A very intense search for these terms has revealed a number of dubious sets which do not combine among themselves as well as one might expect. The term listed as $^21_{3/2}{}^\circ$ may be either the $sp\cdot d\ ^2P_{3/2}$ or the $sp\cdot d\ ^2D_{3/2}$. These further identifications will not be published now pending further investigation in the visible.

The intercombinations given must be considered as tentative classifications. They are consistent with regard to position and intensity with the same transitions in Al I[11] and with certain new classifications in P IV. This latter point is discussed in detail in the following section of this paper. In view of the latest results on the analogous spectrum of N III[12] further intercombinations may be expected among the $sp\cdot 4f$ and $sp\cdot 5g$ doublets and quartets. Rydberg denominators for the doublet system are listed in Table II. The limit has been set by using the g series. The irregularity in the $6g\ ^2G$ is analogous to a similar irregularity in N III. The new classifications comprise fifty-nine lines which locate nineteen new terms. These are listed in Table III and Table IV, respectively. The ionization potential works out to be 30.012 ± 0.003 electron volts.

Table II. *Rydberg denominators in P III. Terms to $3s^2\ ^1S_0$ in P IV.*

Total Quantum Number	$3s^2\cdot ns\ ^2S$	$np\ ^2P_{3/2}$	$nd\ ^2D$	$nf\ ^2F$	$ng\ ^2G$
$n=3$		2.0600	2.7952		
4	2.8058	3.2804	3.7333	3.9089	
5	3.8323	4.4158	4.8010	4.9453	4.9999
6	4.8385		5.8050	5.9510	6.0009
7					6.9995

Triply Ionized Phosphorus P IV

The original classification of this spectrum has been given by Bowen, Millikan[7, 5] and others.[8] In the original Geissler tube exposures this spectrum was fairly weak. The Uppsala spectrograms above 1000A are also of less intensity than

[4] S. Goudsmit and C. J. Humphreys, Phys. Rev. **31**, 960 (1923).
[5] R. A. Millikan and I. S. Bowen, Phys. Rev. **25**, 600 (1925).
[6] I. S. Bowen, Phys. Rev. **31**, 34 (1928).
[7] I. S. Bowen, Phys. Rev. **39**, 8 (1932).
[8] M. O. Saltmarsh, Proc. Roy. Soc. **A108**, 332 (1925).
[9] Desjardin, Can. J. Research **7**, 556 (1928).
[10] P. Geuter, Zeit. f. wiss. Phot. **5**, 1 (1907); (all phosphorus lines in this paper above 2500A taken from this paper except as otherwise noted).
[11] F. Paschen, Ann d. Physik **71**, 537 (1923); R. A. Sawyer and F. Paschen, Ann. d. Physik **84**, 1 (1927).
[12] B. Edlén, Zeits. f. Physik **98**, 561 (1936).

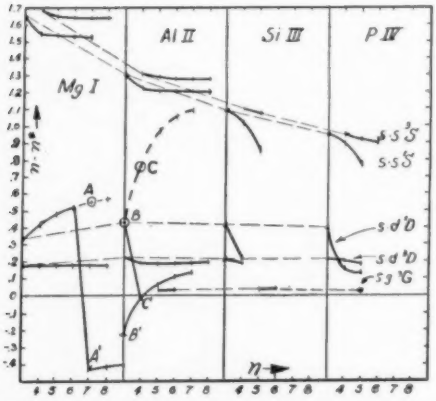

FIG. 1. $n-n^*$ *vs.* n for the s, d and g series of the Mg I-like isoelectronic sequence. The ^1D series is badly perturbed by the $p^2\,{}^1D_2$ term which has inserted itself into the series. The dotted extensions give the series as in Bacher and Goudsmit. The perturbing term according to Shenstone and Russell† is the one at A and B (or C). Removing this term the quantum defects continue from A' and B' (or C'). The singlet then lies above the triplet as would be expected.

those below this limit due to the optical properties of the grazing incidence spectrograph. As a result certain lines (marked B) in Table VII are taken from Bowen who was able to measure them with much greater accuracy than has been possible in this investigation. The group at 656A is badly mixed up with higher orders of strong oxygen lines and has also been taken from Bowen's work.

P IV is a Mg I-like spectrum having $2p^6 \cdot 3s^2\,{}^1S_0$ as a ground state. Spectra of this type are notorious in giving series which are badly perturbed due to interactions between terms going to the $2p^6 3s\,{}^2S$ limit and terms going to the $2p^6 3p\,{}^2P$ limit in P V. These perturbations are still apparent in this case as may be recognized from the irregularities in the Edlén-type diagrams given in Figs. 1 and 2. In a diagram of this type the quantum defect $(n-n^*)$ is plotted against the total quantum number (n) for the

TABLE III. *New classifications in P III.*

INT.	λ (air)	ν (cm⁻¹)	CLASSIFICATION	INT.	λ (vac.)	ν (cm⁻¹)	CLASSIFICATION
1	5203.85	19,211.2	$4d\,{}^2D-5p\,{}^2P_{3/2}$	6	1618.665§	61,779.31	${}^2D_{3/2}-\ {}^2F$
8 II	4587.90	21,790.4	$4f\,{}^2F-5d\,{}^2D$				
8	3978.27	25,129.5	$4f\,{}^2F-5g\,{}^2G$	9	1504.719§	66,457.6	$sp^2\,{}^2D_{3/2}-4p\,{}^2P_{1/2}$
				10	1502.273§	66,565.8	${}^2D_{5/2}-\ {}^2P_{3/2}$
3	3283.20	30,449.3	$p^3\,{}^2D_{3/2}-3d\,{}^2D_{3/2}$	7	1501.551§	66,597.8	${}^2D_{3/2}-\ {}^2P_{3/2}$
2	3280.20	30,477.2	$4d\,{}^2D-5f\,{}^2F$				
3	3277.80	30,499.5	$p^3\,{}^2D_{5/2}-3d\,{}^2D_{5/2}$	5	1492.031	67,022.7	$4s\,{}^2S_{1/2}-{}^21_{3/2}{}^\circ$?
				0	1471.218	67,970.9	$3d\,{}^2D-{}^21_{3/2}{}^\circ$
1	2686.58	37,210.0	$4f\,{}^2F-6g\,{}^2G$				
				2	1447.512	69,084.1	$4s\,{}^2S-sp\cdot s\,{}^2P_{3/2}$
II	2636.77	37,913.8	$sp^2\,{}^2P_{3/2}-p^3\,{}^2D_{3/2}$				
7	2632.62	37,973.7	${}^2P_{3/2}-\ {}^2D_{5/2}$	2	1430.409	69,910.1	$sp^2\,{}^2S-p^3\,{}^2P_{3/2}$
6	2611.05	38,287.3	${}^2P_{1/2}-\ {}^2D_{3/2}$	1	1429.242	69,967.2	${}^2S-p^3\,{}^2P_{1/2}$
	λ (vac.)[l]						
				8	1381.633	72,378.1	$sp^2\,{}^2D_{5/2}-p^3\,{}^2D_{3/2}$
1	2428.58§	41,176.3	$sp^2\,{}^2S-s^24p\,{}^2P_{3/2}$	10	1381.111	72,405.5	${}^2D_{3/2}-\ {}^2D_{3/2}$
1	2420.52§	41,313.4	${}^2S-\ {}^2P_{1/2}$	10	1380.464	72,439.4	${}^2D_{5/2}-\ {}^2D_{5/2}$
				5	1379.873	72,470.4	${}^2D_{3/2}-\ {}^2D_{5/2}$
0	2248.31	44,477.8	$4f\,{}^2F-7g\,{}^2G$				
				1	1374.780	72,738.9	$3s3p3d\,{}^4D_{7/2}-3s3p4f\,{}^4D_{7/2}$
1	1757.68	56,893.2	$3p\,{}^2P_{3/2}-sp^2\,{}^4P_{5/2}$	3	1372.711	72,848.5	${}^4D_{5/2}-\ {}^4D_{3/2}$
0	1756.82	56,921.1	${}^2P_{1/2}-sp^2\,{}^4P_{1/2}$	1	1372.01	72,885.7	${}^4D_{3/2}-\ {}^4D_{5/2}$
				0	1370.39	72,971.8	${}^4D_{1/2}-\ {}^4D_{3/2}$
1	1696.92	58,930.4	$4p\,{}^2P_{3/2}-5d\,{}^2D$				
1	1693.03	59,065.8	${}^2P_{1/2}-\ {}^2D$	0	1354.957	73,803.1	$4s\,{}^2S_{1/2}-5p\,{}^2P_{3/2}$
0	1678.12	59,590.6	$4p\,{}^2P_{3/2}-6s\,{}^2S$	3	1349.110	74,122.9	$3s3p3d\,{}^4P_{1/2}-3s3p4f\,{}^4D_{3/2}$
00	1674.26	59,728.1	${}^2P_{1/2}-\ {}^2S$	0	1348.449	74,159.3	${}^4P_{1/2}-\ {}^4D_{1/2}$
3	1647.546	60,696.3	$sp^2\,{}^2P_{3/2}-p^3\,{}^2P_{3/2}$	0	1347.508	74,211.1	$3s3p3d\,{}^4P_{3/2}-3s3p4f\,{}^4D_{5/2}$
2	1645.914	60,756.5	${}^2P_{3/2}-\ {}^2P_{1/2}$	3	1346.998	74,239.2	${}^4P_{3/2}-\ {}^4D_{3/2}$
1	1637.377	61,073.3	${}^2P_{1/2}-\ {}^2P_{3/2}$				
2	1635.799	61,132.2	${}^2P_{1/2}-\ {}^2P_{1/2}$	10	1344.900§	74,355.0	$3s3p3d\,{}^4P_{5/2}-3s3p4f\,{}^4D_{7/2}$; $3p\,{}^2P_{3/2}-\ sp^2\,{}^2D_{3/2}$
6	1618.944§	61,768.65	$3d\,{}^2D_{5/2}-4f\,{}^2F$				

II, Blend with P II.
IV, Blend with P IV.
§, Lines classified by Bowen, references 5, 6 and 7.
d, Line double.
n, Line nebulous.
l, From here on this list contains all lines classified as P III.

† A. Shenstone and H. N. Russell, Phys. Rev. **39**, 426 (1932).

several members of an isoelectronic sequence. When no perturbations are present the series show regularities along the sequence like that found for the $s \cdot s\ ^3S$ series in Fig. 1. Every one of the other series shows evidence of some outside effect; in all cases the effect can be directly traced to terms in the displaced series. Table V lists the Rydberg denominators for the several series. The limit has been calculated by extrapolation of the $3s5g\ ^3G$ from Al II.[13]

The extension of the singlet system as given here contains only lines which definitely belong to P IV. They have been carefully sorted out by using self-induction in the various circuits. The line at 843.984A appears to be an exception to this but it is closely surrounded by stronger

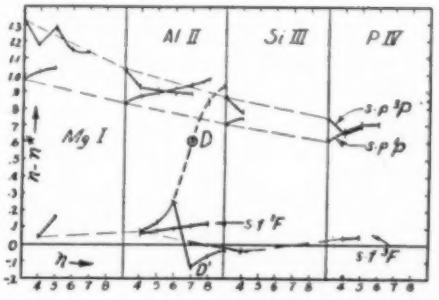

FIG. 2. $n-n^*$ *vs.* n for the p and f series in the Mg I-like isoelectronic sequence, The ^3F series is perturbed by the $3p \cdot 3d\ ^3F$ which has inserted itself into the Al II series at D. Removing this term the quantum defect continues from D'. In this case the term displaces the series partly (Al II) upwards. The irregularities in the $s \cdot p\ ^3P$ series are due both to the $3p4s\ ^3P$ and $3p3d\ ^3P$.

TABLE III.—*Continued.*

INT.	λ (vac.)	ν (cm⁻¹)	CLASSIFICATION
15	1344.343§	74,385.8	$3p\ ^2P_{3/2}-sp^2\ ^2D_{5/2}$ / $3s3p3d\ ^4P_{5/2}-3s3p4f\ ^4D_{5/2}$
1	1343.687	74,422.1	$3s3p3d\ ^4P_{5/2}-3s3p4f\ ^4D_{7/2}$
2	1337.710	74,754.6	$3d\ ^2D_{5/2}-5p\ ^2P_{3/2}$
1	1337.498	74,766.5	$3d\ ^2D_{3/2}-\ ^2P_{3/2}$
10	1334.866§	74,913.9	$3p\ ^2P_{1/2}-sp^2\ ^2D_{3/2}$
1	1325.509	75,442.7	$sp^2\ ^2P_{3/2}-\ ^2I_{3/2}^\circ$
0	1318.91	75,820.1	$^2P_{1/2}-\ ^2I_{3/2}^\circ$
00	1290.134	77,511.3	$sp^2\ ^2P_{1/2}-sp\cdot s\ ^2P_{3/2}$
0	1283.949	77,884.7	$^2P_{3/2}-\ ^2P_{3/2}$
1	1210.600	82,603.7	$sp^2\ ^2P_{1/2}-5p\ ^2P_{3/2}$
2	1093.627	91,438.9	$sp^2\ ^2S_{1/2}-5p\ ^2P_{3/2}$
4	1050.817	95,164.0	$sp^2\ ^2D_{5/2}-p^3\ ^2P_{3/2}$
1	1050.518	95,191.1	$^2D_{3/2}-\ ^2P_{3/2}$
4	1049.824	95,254.1	$^2D_{3/2}-\ ^2P_{1/2}$
10	1003.592§	99,642.1	$3p\ ^2P_{3/2}-sp^2\ ^2S$
8	998.000§	100,200.4	$^2P_{1/2}-\ ^2S$
4	977.888§	102,261.2	$sp^2\ ^4P_{5/2}-p^3\ ^4S$
3	974.776§	102,587.6	$^4P_{3/2}-\ ^4S$
3	972.807§	102,795.3	$^4P_{1/2}-\ ^4S$
1	964.251§	103,707.4	$sp^2\ ^2D_{5/2}-4f\ ^2F$
1 IV	963.993	103,735.1	$^2D_{3/2}-\ ^2F$
5	921.863§	108,475.9	$3p\ ^2P_{3/2}-sp^2\ ^2P_{1/2}$
5	918.706§	108,848.7	$^2P_{3/2}-\ ^2P_{3/2}$
4	917.130§	109,035.8	$^2P_{1/2}-\ ^2P_{3/2}$
5	913.989§	109,410.7	$^2P_{1/2}-\ ^2P_{1/2}$

INT.	λ (vac.)	ν (cm⁻¹)	CLASSIFICATION
1	909.846	109,908.7	$sp^2\ ^2D_{5/2}-\ ^2I_{3/2}^\circ$
8	859.667§	116,324.1	$3p\ ^2P_{3/2}-3d\ ^2D_{5/2}$
0	859.411§	116,358.8	$sp^2\ ^4P_{5/2}-3s3p3d\ ^4P_{5/2}$
1	858.139	116,531.2	$^4P_{5/2}-\ ^4P_{3/2}$
2	856.963	116,691.2	$^4P_{3/2}-\ ^4P_{5/2}$
5	855.618	116,874.6	$3p\ ^2P_{1/2}-3d\ ^2D_{3/2}$
1	854.855	116,978.9	$sp^2\ ^4P_{3/2}-3s3p3d\ ^4P_{1/2}$
1	854.223	117,065.6	$^4P_{1/2}-\ ^4P_{3/2}$
0	853.346	117,185.8	$^4P_{1/2}-\ ^4P_{1/2}$
5	852.679§	117,277.4	$3p\ ^2P_{3/2}-4s\ ^2S$
3d	848.636	117,836.2	$^2P_{1/2}-4s\ ^2S$
1	848.445§	117,862.7	$sp^2\ ^4P_{5/2}-3s3p3d\ ^4D_{3/2}$
2d	848.023§	117,921.3	$^4P_{5/2}-\ ^4D_{5/2}$
3d IV	847.658§	117,972.1	$^4P_{5/2}-\ ^4D_{7/2}$
0 IV	846.494§	118,134.3	$^4P_{3/2}-\ ^4D_{1/2}$
1 IV	846.125§	118,185.8	$^4P_{3/2}-\ ^4D_{3/2}$
1	845.656§	118,251.4	$^4P_{3/2}-\ ^4D_{5/2}$
1	845.047§	118,336.6	$^4P_{1/2}-\ ^4D_{1/2}$
1	844.635§	118,394.3	$^4P_{1/2}-\ ^4D_{3/2}$
1 II	786.244§	127,186.9	$sp^2\ ^4P_{5/2}-3s3p4s\ ^4P_{3/2}$
1	785.392§	127,325.0	$^4P_{3/2}-\ ^4P_{1/2}$
1	783.752§	127,591.4	$^4P_{5/2}-\ ^4P_{5/2}$
1 II	782.977§	127,717.6	$^4P_{1/2}-\ ^4P_{3/2}$
1	781.726§	127,922.0	$^4P_{3/2}-\ ^4P_{5/2}$
00n	581.898	171,851.4	$3p\ ^2P_{3/2}-4d\ ^2D$
00n	579.98	172,420	$^2P_{1/2}-\ ^2D$
2nn	569.90 §	175,469	$3p\ ^2P_{3/2}-5s\ ^2S$
0	568.09	176,028	$^2P_{1/2}-\ ^2S$
00	497.17	201,138	$3p\ ^2P_{3/2}-6s\ ^2S$

[13] A recent extension of this (Mg I) isoelectronic sequence by Edlén (Zeits. f. Physik **103**, 536 (1936)) includes the $s \cdot 3d\ ^3D-s4f\ ^3F$ transition for several of the more highly ionized elements.

TABLE IV. *Complete term table for P III.*

$s^2 3p\ ^2P_{1/2}^\circ$	243,290.0§	559.6		$s^2 5s\ ^2S_{1/2}$	67,249.0§		
$^2P_{3/2}^\circ$	242,730.4§			$s^2 4f\ ^2F^\circ$	64,636.8§		
$sp^2\ ^4P_{1/2}$		206.5	186,370.7§	$3s3p4s\ ^4P_{1/2}^\circ$		185.9	58,836.6§
$^4P_{3/2}$		328.7	186,164.2§	$^4P_{3/2}^\circ$		405.9	58,650.7§
$^4P_{5/2}$			185,835.5§	$^4P_{5/2}^\circ$			58,244.8§
$sp^2\ ^2D_{3/2}$	168,374.9§	29.5		$3s3p3d\ ^2I_{3/2}^\circ$	58,435.9		
$^2D_{5/2}$	168,345.4§			$3s3p4s\ ^2P_{3/2}^\circ$	56,369.3		
$sp^2\ ^2S_{1/2}$	143,088.8§			$s^2 5p\ ^2P_{1/2}^\circ$	———		
$sp^2\ ^2P_{1/2}$	134,254.3§	374.0		$^2P_{3/2}^\circ$	51,650.5		
$^2P_{3/2}$	133,880.3§			$s^2 5d\ ^2D$	42,847.2		
$s^2 3d\ ^2D_{3/2}$	126,416.4§	11.3		$s^2 6s\ ^2S_{1/2}$	42,186.6		
$^2D_{5/2}$	126,405.1§			$s^2 5f\ ^2F^\circ$	40,383.6		
$s^2 4s\ ^2S_{1/2}$	125,455.5§			$s^2 5g\ ^2G$	39,507.3		
$s^2 4p\ ^2P_{1/2}^\circ$	101,914.3§	137.1		$3s3p4p\ ^4P_{1/2}$		116.9	33,351.1§
$^2P_{3/2}^\circ$	101,777.2§			$^4P_{3/2}$		250.3	33,234.2§
$p^3\ ^2D_{3/2}^\circ$	95,967.6	61.9		$^4P_{5/2}$			32,983.9§
$^2D_{5/2}^\circ$	95,905.7			$3s3p4p\ ^4S$			31,950.6§
$p^3\ ^4S^\circ$			83,575.4§	$s^2 6d\ ^2D$	29,307.2		
$p^3\ ^2P_{3/2}^\circ$	73,182.8	− 59.8		$s^2 6f\ ^2F^\circ$	27,888.0		
$^2P_{1/2}^\circ$	73,123.0			$s^2 6g\ ^2G$	27,426.8		
$s^2 4d\ ^2D$	70,860.8§			$s^2 7g\ ^2G$	20,159.0		
$3s3p3d\ ^4P_{5/2}^\circ$		−175.0	69,476.6§	$3s3p4f\ ^4D_{1/2}^\circ$		37.1	4,975.5
$^4P_{3/2}^\circ$		−117.8	69,301.6§	$^4D_{3/2}^\circ$		29.0	4,938.4
$^4P_{1/2}^\circ$			69,183.8§	$^4D_{5/2}^\circ$		31.0	4,909.4
$3s3p3d\ ^4D_{1/2}^\circ$		53.3	68,029.2§	$^4D_{7/2}^\circ$			4,878.4
$^4D_{3/2}^\circ$		62.5	67,975.9§				
$^4D_{5/2}^\circ$		50.6	67,913.4§				
$^4D_{7/2}^\circ$			67,862.8§				

§ Terms from I. S. Bowen, references 5, 6, and 7. Slightly modified on the basis of new measurements.

higher order lines and may be obscured on the hot spark plates. Few singlet systems can be considered as definitely established in their entirety without some outside aid such as that gained from the Zeeman effect. It is nevertheless felt that the additions presented here with the possible exception of $3p3d\ ^1D_2$ and $3p3d\ ^1F_3$ may be considered to be well established. This part of the classification has presented considerable difficulty due to the fact that in most cases the irregular doublet law breaks down due to the large perturbations mentioned before. The $3p^2\ ^1S_0$ and ^1D are completely unidentifiable by this means. Some help is afforded by certain of the relations given by Bacher and Goudsmit.[14]

[14] R. Bacher and S. Goudsmit, Phys. Rev. **46**, 959 (1934).

TABLE V. *Rydberg denominators in P IV.*

TERM	$n=3$	4	5	6
$s^2 \cdot np\ ^3P_2$	2.2536	3.3382	4.3180	
$np\ ^1P_1$	2.3833	3.3464	4.3161	5.3138
$nd\ ^3P_2$	2.7940	3.8083	4.8494	
$nd\ ^1D_2$	2.6180	3.8648	4.8940	
$ns\ ^3S_1$		3.0608	4.0851	5.0945
$ns\ ^1S_0$	2.0586	3.1205	4.2396	
$nf\ ^3F_4$		3.9833	4.9826	
$ng\ ^3G$			4.9859	

TABLE VI. *Irregular doublet law for $3s^2\ ^1S_0 - 3s3p\ ^3P_1$ in P IV.*

	ν (cm^{-1})	$\Delta\nu$
Mg I	21,870.7	
		15,583.1
Al II	37,453.8	
		15,303.8
Si III	52,757.6	
		15,289.0
P IV	68,146.6	

$$(sp^2)[^4P - ^2S] = (p^2)[^3P - ^1S] + \tfrac{1}{2}(sp)[^3P - ^1P]$$

$p^2\ ^1S$ calc. $-225{,}332$ cm^{-1}
obs. $-220{,}474$

$$(sp^2)[^4P - ^2D] = (p^2)[^3P - ^1D]$$

$p^2\ ^1D$ calc. $-250{,}604$ cm^{-1}
obs. $-248{,}918$

also eliminating $p^3\ ^4S$ from the two relations containing it, we get:

$$(p^3)[^2D - ^2P] = \tfrac{2}{3}(p^2)[^1D - ^1S]$$

or numerically $22{,}790 \equiv 18{,}964$.

Thus these three relations show that the intercombination classifications in P III and the classification of these p^2 singlet terms are mutually consistent. The discrepancies are of the

TABLE VII. *New classifications in P IV.*

INT.	λ (air)	ν (cm^{-1})	CLASSIFICATION	INT.	λ (vac.)	ν (cm^{-1})	CLASSIFICATION
I *D*	4291.1	23,298	$4d\ ^1D_2 - 5p\ ^1P_1$	1*d*	1205.513	82,883.5	$3s4p\ ^3P_0 - 3s5d\ ^3D_1$
				1	1204.302	83,035.7	$^3P_1 - {}^3D_2$
3 *d* II	3728.66	26,811.7	$4d\ ^3D_2 - 5p\ ^3P_1$	1	1203.410	83,097.2	$^3P_2 - {}^3D_3$
5 II	3717.62	26,891.3	$4d\ ^3D_2 - 5p\ ^3P_2$	1	1197.822	83,484.9	$3s4p\ ^1P_1 - 3s5d\ ^1D_2$
4	3717.02	26,895.7	$4d\ ^3D_1 - 5p\ ^3P_2$	1	1161.783	86,072.5	$3s4s\ ^1S_0 - 3s5p\ ^1P_1$
0	2547.8	39,237.6	$4p\ ^1P_1 - 4d\ ^1D_2$	4	1118.586	89,398.6	$3s3p\ ^1P_1 - 3p^2\ ^1S_0$
	λ (vac.)*			0	1116.915	89,532.3	$3s3p\ ^3P_2 - 3s3d\ ^1D_2$
				1	1111.127	89,998.7	$^3P_1 - {}^1D_2$
8 II	2498.081	40,030.7	$3p3d\ ^3F_4 - 3s5g\ ^3G$				
1	2479.269	40,334.5	$^3F_3 - {}^3G$	1*B*	1101.65	90,773 §	$3s4s\ ^3S - 3p4s\ ^3P_0$
0	2464.782	40,571.5	$^3F_2 - {}^3G$	2*B*	1098.183	91,059.5 §	$^3S - {}^3P_1$
				2*B*	1093.318	91,464.7 §	$^3S - {}^3P_2$
1 *B*	1910.18	52,351.1 §	$3s4p\ ^3P_2 - 3s5s\ ^3S$				
1 *B*	1904.80	52,499.0 §	$^3P_1 - {}^3S$	4*B* II	1091.442	91,621.9 §	$3s3d\ ^3D - 3p3d\ ^3P_2$
Q	1902.62	52,559	$^3P_0 - {}^3S$	3*B*	1088.608	91,860.4 §	$^3D - {}^3P_1$
				2*B*	1086.943	92,001.1 §	$^3D - {}^3P_0$
10	1888.652	52,947.8 §	$3s3p\ ^1P_1 - 3s3d\ ^1D_2$				
				3	1072.528	93,237.7	$3s4s\ ^3S - 3s5p\ ^3P_2$
1	1691.807	59,108.4	$3s4p\ ^1P_1 - 3s5s\ ^1S_0$	3	1073.373	93,164.3	$^3S - {}^3P_1$
0	1673.759	59,745.6	$3s3p\ ^1P_1 - 3p^2\ ^3P_0$	2*B*	1066.640	93,752.3 §	$3s3d\ ^3D - 3p3d\ ^3D_1$
				3*B*	1065.554	93,847.9 §	$^3D - {}^3D_2$
3	1640.476	60,957.9	$3s3p\ ^1P_1 - 3p^2\ ^1D_2$	3*B*	1064.60	93,932 §	$^3D - {}^3D_3$
Q 2	1614.85	61,925	$3p^2\ ^1S_0 - 3s4p\ ^1P_1$				
				8	1035.505	96,571.2 §	$3s3p\ ^3P_2 - 3p^2\ ^3P_1$
4	1489.101	67,154.6 §	$3s3d\ ^3D - 3s4p\ ^3P_0$	8	1033.099	96,796.1 §	$^3P_1 - {}^3P_0$
4	1487.796	67,213.5 §	$^3D - {}^3P_1$	10	1030.511	97,039.2 §	$^3P_{2,1} - {}^3P_{2,1}$
6	1484.506	67,362.5 §	$^3D - {}^3P_2$	1	1028.093	97,267.5 §	$^3P_0 - {}^3P_1$
				4	1025.564	97,507.2 §	$^3P_1 - {}^3P_1$
1 II	1467.424	68,146.6	$3s^2\ ^1S_0 - 3s3p\ ^3P_1$				
				1	1006.218	99,382.0 §	$3s3d\ ^1D_2 - 3s4p\ ^1P_1$
1	1264.481	79,083.8	$3s4s\ ^1S_0 - 3p4s\ ^1P_1$	1 III	963.993	103,735.1	$p^2\ ^1S_0 - 3p3d\ ^1P_1$

* This is a complete list of all lines classified in the Schumann Region.
II, Blend with P II Lines.
III, Blend with P III Lines.
B, Wave-lengths from Bowen, reference 7.
Q, Wave-lengths from Queney, J. de phys. et rad. (6) **10**, 299 (1929).
D, Wave-lengths from Desjardin, reference 9.
§, Lines classified by Bowen, reference 7.

same order of magnitude as those using these same relations in C, O and N spectra.

The intercombinations in P IV are well established. The line $3s^2\ {}^1S_0 - 3s3p\ {}^3P_1$ obeys the irregular doublet law very well as may be seen in Table VI. This lends further support to the intercombination line classified by Bowen[7] in Si III.

Certain singlet-triplet distances may also be calculated by means of Houston's[15] equations. This is particularly true of the $3s4p\ {}^3P$ and ${}^1P$. In this case the singlet is predicted at 156,755 and found at 156,792 cm^{-1}. The $3s \cdot nd$ terms cannot be so tested and indeed do not obey these equations at all due to the large perturbations. The $3p \cdot 4s\ {}^3P$ separations indicate that the singlet should be lower than the triplet, as is found to be the case, although the separation observed does not check with that calculated. This appears to be general in all such cases.[16] The new classifications comprise fifty-one lines locating twenty-three new terms. They are listed in Table VII and Table VIII, respectively. The ionization potential works out to be 51.106 $\pm$0.013 electron volts (using 1.2336×10^{-4} as conversion factor).

[15] W. Houston, Phys. Rev. **33**, 297 (1929).

Quadruply Ionized Phosphorus P V

The original classification of this spectrum was given by Millikan and Bowen.[17] The main lines are relatively easy to excite and by means of the Uppsala equipment it has been possible to considerably extend the various series as well as to get better measurements for the lines already known. The earlier analysis has been completely substantiated but due to the new

[16] R. F. Bacher, Phys. Rev. **43**, 264 (1933).

[17] R. A. Millikan and I. S. Bowen, Phys. Rev. **25**, 591 (1925).

TABLE VII.—*Continued.*

Int.	λ (vac.)	ν (cm^{-1})	Classification	Int.	λ (vac.)	ν (cm^{-1})	Classification
25	950.662	105,189.9 §	$3s^2\ {}^1S_0 - 3s3p\ {}^1P_1$	6	756.510	132,186.0	$p^2\ {}^1D_2 - 3p3d\ {}^1P_1$
4	908.050	110,126.0	$p^2\ {}^1D_2 - 3p3d\ {}^1F_3$	0	680.570	146,935.7	$p^2\ {}^1D_2 - 3p4s\ {}^1P_1$
2	907.590	110,181.9	$p^2\ {}^1D_2 - 3p3d\ {}^1D_2$	0	649.69	153,920	$3s3d\ {}^3D - 3s5f\ {}^3F_3$
				2	648.507	154,201.3	${}^3D - {}^3F_4$
2	879.310	113,725.5	$3s3d\ {}^3D - 3s4f\ {}^3F_2$				
11	877.493	113,961.0	${}^3D - {}^3F_3$	2B	656.55	152,311 §	$3p^2\ {}^3P_2 - 3p4s\ {}^3P_2$
11	875.132	114,268.4	${}^3D - {}^3F_4$	2B	655.78	152,490 §	${}^3P_1 - {}^3P_1$
				3B	654.86	152,704 §	${}^3P_2 - {}^3P_1$
0	866.84	115,362 §	$3p^2\ {}^3P_2 - 3p3d\ {}^3P_2$	1B	654.54	152,779 §	${}^3P_1 - {}^3P_2$
3	865.04	115,602 §	${}^3P_2 - {}^3P_1$	2B	653.51	153,020 §	${}^3P_0 - {}^3P_0$
3	863.325	115,831.2 §	${}^3P_1 - {}^3P_2$	2B	652.79	153,189 §	${}^3P_1 - {}^3P_1$
1	861.552	116,069.6 §	${}^3P_1 - {}^3P_1$				
2	860.449	116,218.3 §	${}^3P_1 - {}^3P_0$	10	631.790	158,280.4 §	$3s3p\ {}^3P_2 - 3s4s\ {}^3S$
				4	629.920	158,750.3 §	${}^3P_1 - {}^3S$
00	851.09	117,496 §	$3p^2\ {}^3P_2 - 3p3d\ {}^3D_1$	3	629.023	158,976.7 §	${}^3P_0 - {}^3S$
3	850.390	117,593.1 §	${}^3P_2 - {}^3D_2$				
4	849.764	117,679.7 §	${}^3P_2 - {}^3D_3$	00n	522.02	191,564	$3s3p\ {}^1P_1 - 3s4d\ {}^1D_2$
6 III	847.658	117,972.1 §	$3p^2\ {}^3P_1 - 3p3d\ {}^3D_1$	2	472.957	211,435.6	$3s3p\ {}^1P_1 - 3s5s\ {}^1S_0$
5	846.999	118,063.8 §	${}^3P_1 - {}^3D_2$				
				0	445.194	224,621.2	$3s3p\ {}^3P_2 - 3s4d\ {}^3D$
1 III	846.494	118,134.3	$3s3d\ {}^1D_2 - 3p3d\ {}^1F_3$	0	444.249	225,099.0	${}^3P_1 - {}^3D$
2 III	846.125	118,185.8	$3s3d\ {}^1D_2 - 3p3d\ {}^1D_2$	1	415.815	240,491.6	$3s3p\ {}^3P_2 - 3s5s\ {}^3S$
				0	415.022	240,951.0	${}^3P_1 - {}^3S$
2	845.995	118,204.0	$3p^2\ {}^3P_0 - 3p3d\ {}^3D_1$	00n	412.90	242,189	${}^3P_0 - {}^3S$
1	843.984	118,495.6	$p^2\ {}^1S_0 - 3p4s\ {}^1P_1$	6	388.315	257,522.9	$3s^2\ {}^1S_0 - 3s4p\ {}^1P_1$
25	827.932	120,782.9 §	$3s3p\ {}^3P_2 - 3s3d\ {}^3D$	0	359.628	278,065.1	$3s3p\ {}^3P_2 - 3s6s\ {}^3S$
20	824.726	121,252.4 §	${}^3P_1 - {}^3D$				
20	823.181	121,479.9 §	${}^3P_0 - {}^3D$	4	312.443	320,058.3	$3s^2\ {}^1S_0 - 3s5p\ {}^1P_1$
3	776.366	128,805.2 §	$3s3p\ {}^1P_1 - 3s4s\ {}^1S_0$	0n	283.99	352,125	$3s^2\ {}^1S_0 - 3s6p\ {}^1P_1$
00n	765.28	130,671	$3s3d\ {}^3D - 3s5p\ {}^3P_2$				

measurements their ground state has been slightly changed. The Rydberg denominators have been determined logarithmically using the Rydberg constant for phosphorus in place of R_∞. By extrapolation along the Na I isoelectronic sequence $6h\ ^2H$ has been set at $n^*=5.99960$. The lines above 2000A have been taken from Geuter[10] with the exception of 2440.75 and 2441.04 which were obtained by the author by means of the Hilger EI spectrograph located at M.I.T. In Geuter's list these transitions were represented by a single line and it was impossible to give the $4d$ separation accurately. It should be noticed that the $3d\ ^2D$ separation as given is calculated from the difference of the $4p\ ^2P$ difference (as found from the lines 1,000.360 and

TABLE VIII. *Complete term table—P IV.*

$3s^2\ ^1S_0$	414,312.4§		
$3s3p\ ^3P_0^0$			346,400.8§
$^3P_1^0$		227.4	346,173.4§
$^3P_2^0$		468.4	345,705.0§
$3s3p\ ^1P_1^0$	309,122.5§		
$3s3d\ ^1D_2$	256,174.2§		
$3p^2\ ^3P_0$			249,377 §
$^3P_1$		243	249,134 §
$^3P_2$		468	248,666 §
$3p^2\ ^1D_2$	248,168		
$3s3d\ ^3D_{1,2,3}$			224,923.4§
$3p^2\ ^1S_0$	219,723.9		
$3s4s\ ^3S_1$			187,423.8§
$3s4s\ ^1S_0$	180,317.4§		
$3s4p\ ^3P_0^0$			157,768.3§
$^3P_1^0$		58.6	157,709.7§
$^3P_2^0$		148.6	157,561.1§
$3s4p\ ^1P_1^0$	156,792.2§		
$3p3d\ ^1F_3^0$	138,042?		
$3p3d\ ^1D_2^0$	137,987?		
$3p3d\ ^3P_2^0$			133,301 §
$^3P_1^0$		−240	133,061 §
$^3P_0^0$		−140	132,921 §
$3p3d\ ^3D_1^0$			131,170 §
$^3D_2^0$		97	131,073 §
$^3D_3^0$		82	130,991 §

$3s4d\ ^3D_1$			121,078.9§
		5.4	
$^3D_2$			121,073.5§
		7.7	
$^3D_3$			121,065.8§
$3s4d\ ^1D_2$	117,654.6		
$3p3d\ ^1P_1^0$	115,985		
$3s4f\ ^3F_2^0$			111,197
$^3F_3^0$		235	110,962
$^3F_4^0$		307	110,653
$3s5s\ ^3S_1$			105,210.4§
$3p4s\ ^1P_1$	101,234		
$3s5s\ ^1S_0$	97,685.4		
$3p4s\ ^3P_0^0$			96,650 §
$^3P_1^0$		286	96,364 §
$^3P_2^0$		405	95,959 §
$3s5p\ ^1P_1^0$	94,248.9		
$3s5p\ ^3P_0^0$			—
$^3P_1^0$			94,259
$^3P_2^0$		73	94,186
$3s5d\ ^3D_2$			74,676.9
$^3D_2$		−3.8	74,673.1
$^3D_1$		−2.8	74,670.3
$3s5d\ ^1D_2$	73,307.6?		
$3s5f\ ^3F_2$			—
$^3F_3$			71,003
$^3F_4$		281	70,722
$3s5g\ ^3G$			70,624
$3s6s\ ^3S$			67,640
$3s6p\ ^1P_1^0$	62,187?		

§ Terms from I. S. Bowen, references 5, 7, slightly modified on the basis of new measurements.

TABLE IX. *Complete list of classified lines for P V.*

INT.	λ (air)	ν cm⁻¹	CLASSIFICATION	INT.	λ (vac.)	ν cm⁻¹	CLASSIFICATION
3	3204.04§	31,201.61	$4s\ ^2S - 4p\ ^2P_{1/2}$	8	544.914§	183.515.1	$3p\ ^2P_{3/2} - 4s\ ^2S$
5	3175.14§	31,485.60	$^2S - {}^2P_{3/2}$	7	542.567§	184,309.0	$^2P_{1/2} - {}^2S$
3	2978.5 §	33,563	$5g\ ^2G - 6h\ ^2H$	8n	475.610	210,256.0	$3d\ ^2D - 5f\ ^2F$
2	2961.39§	33,758.09	$5f\ ^2F - 6g\ ^2G$	2n	410.073	243,859.0	$3d\ ^2D - 6f\ ^2F$
5	2440.75§	40,958.6	$4p\ ^2P_{3/2} - 4d\ ^2D_{5/2}$	8	390.700	255,950.9	$3p\ ^2P_{3/2} - 4d\ ^2D_{5/2}$
1	2441.04	40,953.7	$^2P_{3/2} - {}^2D_{3/2}$	3	389.500	256,739.0	$^2P_{1/2} - {}^2D_{3/2}$
2	2424.34§	41,235.80	$^2P_{1/2} - {}^2D_{3/2}$	4	348.194	287,192.6	$3p\ ^2P_{3/2} - 5s\ ^2S$
	λ (vac.)			2	347.237	287,987.8	$^2P_{1/2} - {}^2S$
0B	1610.54§	62,089.1	$4f\ ^2F - 5g\ ^2G$	5†	328.768	304,165.9	$3s\ ^2S - 4p\ ^2P_{1/2}$
2B	1447.92§	69,064.5	$4d\ ^2D - 5f\ ^2F$	5†	328.455	304,455.8	$^2S - {}^2P_{3/2}$
0B	1385.11§	72,196.3	$4p\ ^2P_{1/2} - 5s\ ^2S_{1/2}$	4	311.347	321,185.1	$3p\ ^2P_{3/2} - 5d\ ^2D$
10	1128.006§	88,650.9	$3s\ ^2S - 3p\ ^2P_{1/2}$	3	310.579	321,979.2	$P_{1/2} - {}^2D$
15	1117.979§	89,447.1	$^2S - {}^2P_{3/2}$	1	296.112	337,710.0	$3p\ ^2P_{3/2} - 6s\ ^2S$
3	1000.360§	99,963.2	$3d\ ^2D_{3/2} - 4p\ ^2P_{1/2}$	2	280.609	356,367.8	$3p\ ^2P_{3/2} - 6d\ ^2D$
3	997.641§	100,235.6	$^2D_{5/2} - {}^2P_{3/2}$	00	273.13	366,126	$3p\ ^2P_{3/2} - 7s\ ^2S$
15d	871.396§	114,758.4	$3p\ ^2P_{3/2} - 3d\ ^2D_{5/2}$	5*	264.938	377,447	$3p\ ^2P_{3/2} - 7d\ ^2D$
			$^2P_{3/2} - {}^2D_{3/2}$	7	255.688	391,101.7	$3s\ ^2S - 5p\ ^2P_{1/2}$
15	865.435§	115.548.8	$^2P_{1/2} - {}^2D_{3/2}$	7	255.596	391,242.4	$^2S - {}^2P_{3/2}$
10	673.888§	148,392.6	$3d\ ^2D - 4f\ ^2F$	3	229.832	435,100.4	$3s\ ^2S - 6p\ ^2P_{3/2}$
				0	217.220	460,362.8	$3s\ ^2S - 7p\ ^2P$
				00	210.004	476,181.4	$3s\ ^2S - 8p\ ^2P$

§ Lines previously classified by Bowen.
B Wave-lengths from Bowen.
† Obscured by oxygen lines.
* Obscured by 5 × Be 88.

TABLE X. *Complete term table and Rydberg denominators for P V.*

$3s\ ^2S_{1/2}$	524,462.9§		2.28710
$4s\ ^2S_{1/2}$	251,501.8§		3.30273
$5s\ ^2S_{1/2}$	147,823.7§		4.30795
$6s\ ^2S_{1/2}$	97,306		5.3098
$7s\ ^2S_{1/2}$	68,890		6.3105
$3p\ ^2P_{1/2}$	435,811.2§	794.6	
$^2P_{3/2}$	435,016.6§		2.51126
$4p\ ^2P_{1/2}$	220,301.6§	284.0	
$^2P_{3/2}$	220,017.6§		3.53117
$5p\ ^2P_{1/2}$	133,361.2	140.7	
$^2P_{3/2}$	133,220.5		4.53793
$6p\ ^2P_{1/2}$			
$^2P_{3/2}$	89,362.5		5.54070
$7p\ ^2P$	64,100		6.5421
$8p\ ^2P$	48,282		7.5379
$I.P. = 524{,}462.9 \times 1.2336 \times 10^{-4}$ = 64.698 volts			

$3d\ ^2D_{3/2}$	320,265.8	11.2	
$^2D_{5/2}$	320,254.6§		2.92683
$4d\ ^2D_{3/2}$	179,064.5	4.9	
$^2D_{5/2}$	179,059.6§		3.91414
$5d\ ^2D$	113,831.8		4.90920
$6d\ ^2D$	78,649		5.9061
$7d\ ^2D$	57,570		6.9031
$4f\ ^2F$	171,867.6§		3.99526
$5f\ ^2F$	110,004.2§		4.99387
$6f\ ^2F$	76,401.2		5.99226
$7f\ ^2F$	55,933		7.0034
$5g\ ^2G$	109,778.5§		4.99901
$6g\ ^2G$	76,246.1§		5.99832
$6h\ ^2H$	76,215.5§		(5.99960)

§ Terms previously classified by Bowen but modified slightly on the basis of new measurements.

997.641A) and that difference as known from the other pairs containing it. The difference cannot be accurately found from the pair at 871.396 and 865.435 inasmuch as the first line is really double. Twenty new lines have been classified. These locate fourteen new terms. The complete list of classified lines and the complete term table are listed in Tables IX and X, respectively. Using the conversion factor 1.2336×10^{-4} for changing cm^{-1} to electron volts the ionization potential is 69.698 ± 0.003 volts.

ACKNOWLEDGMENTS

The original spectrograms and certain parts of the classifications were made under the guidance of Professor George M. Harrison and Professor J. C. Boyce at M.I.T. to whom I am very grateful. The latter experimental work was carried out while the author was Irving Langmuir Fellow of the American Scandinavian Foundation at the University of Uppsala, Uppsala, Sweden. Both Professor Siegbahn and Docent Bengt Edlén of that University were extremely helpful in innumerable ways.

MAY 1, 1937 PHYSICAL REVIEW VOLUME 51

The Correction of Continuous Spectra for the Finite Resolution of the Spectrometer

CARL ECKART
Ryerson Laboratory, University of Chicago, Chicago, Illinois
(Received March 17, 1937)

The relation between the theoretical intensity function of a continuous spectrum and the intensity measured with an ionization chamber (or counter) and a spectrometer, is discussed. It is shown that while the problem of correcting the observed intensity for the finite resolution of the spectrometer does not always have a mathematically unique solution, the requirement that the theoretical intensity have a smooth graph is sufficient to make the solution practically unique. On this basis, an approximate solution of the problem is given, which involves the first and second differences of a set of equally spaced measurements. A second method of solution is discussed which involves the scansion of a template of the measured intensity wave-length curve by a photoelectric cell connected to a recording galvanometer. This method has practical disadvantages but illustrates several theorems derived analytically in the earlier part of the paper.

INTRODUCTION

THE problem of correcting the measurements of a continuous spectrum for the effect of the finite resolution of the spectrometer has apparently received little attention. It is known that if $I(\lambda)$ is the intensity measured with an ionization chamber or counter, and $\rho(\lambda)$ is the theoretical intensity, the two functions are connected by an equation of the form

$$I(\lambda)=\int_{-a(\lambda)}^{+a(\lambda)} \rho(\lambda+\xi)K(\lambda, \xi)d\xi. \qquad (1)$$

The functions a and K are positive and have been determined for various types of instruments, but the general nature of the relation thus established between I and ρ has not been investigated. Eq. (1) has usually been approximated by

$$I(\lambda)=\alpha(\lambda)\rho(\lambda), \qquad (2)$$

where

$$\alpha(\lambda)=\int_{-a(\lambda)}^{+a(\lambda)} K(\lambda, \xi)d\xi, \qquad (3)$$

but there are cases in which this is not a sufficient approximation, e.g., some of the measurements of continuous beta-ray spectra made for the purpose of determining the mass of the neutrino.[1]

The validity of this approximation is readily estimated as follows: let $\rho_+(\lambda)$ and $\rho_-(\lambda)$ be the largest and smallest values, respectively, of $\rho(\lambda+\xi)$ for $|\xi| \leqslant a(\lambda)$. Then it follows from the positiveness of K that

$$\alpha\rho_- \leqslant I \leqslant \alpha\rho_+. \qquad (4)$$

[1] W. J. Henderson, Proc. Camb. Phil. Soc. **31**, 285 (1935); E. M. Lyman, Phys. Rev. **51**, 5 (1937).

This inequality can be given a graphical interpretation: through any point P of the I, λ curve, draw a straight line parallel to the λ axis, which extends a distance $a(\lambda)$ to either side of P. Then the graph of $\alpha(\lambda)\rho(\lambda)$ will intersect this line. If the point P traces the I, λ curve, the ends of the line will trace two other curves. It cannot be proven rigorously that the graph of $\alpha\rho$ will lie between these two curves at all points, but it will be seen below that it is safe to assume that this will be the case if the spectrum is a continuous one. The two limits thus obtained for $\alpha\rho$ may differ by more than the experimental error in the measurements of I; if this is the case, then Eq. (2) is usually not a sufficiently good approximation. It is ordinarily difficult to diminish the difference between the two limits, since this depends on the spectrum and on the resolving power of the spectrometer. The error in the measurement of I on the other hand, can be decreased with comparative ease; it may therefore be desirable to work under conditions that invalidate Eq. (2), and to devise more elaborate methods of calculating ρ from I.

General Theory of Eq. (1)

If Eq. (1) is considered as an equation for determining ρ in terms of I, a number of general theorems concerning its solutions may be proven. It is easily seen that its solution is not unique unless certain data analogous to boundary conditions are available. To see this, it may be noted that if f is the difference of two solutions of Eq. (1), then it must satisfy the homogeneous equation

$$0=\int_{-a(\lambda)}^{+a(\lambda)} f(\lambda+\xi)K(\lambda,\xi)d\xi, \qquad (5)$$

and conversely, if f is a solution of this equation, and I_1 a solution of Eq. (1), then $I_2=I_1+f$ will be another solution of the latter. Of course, it might be that Eq. (5) has no solution other than $f\equiv 0$, but this does not seem likely. As an example, let a and K be constants; then any periodic function of λ, of period $2a$, whose integral over one complete period vanishes, will be a solution of Eq. (5). This illustration seems to be typical of the general case that arises in practise.

The characteristics of the practical case are (a) that $K(\lambda,\xi)\geq 0$ and has only a finite number of roots when $|\xi|\leq a(\lambda)$, i.e., it does not vanish identically over any whole interval of ξ; (b) that both $\lambda-a(\lambda)$ and $\lambda+a(\lambda)$ are monotonically increasing functions of λ.

For convenience, let the interval on the λ axis from $\lambda-a(\lambda)$ to $\lambda+a(\lambda)$ be called the r interval at λ. It then follows from (a) that any solution of Eq. (5) must change sign at least once in any r interval, or else be zero throughout that interval. Confining attention to regular solutions, it follows from this and (b) that if such a solution is zero throughout one r interval, it is zero everywhere. For, suppose that f is a solution of Eq. (5) that vanishes throughout the r interval at λ_0 but is not zero in the interval from $\lambda_0+a(\lambda_0)$ to $\lambda_1>\lambda_0+a(\lambda_0)$. It will then be possible to choose λ_1 so that f does not change sign in the last mentioned interval. Because of (b), there will then be an r interval ending at λ_1 in which f neither changes sign nor is everywhere zero. This possibility has already been excluded, hence the supposition is false.

These results have several consequences for the solutions of Eq. (1): thus the graphs of any two of its solutions will intersect at least once in every r interval. Therefore there is, practically speaking, at most one solution that has a smooth graph. More precisely, if two solutions differ by an appreciable amount at even one point, at most one of them can have a smooth graph. This remark justifies the trial-and-error method of solution used by Henderson.[1]

However, the requirement that ρ have a smooth graph does not determine the solution with mathematical uniqueness. In order to accomplish this, it is necessary that the values of ρ be specified throughout one complete r interval. This specification thus plays much the same role in the theory of Eq. (1) as do the initial values in the theory of differential equations. However, this datum is not always available, unless the spectrum has a limit, beyond which the function ρ vanishes identically. In this case, the precise location of the limit need not be known (theoretically) in order to find the solution required.

There are several special examples of Eq. (1) for which the general solution can be obtained. The calculations that would be required for their application to practical problems would be very laborious and the effects of experimental error

would be cumulative. Furthermore, it would ordinarily be necessary to have recourse to the method of trial and error in order to find the correct initial conditions (or spectrum limit) and this would multiply the labor. Consequently the general solution will not be very useful, even when found, and it seems preferable to develop systematic approximate methods for finding a smooth solution.

Approximate Determination of a Smooth Solution

The remaining considerations of this paper will be based on the assumption that a and K are both independant of λ, so that Eq. (1) becomes

$$I(\lambda)=\int_{-a}^{+a}\rho(\lambda+\xi)K(\xi)d\xi. \tag{1.1}$$

Then α, defined by Eq. (3) is a constant, and it may be supposed that the units of ρ and I have been so chosen that its value is unity. The following definitions will also be useful:

$$\eta=\int_{-a}^{+a}\xi K(\xi)d\xi,$$
$$\zeta^2=\tfrac{1}{2}\int_{-a}^{a}(\xi-\eta)^2K(\xi)d\xi; \tag{6}$$

both $|\eta|$ and ζ are less than a. If the function K is symmetric, η will be zero. The quantity ζ may be called the half-width of K. It will be supposed that measurements have been made at equally spaced intervals of λ: $\lambda_n=\lambda_0+nb$, $I(\lambda_n)=I_n$, etc.

It is next necessary to formulate the requirement that ρ have a smooth graph in such a manner that it can be utilized analytically. It is characteristic of a smooth curve that it can be approximated by parabolas over relatively long intervals; hence it may be required that if

$$\rho(\lambda+x)=\rho(\lambda)+x\rho'(\lambda)+\tfrac{1}{2}x^2\rho''(\lambda)+R(\lambda,x), \tag{7}$$

then $|R(\lambda,x)|<\epsilon$ whenever $|x|\leqslant a+b$, (8)

where ϵ is a negligible quantity. It is always questionable whether, for a given I, there is a solution that satisfies this requirement. If there is such a solution, then the graph of I must be approximable by a parabola in any interval of length $2b$, with an error less than ϵ. It is very likely that this will also be a sufficient condition for all spectra that can properly be classed as continuous with respect to the resolving power of the spectrometer. In fact, this might well be adopted as a criterion for this relation,[2] with the additional proviso that $b>a$ (see below), and that ϵ be the experimental error in the measurements of I.

The Eq. (7) may be used, with $\lambda=\lambda_n$, to calculate I_{n+1}, I_n and I_{n-1}:

$$\begin{aligned}I_{n+1}&=\rho_n+(\eta+b)\rho_n'+\tfrac{1}{2}[(\eta+b)^2+2\zeta^2]\rho_n'',\\ I_n&=\rho_n+\eta\rho_n'+\tfrac{1}{2}[\eta^2+2\zeta^2]\rho_n'',\\ I_{n-1}&=\rho_n+(\eta-b)\rho_n'+\tfrac{1}{2}[(\eta-b)^2+2\zeta^2]\rho_n''.\end{aligned} \tag{9}$$

These equations are approximate, but the error is in each case less than ϵ. They may be solved for ρ_n:

$$\rho_n=I_n-(\eta/2b)\Delta_2I_n+[(\eta^2-2\zeta^2)/2b^2]\Delta^2I_n, \tag{10}$$

in which the abbreviations

$$\begin{aligned}\Delta_2I_n&=I_{n+1}-I_{n-1},\\ \Delta^2I_n&=I_{n+1}-2I_n+I_{n-1},\end{aligned} \tag{11}$$

have been used. The magnitude of the error in ρ_n is readily estimated: it is certainly less than

$$(1+a/b+4a^2/b^2)\epsilon.$$

If $b\gg a$ then the error will approach ϵ, but it must be recalled that b cannot be indefinitely increased without affecting the validity of Eq. (8). In any event, the errors of the calculation are not cumulative, since the result for ρ_n does not depend on the result for ρ_{n-1}.

A Photoelectric Method of Approximate Solution

The foregoing method of approximate solution leaves little to be desired in the way of computational simplicity. The method to be discussed in this section is not as simple, and the solutions obtained by it are subject to cumulative errors. It is presented rather as an instructive mathematical curiosity than as a feasible alternative to the previous method.

[2] It should be noted that this criterion can always be fulfilled for any spectrum if the measurements are sufficiently inaccurate. Conversely, if the measurements are extremely accurate, it becomes an exceedingly stringent criterion. From this point of view, it may be regarded as determining the desirable accuracy of the measurements for a given spectrum and spectrometer.

In Eq. (7), replace λ by $\lambda-x$, and x by $x+\xi$, and then substitute into Eq. (1.1). The result will be

$$I(\lambda)=\rho(\lambda-x)+(x+\eta)\rho'(\lambda-x) +\tfrac{1}{2}[(x+\eta)^2+2\zeta^2]\rho''(\lambda-x), \quad (12)$$

with an error that is less than ϵ provided that $x<b$. Next suppose that an opaque template of the I, λ curve is scanned by a photoelectric cell connected to a recording galvanometer. The ordinate of the trace, G, will be a function of λ that satisfies the equation

$$I(\lambda)=G(\lambda)+AG'(\lambda)+BG''(\lambda), \quad (13)$$

where A and B are constants and the unit of G has been conveniently chosen.

Eqs. (12) and (13) suggest that one inquire whether matters can be so arranged that

$$A=(x+\eta), \quad B=\tfrac{1}{2}[(x+\eta)^2+2\zeta^2]. \quad (14)$$

The disposable parameters are

the period of the galvanometer: $T=2\pi/\omega$ sec.;
its damping constant: p sec.$^{-1}$;
the speed with which the template is scanned: s (units of λ)/sec.;
the constant: x (units of λ).

The quantities η and ζ are to be considered as fixed, and of the four disposable parameters, s and x are the most readily varied. In terms of these quantities, the Eq. (14) becomes

$$\begin{aligned}(x+\eta)&=2ps/(\omega^2+p^2),\\ \tfrac{1}{2}(x+\eta)^2+\zeta^2&=s^2/(\omega^2+p^2),\end{aligned} \quad (14.1)$$

whose solutions for x and s are

$$\begin{aligned}x&=-\eta\pm 2p\zeta/(\omega^2-p^2)^{\frac{1}{2}},\\ s&=\pm\zeta(\omega^2+p^2)/(\omega^2-p^2)^{\frac{1}{2}},\end{aligned} \quad (15)$$

the undetermined sign being the same in both equations.

In order that x and s shall both be real, it is necessary that $\omega>p$; in other words, the galvanometer must be under-damped, even though p need not be zero. It can also be seen that $sT>2\pi\zeta$: during the period of one free oscillation of the galvanometer, an interval of the I, λ curve must be scanned that is greater than the half-width of K. These two requirements may be contrasted with the characteristics of an ordinary microphotometer, whose galvanometer is critically damped ($\omega=0$) and whose scanning speed is normally such that $sT\ll\zeta$. It is thus quite obvious that if the requirements of Eq. (15) were imposed on a microphotometer intended for use in registering line spectra, the results obtained with it would not be very sensible. This finds its mathematical explanation in the fact that the graph of a line spectrum will not satisfy the smoothness criterion unless ϵ is given a very large value, greater than the experimental error in the measurements. The method is thus restricted to continuous spectra.

Supposing that Eq. (15) is satisfied, it still does not follow that $G(\lambda)$ and $\rho(\lambda-x)$ are identical. The galvanometer trace will depend, not only on $I(\lambda)$ but also on the initial conditions of the galvanometer motion. Common sense indicates that the galvanometer should be at rest when the scansion begins: there should be no "galvanometer wiggles" in the trace. This conclusion is justified by a more detailed examination of the mathematics. It can easily be shown from Eq. (15) that the trace of a free vibration of the galvanometer is not a smooth curve unless its amplitude is considerably less than ϵ. This remark serves to establish a convenient standard for the estimation of smoothness. The further theorem, that if both $G(\lambda)$ and $\rho(\lambda-x)$ have smooth graphs their difference is less than ϵ, cannot be proven with complete rigor, since Eq. (12) is only approximate. Ignoring this source of error, the theorem is valid. However, this source of error may very easily be important, since it may result in systematically cumulative differences between the calculated and theoretical ρ functions. Consequently the method is not to be recommended for actual use, and is of interest largely because of the close analogy between the "galvanometer wiggles" and the solutions of the homogeneous integral equation, Eq. (5).

Pressure Effect in Bands of Several Dipole Molecules*

S. D. CORNELL
Sloane Physics Laboratory, Yale University, New Haven, Connecticut
(Received March 11, 1937)

Several photographic infrared bands, of H_2O, HCN, and NH_3, have been investigated for line broadening due to increased pressure of the vapors themselves. The half-widths at one atmosphere have been found, and the excess broadening per atmosphere calculated in each case. Comparison with simple dipole interaction theory has been made. Conformity is found for one H_2O band, compared with HCN. Lack of conformity for another H_2O band, and for two NH_3 bands, is discussed. For HCN a variation of half-width with J is found, in accord with theoretical considerations of a qualitative nature, leading to broader lines in the neighborhood of the thermal maximum of the rotational velocity distribution. Effect of change in slit width on the observed line width and rate of broadening, and the consequent precautions necessary, are discussed.

1. INTRODUCTION

AN investigation of the absorption spectrum of HCN in the far photographic infrared was carried out in 1934 by Herzberg and Spinks.[1] In particular, the intense (0,0,3,0) band at 1.038μ was photographed at various HCN vapor pressures, from 130 mm to 650 mm, and the authors concluded, from visual inspection of their spectrograms, that the pressure broadening present was exceptionally large, because of a strong interaction between HCN molecules at relatively large distances. A later investigation by Watson and the author,[2] using a somewhat larger slit width, indicated that no excessive increase in line width with pressure was present. This divergence of results led to the question of whether the apparent disagreement could have arisen entirely from the difference in slit widths used. Herzberg and Spinks[1] also concluded, from visual inspection, that the broadening decreases with increasing molecular rotation, the lines of high J (>20) in particular being less broadened than those of lower J value. Microphotometer measurements of the spectrograms of Herzberg and Spinks have been made by Watson,[3] and a broadening of about 1 cm^{-1} per atmosphere found. Because of the plate grain and high background fog of the early Agfa plates used, no certain conclusions could be reached regarding any variation of the broadening with the value of J. These two questions, of the rate of broadening with pressure, and of variation with J, for HCN, are taken up in the present investigation, along with some less extensive work on two other dipole molecules, H_2O and NH_3.

2. EXPERIMENTAL PROCEDURE

The light source used throughout was a 100 C.P. Point-O-Lite lamp. Exposures ranged from 10 minutes to 24 hours, using in each case the type of Eastman spectroscopic plate appropriate for the wave-length region under observation. All spectrograms were taken in the first order of the 21-foot concave grating in a stigmatic mounting, the dispersion varying from 3.55 to 7.84 cm^{-1}/mm. All the microphotometer plates were made with the 40 : 1 magnification of a Koch-Goos registering microphotometer.

In the case of H_2O two different experimental conditions were used. To obtain a sort of reference exposure, indicating the extent of the broadening influence of nonpolar foreign gas molecules alone, one spectrogram for each band was taken with no absorption tube in the light path, so that the absorption was due entirely to atmospheric water vapor present in the slit room and grating room. To obtain spectrograms of H_2O broadened by H_2O, an 80 cm Pyrex absorption cell was used, containing only water and water vapor, heated to about 100° by an electric furnace. The slit width was 0.04 mm. Only those lines in each band showing good intensity, with no apparent overlapping, were chosen for microphotometering. The 9400A band and the

* Part of a dissertation to be presented to the faculty of the Graduate School of Yale University in candidacy for the degree of Doctor of Philosophy.

[1] G. Herzberg and J. W. T. Spinks, Proc. Roy. Soc. **A147**, 434 (1934).

[2] S. D. Cornell and W. W. Watson, Phys. Rev. **50**, 279 (1936).

[3] W. W. Watson, J. Phys. Chem. **41**, 61 (1937).

11,350A band were photographed under the above two conditions.

For HCN a steel absorption tube 21 feet in length was employed, to provide more absorption than had previously been used, in an effort to get more accurately measurable microphotometer traces. HCN was generated by dropping a concentrated solution of sodium cyanide into concentrated sulfuric acid. After passing through a calcium chloride drying tube it was introduced into the previously evacuated absorption tube. The 10,380A band was photographed at HCN pressures of 120 mm, 340 mm, and 545 mm, using three different slit widths, 0.04 mm, 0.05 mm, and 0.06 mm, at each pressure. This band has a simple P, R branch structure on account of the linear nature of the molecule. The P branch, showing a line spacing sufficient to prevent overlapping, was in each case microphotometered to as high a J value as possible.

NH_3, to a pressure slightly above atmospheric (about 78 cm), was introduced from a commercial tank into the evacuated 21-foot tube. The 7920A band and the 10,230A band were photographed at this pressure, and again only fairly sharp lines of good intensity were chosen for microphotometering.

The half-widths were measured with a millimeter scale from traces of the microphotometer plates. In tracing, the fluctuations due to plate grain were smoothed out as much as possible.

It is well to emphasize here the magnitude of the errors involved in half-width measurements, especially in the far photographic infrared. In plates sensitized for this region, the plate grain is generally large, and in the microphotometer may cause short period deflections of comparable magnitude to the line deflections themselves. Thus the line contours finally measured from the trace of the microphotometer plate become quite sensitive to the process of smoothing out the plate grain in tracing, especially in the case of lines of relatively low intensity, approaching the limit of sensitivity of the microphotometer. Likewise, in the case of lines which have a breadth comparable to their maximum height, since the half-width is measured along an abscissa drawn at one-half the maximum ordinate, the measured $\Delta\nu_{\frac{1}{2}}$ is very sensitive to the accuracy with which the maximum ordinate is determined and bisected. As a consequence of these two facts in particular, the individual measurements have at best only a very low order of accuracy. In every case, therefore, a mean of as many lines as possible has been taken for any given band at a given pressure, and the mean deviation of the individual measurements from this mean has been found. This calculated error, then, gives an indication of the consistency of the measurements among themselves, but also, of course, is increased by any actual variation in half-widths within the band in question.

3. Excess Broadening

The forces between dipole molecules leading to broadening of their spectral lines are in general made up of three principal components: (1) London's dispersion effect, (2) Debye's induction effect, and (3) the effect of dipole alignment.[4] The complicated manner in which these three effects combine to make up the total line width is known theoretically, but has not been worked out on a practical basis. The dispersion effect, involving the mutual polarization of the electronic structures of the interacting molecules, is, of course, present in interactions between molecules which have no permanent dipole moment, as well as in the dipole case here considered. Consequently, if the dispersion broadening influence can be measured and subtracted from the total effect, we should, on the assumption of approximate additivity, obtain a fair idea of the broadening due to dipole interactions alone. From London's[4] work on intermolecular forces, it appears that even for dipole molecules having dipole moments μ of ordinary magnitude, about 10^{-18} e.s.u., the dispersion effect is strongly predominant, but that for μ

Table I. *Average values of half-width of band lines.*

Substance	Band	Pressure	$\Delta\nu_{\frac{1}{2}}$ (cm^{-1})	Average of
H_2O	9400	Atmos. Abs.	0.57±0.06	37 lines
		0.8 Atmos.	0.67±0.07	34
	11,350	Atmos. Abs.	0.40±0.04	14
		0.8 Atmos.	0.63±0.06	19
HCN	10,380	120 mm	0.56±0.08	19
		340 mm	0.88±0.10	24
		545 mm	1.24±0.16	23
NH_3	7920	78 cm	1.45±0.27	14
	10,230	78 cm	0.81±0.19	10

[4] F. London, Zeits. f. Physik **63**, 245 (1930).

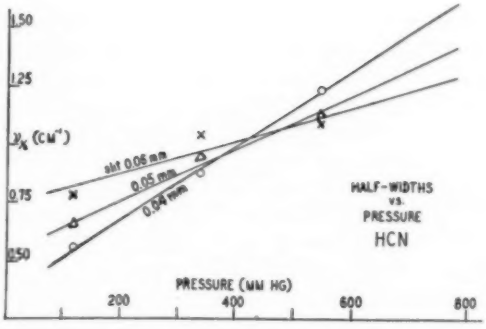

FIG. 1. Half-widths of the lines of the 1.038μ HCN band as a function of pressure for three different slit widths.

larger, about 2×10^{-18} e.s.u., the alignment effect becomes of comparable magnitude with the dispersion effect, and may become predominant for exceptionally large values of μ. This dipole interaction broadening may be thought of as an "excess broadening," present only in dipole molecules, and appreciable only in dipole gases of relatively large dipole moments. London's[4] Eq. (26) gives the interaction energy for the case of two linear dipoles, of dipole moment μ and moment of inertia A (perpendicular to μ), a distance R apart:

$$\epsilon_{lk}^{(2)} = \frac{8\pi^2}{R^6}\frac{\mu^4 A}{h^2} \times \text{a function of } l \text{ and } k,$$

where l and k are the angular momenta of the perturbed and perturbing molecules, respectively. The condition of large intermolecular distances, necessary for the validity of this expression, is best fulfilled at low pressures, such as are here used (<1 atmosphere). Resonance interactions, between molecules for which l and k differ by one unit, are, of course, present, but nevertheless the excess broadening might be expected to be roughly proportional to μ^4.

Table I gives the average values of $\Delta\nu_{\frac{1}{2}}$, the half-width in cm^{-1}, found at the various pressures for H_2O, HCN, and NH_3, together with the mean deviations from the mean for each, and the number of lines represented in each average. It is to be noted that for comparison purposes, the relative vapor densities are important, or the relative pressures at constant temperature. Consequently, the H_2O vapor pressures of 1 atmosphere, at 100°, have been reduced to room temperature (20°) for comparison with the other pressures, all of which were obtained at room temperature, leading to a corrected pressure of 0.8 atmosphere. In the case of absorption by atmospheric H_2O alone, the H_2O pressure is only a few millimeters (about 1.5 cm or less for relative humidity 60 percent), and N_2 and O_2 molecules, at a total pressure of 1 atmosphere, are the perturbers. The half-widths found under these conditions, then, may be considered to represent the breadth due to all such effects as apparatus width, dispersion forces, and the small contributions of Doppler broadening and natural line width. The two values found, for the 9400A and 11,350A bands, do not agree within the approximate errors. Part of the discrepancy may be explainable on slit width considerations, which will be taken up later. On the whole, however, the difference has found no satisfactory explanation. However, if we take a mean of the two, we may assume that the half-width for these forces alone lies between 0.45 cm^{-1} and 0.50 cm^{-1}. Such a value is supported by other measurements, such as those on CH_4 and C_2H_2 mentioned by Watson,[3] which indicate that the half-width for dispersion and collision forces alone is in general in this region.

Now, the half-width *vs.* pressure relation for HCN (Fig. 1) is linear (the curve for slit 0.04 mm is the one under consideration) and gives a value for the half-width, at 1 atmosphere, of 1.55 cm^{-1}, assuming linearity up to one atmosphere, an assumption apparently justified.[2] The excess broadening, then, would appear to be in the neighborhood of 1.05 to 1.10 cm^{-1} per atmosphere. For HCN, μ is 2.5 to 2.6×10^{-18} e.s.u.; μ for H_2O is 1.87×10^{-18} e.s.u. The ratio $\mu^4_{HCN} : \mu^4_{H_2O}$ is about 3.45. This ratio indicates an expected broadening for H_2O of roughly 0.3 cm^{-1} per atmosphere. From the data of Table I the excess broadening for the 11,350A band of H_2O is found to be 0.29 cm^{-1} per atmosphere, in good agreement with the expected value. For the 9400A band, however, a value of 0.13 cm^{-1} per atmosphere is calculated, for which no explanation has been found, unless it be in a variation in μ for the upper states in vibrational transitions, or possibly in the effect of slit width on observed line width at different wave-lengths, a question which will be taken up below.

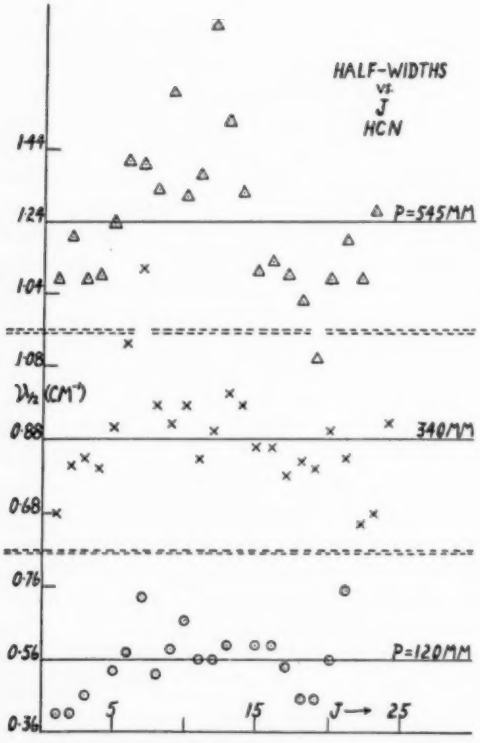

FIG. 2. Variation of the half-widths in the 1.038μ HCN band with the rotational quantum number, J, for three different pressures.

For NH_3, $\mu = 1.44 \times 10^{-18}$ e.s.u., smaller than for H_2O. And yet, for the 10,230A band Table I indicates an excess broadening slightly larger than that for the H_2O 11,350A band. The 7920A band shows a very much larger excess broadening, but comparison may be risky because of wavelength and slit width considerations. Although the actual measurements on NH_3 are very unreliable, as indicated by the small number of lines found suitable for microphotometering, and the large mean deviations, half-widths of this order are indicated also in other work on NH_3.[5] There are, however, some promising explanations for this unexpectedly large excess broadening. The symmetrical top structure, of which NH_3 is an example, shows, as is well known, a first-order Stark effect, and hence first-order van der Waals forces.[6] London[4] did not consider this type of van der Waals interaction. Margenau and Warren[6] have made some absolute calculations on the interactions between symmetrical top dipoles, indicating that $\Delta\nu_{\frac{1}{2}}$ for NH_3 at one atmosphere might be expected to be of the order of 1.5 cm^{-1}. Comparison with experiment is of no quantitative reliability because of the uncertainty of the effect of slit width on the observed value, but at least it can be said that a considerably larger value is to be expected than that calculated from the H_2O or HCN line widths by the simple μ^4 ratio. These top interactions increase with J, and consequently a comparable effect would not be expected in H_2O, which is a top structure (asymmetrical), because for most of the observable band lines in H_2O, J is not greater than 4, as has been pointed out by Dennison.[7]

4. Half-Width Variation with J

In earlier quantitative work on HCN[2, 8] no reliable evidence could be found for any variation of the half-width with rotational quantum number J, although Herzberg and Spinks[1] had reported, as has been mentioned, an apparent lessening of the broadening for the highest observable values of J. The simple P, R branch structure renders HCN particularly suitable for comparison of lines of different J, and the experimental conditions in the present investiga-

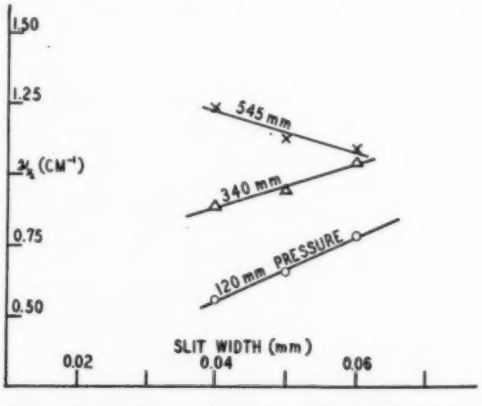

FIG. 3. Half-width as a function of slit width for three different pressures of HCN.

[5] S. H. Chao, Phys. Rev. **50**, 27 (1936).

[6] H. Margenau and D. T. Warren, Phys. Rev. **51**, 748 (1937).

[7] D. M. Dennison, Rev. Mod. Phys. **3**, 280 (1931).

[8] G. Herzberg, J. W. T. Spinks and W. W. Watson, Phys. Rev. **50**, 1186 (1936).

tion are more favorable than before for detecting any true J dependence, because of the considerably increased absorption path used.

It has been pointed out by Watson and Margenau[9] on the basis of qualitative theoretical considerations, that, ignoring the London dispersion effect and the Debye static induction effect, and assuming the dipole alignment effect alone to be present, a slight variation with J is to be expected, the selectivity of dipole interactions for rotational states of nearly equal quantum number giving rise to a noticeable maximum broadening for values of J in the neighborhood of the maximum of the Maxwell distribution of rotational velocities. In the case of HCN the alignment effect is strong, certainly comparable to the other effects present, because of the rather large value of μ for HCN. A variation in half-width with J, then, from the above considerations, is to be expected, leading to somewhat broader lines in the neighborhood of $J=7$ or 8, where the maximum of the rotational velocity distribution occurs. The HCN measurements bear out this theory in a convincing manner. For one thing, Table I shows that the mean deviations from the mean half-widths for HCN are somewhat larger, amounting to from 11 percent to 14 percent, than for H_2O, where 10 percent seems to be a fairly consistent value, and this despite the fact that any difference in quality of the lines, for measuring purposes, was quite negligible. Thus a definite trend of some sort is indicated. Fig. 2 shows the half-widths, $\Delta\nu_{\frac{1}{2}}$, plotted against J for the three pressures of HCN used. Obviously, the individual measurements for a given pressure show a very large spread, which in large part is to be expected from the error considerations discussed above. Greater average consistency than about 10 percent can scarcely be hoped for under the photographic conditions obtaining in this region of the infrared. Striking, however, is the fact that superposed on this random variation from line to line there is a marked tendency, unmistakable at all three pressures, toward maximum half-widths in the expected region.

In connection with a narrowing for high J values such as Herzberg and Spinks[1] thought to be present, it should be emphasized that the intensity at $J=20$ and above is falling off very rapidly, making it impossible to measure lines much farther out. Up to $J=24$, however, as is clear from Fig. 2, no narrowing is evident, the tendency, if any, being to slightly wider lines at the high values of J.

5. Effect of Slit Width

In most absorption work at high dispersion in the photographic infrared, slit widths of about 0.05 mm are found to give the best results, as regards intensity, resolving power, etc. The disagreement in the measured rate of broadening from two earlier investigations,[1,2] as has been mentioned, gave rise to the question of whether this disagreement could be attributed entirely to the difference in slit widths used. The evidence found is certainly in the affirmative, and both previous results are confirmed for the conditions prevailing. Fig. 1 and Fig. 3 show clearly how the measured, or apparent, rate of broadening decreases as the slit is widened from 0.04 mm to 0.06 mm, the curves of Fig. 1 intersecting each other in a very indefinite region, between 30 and 50 cm pressure. This is confirmed by other data, such as that obtained by Watson[8] from the plates of Herzberg and Spinks, and by Watson and the author.[2] An interesting consequence, then, is that for pressures above this region, the measured half-width decreases as the slit width is increased from 0.04 mm to 0.06 mm. Nothing can be said concerning the quantitative relation between the slopes for the three slit widths in Fig. 1, but qualitatively their relative order is definitely established.

It is quite possible that for sufficiently narrow slits, the measured half-widths and rate of broadening would approach definite limiting values, in which case the curves of Fig. 1 would approach a definite slope, somewhat greater than the one shown for 0.04 mm, and those of Fig. 3 would become horizontal at some point below 0.04 mm. Because of this uncertainty the lines of Fig. 3 have not been extrapolated beyond the observed points.

From the work of Stockbarger and Burns[10] it appears that the effect of slit width on observed

[9] W. W. Watson and H. Margenau, Phys. Rev. **51**, 48 (1937).

[10] D. C. Stockbarger and L. Burns, J. Opt. Soc. Am. **23**, 379 (1933).

line width may depend to some extent on the particular wave-length used. (The wave-length enters linearly in the expression for optimum slit width.) It must, of course, be remembered that this work was done only for narrow emission lines, and, so far as the author is aware, no comparable investigation has been made for the case of broad lines in absorption, which are in question here. Moreover, in infrared absorption work, slits much wider than the narrow optimum slits calculated by Stockbarger and Burns for emission work are generally used. However, some effect of wave-length is to be expected, although its nature and exact extent are unknown. It may be stated, then, that comparison of half-widths at the same slit widths for bands of widely different wave-length is probably risky. Just what conditions must obtain for reliable comparison is a matter of question. These considerations may enter in when the 7920A NH_3 band is compared with the 1.038μ HCN band, and when the two H_2O bands are compared with each other. But for comparison of the H_2O bands and the longer wave-length NH_3 band with HCN, all are certainly nearly enough in the same spectral region so that any error from this source is overshadowed by the large inherent errors in measurement.

The value of the broadening per atmosphere for HCN measured from the plates of Herzberg and Spinks, using a slit of 0.05 mm, is 1.17 cm^{-1}. The value found for the case of 0.04 mm slit in the present work is 1.22 cm^{-1}. These two, within the approximate errors in each, are sensibly the same, indicating that what might be called the "apparatus width" was about the same in both cases. The conclusion is, then, that for comparison of pressure broadening effects in one band, or in several bands in the same region of the spectrum, at the slit-widths generally used in this work, care must be taken that all comparisons involve the same apparatus width, or, preferably, the same apparatus and slit width.

I wish to express my appreciation to Professor W. W. Watson for much helpful advice and for his many suggestions in connection with this work, and to Professor H. Margenau for valuable discussions on several points.

MAY 1, 1937 PHYSICAL REVIEW VOLUME 51

Drift of Ions and Electrons in a Magnetic Field

LEWI TONKS
General Electric Company, Schenectady, New York
(Received March 6, 1937)

Townsend's equations for the drift motion of ions under the combined action of magnetic field, concentration gradient and electric field are shown to be inconsistent with the Boltzmann equation. Other relations according to which a gradient contributes a perpendicular component to the drift are shown to be satisfactory in this respect. It is proved that such contributions exist and the fallacy in the demonstration that they do not exist is exposed. These equations lead to the simple result that the drift speed is the same as would occur if the components of concentration gradient and electric field perpendicular to it, as well as the magnetic field itself, did not exist. All of the equations are only semiquantitatively correct and are subject to refinement by a more adequate statistical treatment.

THE most complete analysis of the motion of ions through a gas in the presence of a magnetic field has been given by Townsend.[1, 2] Basing his definition of diffusion coefficient upon the time rate of increase of the mean square of the distance of particles from a line, he derived the fact that the coefficient of diffusion K_H at right angles to a magnetic field is given by

$$K_H = K(1+\omega^2\tau^2)^{-1}, \qquad (1)$$

where K is the normal coefficient, $\omega = eH/mc$ and

[1] Townsend, Proc. Roy. Soc. **86**, 571 (1912).
[2] Townsend, *Electricity in Gases*, §§ 89–92.

τ is the mean free time between impacts, and $e=-4.775\times10^{-10}$ for electrons.

This result he applied directly to the component drifts of ions in a concentration gradient, putting

$$nu/K_H=-\partial n/\partial x,\qquad nv/K_H=-\partial n/\partial y \tag{2}$$

for a magnetic field in the z direction, concentration n and drift components u and v.

Further analysis in the case where ion density is constant but an electric field X (in the x direction) causes drift of the ions led him to the equations

$$nu/K_H=enX/kT,\qquad nv/K_H=-\omega\tau enX/kT. \tag{3}$$

Combination of the two cases then gave for the simultaneous action of magnetic and electric fields and concentration gradient

$$nu/K_H=-\partial n/\partial x+enX/kT, \tag{4}$$

$$nv/K_H=-\partial n/\partial y-\omega\tau enX/kT. \tag{5}$$

Townsend used these relations to interpret a series of experiments in some of which ions moved under the threefold action of electric field, magnetic field and concentration gradient, and the results were consistent with the above theory. These experiments, however, did not constitute a complete test to the extent that in the plane perpendicular to the magnetic field only drift in the line of the concentration gradient and not perpendicular to it was observable. How important such a drift component is for the theory will appear below.

From the realm of electric conduction in gases we get direct evidence that Eqs. (4) and (5) must be modified. An anode arm (radius 14.5 cm) of a steel tank rectifier in which the condensed mercury temperature is 50°C easily carries a peak of over 2500 amperes. Allowing for temperature rise in the mercury vapor we estimate the electron's mean free path to be 1.3 cm and its mean velocity to be 6.24×10^7 cm/sec. ($T_e=10^4$ deg K) whence τ is 2×10^{-8} sec. At the anode arm wall the value of ω is 6×10^8 giving an $\omega\tau$ value of 12. By Eq. (1) the effect would be to cut down the current flow near the wall to less than 1 percent of its "normal" value, thus confining the arc current to a narrower column. The decrease in radius would further augment the magnetic field and hence the flow resistance at the edge of the flow region and this progressive constriction would make conduction of current impossible. Only a strong reversal of the normal transverse potential gradient, i.e., a strong field drawing the electrons (instead of the ions) radially outward, could account for the high longitudinal conductivity in this case. But such a concept leads to other difficulties.

More serious than this is a fundamental theoretical contradiction to which these equations lead. To show this we shall adopt another pair of equations whose theoretical consistency will be demonstrated, after which it will be evident that the present equations are theoretically wrong.

Strangely enough, these formulas

$$nu/K=-\partial n/\partial x+\omega\tau nv/K, \tag{6}$$

$$nv/K=-\partial n/\partial y-\omega\tau nu/K, \tag{7}$$

$$nw/K=-\partial n/\partial z, \tag{8}$$

which are not new, have been rejected by Townsend by an argument the fallacy of which will be demonstrated later.

In support of these relations it is to be noted that a drift velocity v constitutes a current in the y direction, which, interacting with the magnetic field, gives rise to a transverse force which, in turn, acting upon the ions, creates an x component of drift. The second terms of the right members of Eqs. (7) and (8) yield just such contributions but Eqs. (2) are entirely deficient in this respect.

Solving (6) and (7) for u and v we find

$$nu/K_H=-\partial n/\partial x-\omega\tau\partial n/\partial y, \tag{6'}$$

$$nv/K_H=-\partial n/\partial y+\omega\tau\partial n/\partial x, \tag{7'}$$

differing from Eqs. (2) in the inclusion of transverse gradients.

That these equations are consistent with the definition of $K_H=(1/4)d(\rho^2)_{Av}/dt$, where ρ is the distance of an ion from the z axis, follows immediately by using the same method employed by Townsend, for in applying the equation of continuity

$$\partial n/\partial t=-\partial(nu)/\partial x-\partial(nv)/\partial y-\partial(nw)/\partial z$$

the terms containing the transverse gradients form cross derivatives which cancel each other.

The conclusive demonstration of the validity of the Eqs. (6′) and (7′) follows upon the combination of these with the mobility equations (3) to give:

$$nu/K_H=(neX/kT-\partial n/\partial x)-\omega\tau\partial n/\partial y, \quad (9)$$

$$nv/K_H=-\partial n/\partial y-\omega\tau(neX/kT-\partial n/\partial x). \quad (10)$$

Suppose now that the ion-containing gas is in a potential field of cylindrical symmetry about the z axis. In cylindrical coordinates, using R for radial field, Eqs. (9) and (10) become:

$$nu_r/K_H=(neR/kT-\partial n/\partial r)-\omega\tau\partial n/r\partial\theta, \quad (11)$$

$$nu_\theta/K_H=-\partial n/r\partial\theta-\omega\tau(neR/kT-\partial n/\partial r). \quad (12)$$

In the steady state, and either in the presence or absence of a magnetic field parallel to z, these relations must be consistent with the Boltzmann equation. In the steady state not only u_r and u_θ but also $\partial n/\partial_\theta$ are zero. In the absence of magnetic field ω is zero and Eq. (12) becomes zero in all its terms, but Eq. (11) becomes

$$-\partial n/\partial r+neR/kT=0.$$

This is a form of the Boltzmann equation. In the presence of a magnetic field Eq. (12) also reduces to this form, but only by virtue of the presence of the cross-drift terms which were excluded by Townsend. Actually, the omission of these terms leads to the inconsistent relation

$$0=nu_\theta/K_H+\partial n/r\partial\theta+\omega\tau neR/kT,$$

in which all terms but the last are zero.

The fallacy in the argument[1] which led to the exclusion of the cross-drift terms has now to be exposed.

Imagine an ion-containing gas with an ion concentration independent of x and z and increasing with y in a magnetic field parallel to the z axis. Let P of Fig. 1 be an imaginary plane parallel to the yz plane. To either side of P and equidistant from it we consider two equal infinitesimal volumes, A and B, which lie at the same height above the xz plane.

The argument is that though the paths of ions which made their last collisions within A and B are curved as indicated in the figure, those paths reaching to the right from A are curved

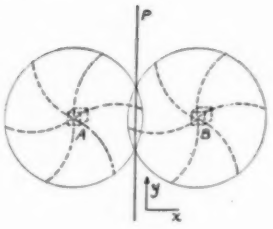

FIG. 1.

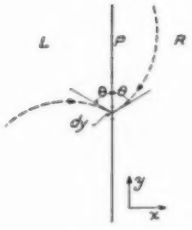

FIG. 2.

to the same degree as those going to the left from B, so that symmetry is preserved; equal numbers cross P in the two directions and there is no drift parallel to x.

The error lies in the failure to consider the relative positions of all portions of the two regions in which ions must have suffered their last collisions if they are to cross a given element ds of P from either one direction or the other.

For simplicity let us neglect motion parallel to z and suppose that all ions travel with the same speed in the xy plane, so that they describe arcs of equal curvature.

Let us now compare the flow of ions across an element dy of P in Fig. 2 from the two sides according to the angle that their paths make at crossing with the positive y direction. Thus in the figure the number of ions from L whose path angles at dy lie within θ, $d\theta$ limits are to be compared with the R ions in the same limits. In the absence of a concentration gradient the two fluxes are equal, for the magnetic field does not disturb the uniformity of the angular distribution of velocity. But the circumstance that on the average, for any θ, the R ions come from larger values of y means that if there is a concentration gradient, n increasing with y, there is consequently a greater flow across dy from R to L than *vice versa*. That some of the R ions, particularly for small θ, have come from impacts on the L side, and *vice versa* for large θ, creates no real difficulty, for the first crossing of P in either case will be counted in another element of P when the summation over a finite area of P is made.

It is now apparent that the fallacy in Townsend's treatment is that it fails to recognize that the center of flow of ions crossing P from B lies below B while the center of flow from A lies

above, which is the very factor taken into account in the present argument.

An interesting and significant deduction follows from the relations which have here been justified. In more general form, including an electric field component parallel to the y axis as well as to the x axis, Eqs. (9) and (10) become

$$nu/K_H=(neX/kT-\partial n/\partial x)+\omega\tau(neY/kT-\partial n/\partial y), \quad (13)$$

$$nv/K_H=(neY/kT-\partial n/\partial y)-\omega\tau(neX/kT-\partial n/\partial x). \quad (14)$$

(With the equations in this form it becomes evident that considerations of symmetry and the Boltzmann equation require that electric field and concentration gradient should not appear singly but only in the present combination.)

Now suppose that concentration gradients and field components have so adjusted themselves that there is no net motion in the y direction. Eqs. (13) and (14) then reduce to

$$nu/K_H=\omega\tau(neY/kT-\partial n/\partial y)+(neX/kT-\partial n/\partial x), \quad (15)$$

$$neY/kT-\partial n/\partial y=\omega\tau(neX/kT-\partial n/\partial x). \quad (16)$$

Combining to eliminate $(\partial n/\partial y-neY/kT)$ and using Eq. (1), gives the simple result

$$nu/K=neX/kT-\partial n/\partial x. \quad (17)$$

Thus, if at any point in the gas we resolve the drift into two components, one in the magnetic field direction and the other perpendicular thereto, it is evident that each component drift takes place with respect to the component gradient and field in its direction as if those gradients and fields alone were acting, with no magnetic field present. The same is then true of the resultant drift with respect to the components of gradient and field which lie in its direction.

Relative to fixed directions in space, the conclusion appears in a different form: If the combined action of concentration gradient and electric field produces no drift motion in some direction perpendicular to the direction of the magnetic field, then at right angles to both directions the drift is the same as would result simply from the existing gradient and field components in that direction in the absence of the magnetic field.

This simplifying theorem finds direct application in the theoretical treatment of the effects of a magnetic field on the positive column of low pressure arcs. With a magnetic field perpendicular to the column axis the no-drift condition obtains in the direction of a tube radius and unimpeded longitudinal flow then occurs.

Some unpublished experimental work by T. J. Killian, done while working in this laboratory, indicates that this ideal condition is not completely fulfilled, for there is an increase in arc gradient with the application of a transverse magnetic field. It is to be noted, however, that the increase in resistance is far less than corresponds to a decrease in electron mobility from Ke/kT to K_He/kT and the redistribution of potential and electron concentration in the column cross section are at least in qualitative agreement with the newer equations. It should be noted too that other factors not covered by the present theory such as the increase in current density in the arc may contribute to the discrepancy.

Finally, we should recognize that while the equations involving ω and inclusive of Eq. (17) are roughly correct, their original derivation rests upon only approximate methods of averaging and without full regard to the maintenance of a constant distribution function for the ions.[3] We may, therefore, expect a more accurate analysis to introduce small numerical factors and even higher order terms in $\omega\tau$. As a result, a coefficient differing somewhat from unity and varying with $\omega\tau$ will undoubtedly appear as a multiplier of the left member of Eq. (17). Nevertheless, this expression in its present form promises to be of considerable value in analyzing magnetic effects in arcs.

[3] L. G. H. Huxley, Phil. Mag. **23**, 210 (1937) attempts to give a more exact analysis, without, however, setting up the distribution function. The present author has made some similar calculations leading to different results. Any calculations which are not based on the distribution function are probably of doubtful accuracy. This has been true for no magnetic field and is all the more likely with one. Huxley's final Eqs. (27) also omit the indispensable transverse gradient terms.

Long Range Interactions Between Dipole Molecules

HENRY MARGENAU AND DANA T. WARREN
Sloane Physics Laboratory, Yale University, New Haven, Connecticut
(Received February 23, 1937)

The first-order van der Waals forces between symmetrical top molecules which carry a dipole along their figure axis are calculated. Their strength is compared with that of other interactions, and found to be greater than London's second-order effect for linear dipoles over the main part of the range of the latter. A simple preliminary theory of the effect of these forces on the width of spectral lines in bands of polyatomic molecules is given, and it is shown that they lead to results of the correct order of magnitude.

THE van der Waals forces between dipole molecules have been worked out on the basis of quantum mechanics, and classified in a systematic manner, chiefly by F. London.[1] He finds that, in general, greatest importance is to be ascribed to the attractive forces arising from the dispersion effect, the electronic perturbations of high frequency. This is common to all molecular interactions and is independent of the presence of permanent poles. The potential due to dispersion forces varies (asymptotically) like $-1/R^6$, R being the distance between interacting partners.

Besides this, there are the following effects specifically connected with dipole molecules: (1) The induction of an additional dipole moment due to the permanent moment of a partner, producing a small potential proportional asymptotically to $-1/R^6$. (2) The effect of molecular alignment which depends on the rotational quantum number and hence on the temperature distribution of the molecules. Its potential varies, at large distances, as $\pm 1/R^6$, but for close approach becomes proportional to $-1/R^3$, and relatively strong, for molecules in the lowest rotational state. The transition from the $1/R^6$ to the $1/R^3$ law takes place at distances of approach for which the perturbation energy becomes comparable with the normal separation of the rotational levels. (3) Resonance forces due to the possibility of exchanging a quantum of radiation, come into play when two interacting partners have rotational quantum numbers, J, differing by unity. They correspond to first-order interactions, have a potential proportional to $\pm 1/R^3$, and produce a symmetrical splitting of the rotational levels, which are, however, in general also lowered as a result of the other types of interaction mentioned above. These forces, clearly, have therefore the longest range, but their average over all orientations of the molecules is zero. Thus they are unimportant when interest is confined to properties of a dipole gas which depend on long time averages. But phenomena like the broadening of spectral lines depend on them quite essentially.

The present classification is sufficient as long as one is dealing with linear or diatomic dipole molecules, which indeed London chose as the model for his calculations. These exhibit no first-order Stark effect; hence their interactions bring about no removal of space degeneracy. With polyatomic dipoles the situation is different, for the symmetrical top gives rise to a linear Stark effect. We expect, therefore, a first-order splitting of the rotational levels on approach of two symmetrical top molecules. A calculation of this effect will be presented below. Although the treatment has not been extended to asymmetrical molecules, the results obtained will hold qualitatively for such cases as well.

We suppose that the top carries a dipole of moment μ along its figure axis. If the axes of two similar tops make angles θ_1 and θ_2 with the line, of length R, joining the molecular centers, their azimuths being φ_1 and φ_2, then the classical perturbation energy is

$$V = -\mu^2/R^3[2\cos\theta_1\cos\theta_2 - \sin\theta_1\sin\theta_2\cos(\varphi_1-\varphi_2)]. \quad (1)$$

To set up the secular equation it is necessary to calculate the matrix elements of (1) between the unperturbed degenerate states of the top. These depend on the three quantum numbers J, K, M

[1] F. London, Zeits. f. Physik **63**, 245 (1930).

corresponding to the three Eulerian degrees of freedom θ, φ, χ.[2] V does not contain χ; the matrix elements are therefore diagonal in K.

If the two interacting molecules have quantum numbers J, K, M and J', K', M', the unperturbed function representing their combined state is

$$\psi_{J,K,M;J',K',M'} = N(J,K,M)N(J',K',M')\Theta_{J,K,M}(\theta_1)\Theta_{J',K',M'}(\theta_2)e^{i(M\varphi_1+M'\varphi_2+K\chi_1+K'\chi_2)},$$

where the N's are normalizing factors. We require the matrix elements for fixed values of J, K, J', K', between the various permitted sets M_i, M'_i and M_j, M'_j. Since M runs from $-J$ to $+J$ and M' from $-J'$ to $+J'$, our secular determinant will have $(2J+1)(2J'+1)$ rows and columns. In forming the elements, the integrations over the χ's and φ's can be carried out immediately, the result at that stage being:

$$\begin{aligned} V_{J,K,M_i,J',K',M'_i;J,K,M_j,J',K',M'_j} &= -(\mu^2/R^3)N(M_i)N(M'_i)N(M_j)N(M'_j)\{32\pi^4 I_1(J,K,M_i)I_1(J',K',M'_i)\delta(M_j,M_i)\delta(M'_j,M'_i) \\ &\quad -8\pi^4 I_2(J,K,M_i)I_2(J',K',M'_i)\delta(M_j,M_i-1)\delta(M'_j,M'_i+1) \\ &\quad -8\pi^4 I_3(J,K,M_i)I_2(J',K',M'_i)\delta(M_j,M_i+1)\delta(M'_j,M'_i-1)\} \end{aligned} \quad (2)$$

with the following definitions of the integrals:

$$\left.\begin{aligned} I_1(J,K,M_i) &= \int_0^\pi \cos\theta\,\Theta^2_{J,K,M_i}\sin\theta\,d\theta = 2\int_0^1 (1-2x)\,\Theta^2_{J,K,M_i}(x)\,dx, \\ I_2(J,K,M_i) &= \int_0^\pi \sin\theta\,\Theta_{J,K,M_i}\Theta_{J,K,M_i-1}\sin\theta\,d\theta = 4\int_0^1 x^{\frac{1}{2}}(1-x)^{\frac{1}{2}}\Theta_{J,K,M_i}(x)\,\Theta_{J,K,M_i-1}(x)\,dx, \\ I_3(J,K,M_i) &= \int_0^\pi \sin\theta\,\Theta_{J,K,M_i}\Theta_{J,K,M_i+1}\sin\theta\,d\theta = I_2(J,K,M_i+1). \end{aligned}\right\} \quad (3)$$

The Θ functions are Jacobi polynomials, and the transformation from θ to x is the usual one: $x=\frac{1}{2}(1-\cos\theta)$. I_1 is the integral which appears in the theory of the linear Stark effect; it has been calculated by Reiche and Rademacher, and by Manneback.[2] Its value is given by

$$N^2(M_i)I_1(J,K,M_i) = KM_i/(4\pi^2 J(J+1)). \quad (4)$$

We have calculated I_2 by the reduction method as explained by Reiche and Rademacher. The details of the calculation are straightforward and hardly of sufficient interest to be set down here. The result is

$$N(M_i)N(M_i-1)I_2(J,K,M_i) = \frac{\pm K[(J-M_i+1)(J+M_i)]^{\frac{1}{2}}}{4\pi^2 J(J+1)}. \quad (5)$$

Here the $-$ sign holds if the numerically greater of K or M is positive, the $+$ sign if it is negative, or if $K=-M$. (Except for its sign, Eq. (5) may be checked against Dennison's[2] intensity formulae to which it is related by the definition (3) of I_2.)

On putting these values of I_1, I_2 and I_3 into (2) we find, leaving off the fixed subscripts from V,

$$\begin{aligned} V_{M_i,M'_i;M_j,M'_j} = \frac{\mu^2}{R^3}\frac{KK'}{J(J+1)J'(J'+1)}\{&-2M_iM'_i\delta(M_j,M_i)\delta(M'_j,M'_i) \\ &\pm\tfrac{1}{2}[(J-M_i+1)(J+M_i)(J'-M'_i)(J'+M'_i+1)]^{\frac{1}{2}}\delta(M_j,M_i-1)\delta(M'_j,M'_i+1) \\ &\pm\tfrac{1}{2}[(J+M_i+1)(J-M_i)(J'-M'_i+1)(J'+M'_i)]^{\frac{1}{2}}\delta(M_j,M_i+1)\delta(M'_j,M'_i-1)\}. \end{aligned} \quad (6)$$

[2] Cf. the familiar papers by Reiche and Rademacher, Manneback, Kronig and Rabi, and Dennison. The present notation is illustrated in Pauling and Wilson, *Introduction to Quantum Mechanics*, p. 276. For references cf. D. M. Dennison, Rev. Mod. Phys. 3, 280 (1931).

With the use of these matrix elements we wish to determine the roots ΔE of the secular equation, $\det(V_{ij}-\Delta E\delta_{ij})=0$. If arranged properly, all elements of the determinant will be zero except those in, and adjacent to, the principal diagonal. The most convenient way of factoring the determinant is the following.

We observe by inspecting (6) that a state function characterized by $M_iM'_i$ gives a non-vanishing matrix element only by combination with another state $M_jM'_j$ if $M_j+M'_j=M_i+M'_i$. Thus if the states $M\,M'$ are divided into sets so that, for each set, $M+M'$ is constant, and if we number the members of each set consecutively, the determinant consists of diagonal squares and hence factors immediately. Since there is but one member, namely $M=J$, $M'=J'$, in the set for which $M+M'=J+J'$, this particular state combines only with itself, and the corresponding matrix element is a root of the secular equation. Closer analysis shows that it is not in general the largest root, but that it lies near the edge of the pattern. It may therefore serve as an indication of the magnitude of the splitting. Its value is obtained, of course, from (6) by putting $M_i=M_j=J$, $M'_i=M'_j=J'$, which yields

$$\Delta E_1=-\frac{2\mu^2}{R^3}\frac{KK'}{(J+1)(J'+1)}. \tag{7}$$

This is a double root, because it results also from the diagonal element of the state $M=-J$ and $M'=-J'$. (7) suggests at once the formula for the linear Stark effect

$$\Delta E_1=\mu F\frac{KM}{J(J+1)}$$

and shows its relation with the interaction here considered, since the greatest Stark displacement is given by $\mu FK/(J+1)$ which is very similar to (7).

The arrangement of the elements in sets just discussed causes the determinant to consist of square blocks along the diagonal, increasing in size up to the $(2J+1)^{\text{rst}}$ which has the maximum number $(2J+1)$ of rows and columns.[3] They continue to have this size up to the $(2J'+1)^{\text{rst}}$ block and then decrease again. The entire determinant is symmetrical about the midpoint of the principal diagonal. Hence all roots, except those arising from the central block, are double.

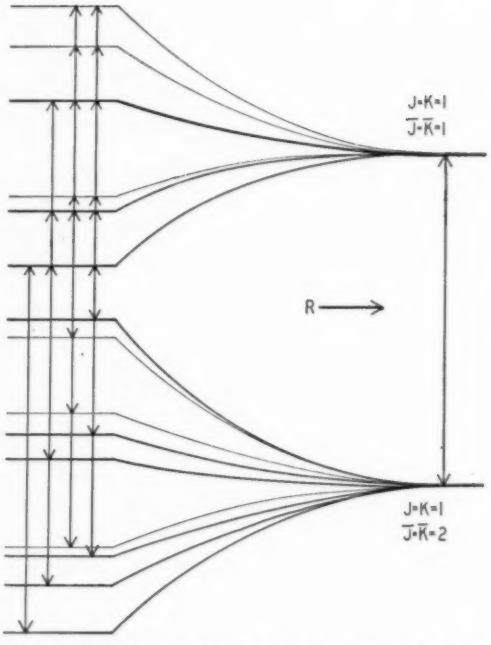

FIG. 1. Splitting of energy levels on approach of two molecules, one in the state $J=K=1$, the other in state $J'=K'=1$ for the upper diagram, $J'=K'=2$ for the lower diagram. Light lines indicate single levels, heavy lines double levels. The arrow heads on the vertical lines mark the allowed transitions (40 in all).

In the general case, many of the roots are irrational, and no closed formula can be given for the splitting of the levels. But it can always be computed with relative ease by the method just outlined. As seen from (6), the lowest level ($J=0$) undergoes no perturbation of the kind in question, because its K value is zero. For the case of two tops, with $|K|=|K'|=1$, each having one quantum of rotational energy, the roots are

$$-2,\ -1,\ 1-\sqrt{3},\ +1,\ +2,\ 1+\sqrt{3}$$

in units $\mu^2/4R^3$. The first, second and fourth of these are double, the others single. This situation is illustrated in Fig. 1. In Fig. 1 we have also plotted as another example the splitting of the levels occurring when two molecules, one with $J=1$, the other with $J'=2$, approach each other.

[3] We are assuming here that $J'>J$. There are thus altogether $2\sum_{n=1}^{2J}n+(2J'-2J+1)(2J+1)=(2J+1)(2J'+1)$ rows.

That the present effect cannot take place for molecules with only one moment of inertia is clear. The eigenfunctions and energies of a symmetrical top go over into those of a linear molecule if we let K be zero. But then all the matrix elements (6) vanish.

II

To calculate the second-order interactions between two symmetrical tops would not be difficult. But one would expect the result to be very similar to that obtained by London[1] for diatomic molecules. Let us then, in order to arrive at an estimate of relative magnitudes, compare the present results with those of London. For the lowest rotational state, the second-order forces are the only ones present. If $J=1$, $J'=1$, however, the first-order forces here computed are generally predominant. To illustrate this we recall that, for $|K|=|K'|=1$, (taking the second largest root)

$$|\Delta E^{(1)}|=\frac{1}{2}\frac{\mu^2}{R^3}, \tag{8}$$

while

$$|\Delta E^{(2)}|=\frac{1}{6B}\frac{\mu^4}{R^6}, \quad B=\frac{h^2}{8\pi^2 A}. \tag{9}$$

Both these formulae are valid only as long as the perturbation energy is considerably smaller than the normal separation of the lines; i.e., if $\Delta E<B$. What happens on closer approach is discussed by London. Now

$$\frac{|\Delta E^{(1)}|}{|\Delta E^{(2)}|}=3B\frac{R^3}{\mu^2}.$$

If we assume $B=1.8\times10^{-15}$ ergs, $\mu=1.5\times10^{-18}$ e.s.u., this ratio is unity for $R\approx7$A. Thus for distances greater than this, $\Delta E^{(1)}$ predominates, and $\Delta E^{(2)}$ becomes rapidly insignificant in comparison with it. It might also be remarked that at $R=7$A, ΔE is already greater than B, so that there is in this example no range at all in which formula (9) is both accurate and important. This situation is quite general for large values of K and K', as may be seen from (7).

The equation of state of dipole gases is not affected by the interactions considered in this paper, except at low temperatures. It is known that for ordinary temperatures, at which most measurements are made, the sum of state is sufficiently well approximated by the classical phase integral.

The influence on the broadening of molecular band lines should be more appreciable. The present inquiry has indeed been stimulated by a suggestion due to Watson[4] who concludes, on the basis of a survey of experimental data regarding pressure effects, that the lines of some polyatomic molecules seem more effectively broadened than those of linear ones. The experimental data are as yet very qualitative. Great difficulties arise from lack of resolution of the lines and from the fact that an exact assignment of quantum numbers has not been achieved. Moreover, in the case of parallel type bands, where the structure is most intelligible, the band lines are composite, consisting of a superposition of lines for all values of K. Since the splitting of the levels is proportional to K, the broadening of a spectral line is due to a superposition of patterns of the type shown in Fig. 1, but on different scales. For each value of K, the actual pattern is further greatly complicated by the velocity effect.

To get a rough measure of line widths, we first calculate the average spread of a pattern for given J, J', K, K'. Let the roots of the secular determinant whose matrix elements are given by (6), if measured in units of

$$\frac{\mu^2}{R^3}\frac{KK'}{J(J+1)J'(J'+1)},$$

be denoted by $\epsilon_1, \epsilon_2, \cdots \epsilon_n$, where

$$n=(2J+1)(2J'+1),$$

and each root is counted as many times as it occurs. Then the secular equation becomes

$$\det(V_{ij}-\epsilon\delta_{ij})=\prod_{i=1}^{n}(\epsilon-\epsilon_i)$$
$$=\epsilon^n-a\epsilon^{n-1}+b\epsilon^{n-2}-\cdots+x=0. \tag{10}$$

The form of the determinant shows at once that

$$a=\sum_i\epsilon_i=\sum_i V_{ii}.$$

[4] W. W. Watson, J. Phys. Chem. **41**, 61 (1937), especially symposium discussion in later issue. We wish to express our thanks to Professor Watson for many interesting discussions.

But the sum of the diagonal elements of (6) is

$$\sum_{M_i=-J}^{J}\sum_{M'_i=-J'}^{J'} 2M_iM'_i=0.$$

We see thus that there is no shift in the weighted mean of the perturbed energy levels. Next, let us find the root mean square displacement. Consider the coefficient b of (10).

$$b=\sum_{i>j}(V_{ii}V_{jj}-V_{ij}^2)$$
$$=\tfrac{1}{2}\sum_i\epsilon_i\sum_j\epsilon_j-\tfrac{1}{2}\sum_i\epsilon_i^2=-\tfrac{1}{2}\sum_i\epsilon_i^2. \qquad (11)$$

On the other hand,

$$\sum_{i>j}(V_{ii}V_{jj}-V_{ij}^2)=\sum_{i,j}\tfrac{1}{2}V_{ii}V_{jj}-\sum_i\tfrac{1}{2}V_{ii}^2-\sum_{i>j}V_{ij}^2.$$

If now we insert values from (6) we obtain

$$b=2\sum_{M_i,M_j}\sum_{M'_i,M'_j}M_iM'_iM_jM'_j-2\sum_{M_i,M'_i}M_i^2M'^2_i$$
$$-\tfrac{1}{4}\sum_{M'_i,M'_i}(J^2-M_i^2+J+M_i)(J'^2-M'^2_i+J'-M'_i)$$
$$=0-\tfrac{2}{3}J(J+1)(2J+1)J'(J'+1)(2J'+1)$$
$$-\tfrac{1}{4}[(J^2+J)(2J+1)-\tfrac{1}{3}J(J+1)(2J+1)]$$
$$\times[(J'^2+J')(2J'+1)-\tfrac{1}{3}J'(J'+1)(2J'+1)]$$
$$=-\tfrac{1}{3}J(J+1)(2J+1)J'(J'+1)(2J'+1).$$

By reason of (11), this expression, if multiplied by -2, is the sum of the squares of all the roots. To get the root mean square spread of the levels, we divide by n and extract the square root. Hence

$$(\epsilon_i^2)_{\text{Av}}^{\frac{1}{2}}=[\tfrac{2}{3}J(J+1)J'(J'+1)]^{\frac{1}{2}},$$
$$[(\Delta E)^2]_{\text{Av}}^{\frac{1}{2}}=\left(\frac{2}{3}\right)^{\frac{1}{2}}\frac{\mu^2}{R^3}\frac{KK'}{[J(J+1)J'(J'+1)]^{\frac{1}{2}}}. \qquad (12)$$

Inasmuch as the present type of interaction causes no mean shift, and is proportional to R^{-3}, it is very similar to resonance forces between atoms. But if spectral lines are broadened by resonance interactions for which the potential has the form

$$\Delta E=\pm B/R^3,$$

the lines are known[5] to have an approximate half-width $\Delta\nu_{\frac{1}{2}}\approx\frac{4}{3}\pi^2B/h\cdot N$, where N is the number of atoms per cc. Now while it is indefensible in detail to identify the splitting patterns calculated in part I with *any* pattern which has the same standard deviation, an approximate estimate of the line width may certainly be obtained by identifying the constant B in the law for resonance forces with the constant

$$\left(\frac{2}{3}\right)^{\frac{1}{2}}\frac{\mu^2}{h}|KK'|[J(J+1)J'(J'+1)]^{-\frac{1}{2}}$$

in (12). We find

$$\Delta\nu_{\frac{1}{2}}\approx\pi^2\frac{\mu^2}{h}N|KK'|[J(J+1)J'(J'+1)]^{-\frac{1}{2}}. \qquad (13)$$

This is, approximately, the line width caused by the effect here considered. Its isolation from other effects is, of course, an idealization, since line widths due to various causes may not be simply added. But at lower pressures it is likely to be the dominant cause of line broadening in polyatomic molecules.

Formula (13) refers only to one set of values J, K, J', K', whereas a spectral line involves two, the one just mentioned, and $J\pm1$ or 0, $K\pm1$ or 0, J', K'. The diffuseness of both will appear in the line. The exact manner in which they are to be combined is complicated. For the present purpose it will suffice to regard the quantum numbers appearing in (13) as mean values for the two states in question, since they do not differ by more than unity. The breadth is seen to depend on J, J' in a different way than it does for linear molecules.[6]

In any practical application of formula (13) to the spectra of polyatomic molecules one is confronted with the difficulty that the quantum numbers are not in general known, and that a single line may involve numerous different values of K. It will be observed, however, that the factor $|KK'|[J(J+1)J'(J'+1)]^{-\frac{1}{2}}$ is always smaller than unity and has a weighted mean around $\frac{1}{2}$. Remembering this, the effect (13) is found to be about 20 times as weak as the self-broadening of atomic resonance lines.

[5] H. Margenau and W. W. Watson, Rev. Mod. Phys. **8**, 43 (1936).

[6] Line widths for linear dipole molecules were discussed recently by W. W. Watson and H. Margenau, Phys. Rev. **51**, 48 (1937).

For NH_3 at atmospheric pressure, the value of $\Delta\nu_i \approx \frac{1}{2}\pi^2(\mu^2/h)N$ comes out to be 4.5×10^{10} sec.$^{-1}$ $=1.5$ cm^{-1}. Cornell,[7] in measurements made in this laboratory, finds an average half-width of 1.45 cm^{-1} in the 7920A band of NH_3, and of 0.81 in the 10,230A band. The agreement as to order of magnitude is gratifying in view of the present inaccuracies in both experiment and theory.

[7] S. D. Cornell, Phys. Rev. this issue. We are indebted to Mr. Cornell for the use of his material before publication.

MAY 1, 1937 PHYSICAL REVIEW VOLUME 51

Vapor Pressure of Caesium by the Positive Ion Method

JOHN BRADSHAW TAYLOR* AND IRVING LANGMUIR
General Electric Company, Schenectady, New York

(Received February 23, 1937)

The positive ion currents from pure tungsten filaments in saturated caesium vapor at bulb temperatures from −35°C to +73°C were measured for filament temperatures from 1000° to 1800°K. The results were corrected for the cooling effect of the leads and for photoelectric emission from the caesium film on the platinum deposited on the bulb which was used as an ion collector. The vapor pressures in mm of Hg are given for solid Cs ($T<302$°K) by

$$\log_{10} p_S = 10.5460 - 1.00 \log_{10} T - 4150/T$$

and for liquid Cs ($T>302$°K) by

$$\log_{10} p_L = 11.0531 - 1.35 \log_{10} T - 4041/T.$$

The vapor pressures given by these equations are believed to be accurate to within one percent from 220° to 350°K, within 3 percent up to 600° and within about 8 percent at 1000°K.

IN some early studies of the effects of caesium vapor on thermionic phenomena[1, 2] it was observed that with a negatively charged cylinder surrounding a hot filament, positive ion currents were obtained which are independent (over wide ranges) of filament temperature and of voltage, but increase rapidly as the caesium vapor pressure is raised. These results were interpreted as indicating that every caesium atom which strikes a filament (above about 1200°K) is converted into an ion. The ion current thus serves as a measure of the pressure.

The vapor pressure p of caesium, in baryes, was found to be accurately expressed (in a temperature range from 0 to 40°C) by the equation

$$\log_{10} p = 10.65 - 3992/T. \quad (1)$$

The experimental data and the details of the method by which this equation was obtained have not been published.

These results have been criticized by Rowe[3] who compared them with measurements of Kröner[4] in the range from 250° to 350°C. Rowe found that Kröner's data could be expressed by

$$\log_{10} p_{mm} = 7.165 - 3966/T, \quad (2)$$

while Eq. (1) expressed in the same units is

$$\log_{10} p_{mm} = 7.525 - 3992/T. \quad (3)$$

The Langmuir-Kingdon (L-K) values of Eq. (3) are greater than those calculated from Kröner's data by a factor that varies from 1.85 at 27°C to 2.02 at 327°C. Rowe believed that the positive ion method is at fault, and that the discrepancy can be explained by assuming that the caesium ions that leave the filament have a double charge.

More recently Taylor and Langmuir[5] have measured the limitations of the caesium ion current by space charge in a cylindrical collector.

* Dr. Taylor died January 22, 1937.

[1] I. Langmuir and K. H. Kingdon, Phys. Rev. **21**, 380 (1923) and Science **57**, 58 (1923).

[2] I. Langmuir and K. H. Kingdon, Proc. Roy Soc. **107**, 61 (1925).

[3] H. Rowe, Phil. Mag. **3**, 544 (1927).

[4] A. Kröner, Ann. d. Physik (4) **40**, 438 (1913).

[5] J. B. Taylor and I. Langmuir, Phys. Rev. **44**, 423 (1933); see especially p. 442.

These measurements prove that the value of e/m for the ions is within 1.5 percent of that of singly charged ions. The high energy (23 volts) required to remove a second electron from a Cs atom would preclude the possibility of double ionization by thermal means.

de Boer and Dippel[6] have examined available data on caesium vapor pressure and conclude that Kröner's data, Eq. (2), give the best values and imply that the L-K values of Eq. (3) are too high by a factor of about 2, although they consider that the temperature coefficient of Eq. (3) is probably accurate. They call attention to the fact that the equations for solid and liquid caesium should be different.

de Boer in his book[7] proposes other possible explanations for the high pressures that L-K obtained. He suggests that the freeing of electrons from the ion collecting surface by ion bombardment and by photoelectric emission may have increased the current. Also he thinks that the caesium pressure in the tube may have been higher than that corresponding to the bulb temperature because of the heating of the cylinder by the radiation from the filament.

As a matter of fact, Kingdon before 1924 was thoroughly familiar with all of these possible sources of error and took precautions to avoid them. The remarkable constancy of ion current as the filament temperature and the voltage on the collector are raised was described,[1] and these facts prove that the errors suspected by de Boer could not have been present in the experiments.

Recently van Liempt[8] has reviewed all the literature on this subject and proposes the following equation for the whole temperature range from 0°C to 700°C,

$$\log_{10} p_{mm} = 6.62 - 3701/T. \qquad (4)$$

Eucken[9] has developed general equations based on the second and third laws of thermodynamics for the vapor pressures of metals, taking into account the specific heats of the liquid and vapor phases in order to get the temperature coefficient of the latent heat. For caesium, using the data of Kröner,[4] Hackspill,[10] L and K[2], he obtains

$$\log_{10} p_{mm} = 11.38 - 1.45 \log_{10} T - 4075/T. \qquad (5)$$

A comparison of the vapor pressures of caesium at various temperatures from all these equations is given in Table I.

Eucken's equation is the only one that gives reasonably good agreement with the various experimental determinations over the whole range of temperature. It should be noted that while Rowe and de Boer believe that the true vapor pressure is only 50 percent of that given by L and K, Eucken from the same experimental data obtains a value only 3 percent lower than L and K. In view of the lack of agreement shown by the data in Table I more accurate vapor pressure determinations by the positive ion method are needed, over as wide a range of temperature as possible.

The Positive Ion Method[11]

With a given pressure of caesium and with a sufficiently strong accelerating field for ions to overcome space charge, there is a critical filament temperature, T_c, above which every caesium

[6] J. H. de Boer and C. J. Dippel, Zeits. f. physik. Chemie **B21**, 273 (1933).
[7] J. H. de Boer, *Electron Emission and Adsorption Phenomena* (Cambridge University Press, 1935), p. 65.
[8] J. A. M. van Liempt, Receuil des trau chimiques d. Pay.-Bas. **55**, 157 (1936).
[9] A. Eucken, Metallwirtschaft **15**, 27, 63 (1936).
[10] L. Hackspill, Ann. chim. phys. [8] **28**, 611 (1913).
[11] Reference 5. See particularly Fig. 18, pp. 440, 445 and 447.

Table I. *A comparison of vapor pressure data for caesium. Pressures in mm of Hg.*

t °C	T °K	L-K Eq. (3) 0–60°C	Kröner Eq. (2) 250–350°C	v. Liempt Eq. (4) 0–700°C	Eucken Eq. (5) 0–700°C	T–L Eq. (16) or (17)
26.9	300	1.654×10^{-6}	8.85×10^{-7}	1.92×10^{-6}	1.603×10^{-6}	1.721×10^{-6}
126.9	400	3.51×10^{-3}	1.78×10^{-3}	2.33×10^{-3}	2.63×10^{-3}	2.74×10^{-3}
226.9	500	0.348	0.1714	0.165	0.207	0.212
326.9	600	—	3.60	2.83	3.63	3.70
526.9	800	—	161.4	98.6	119.3	121.
726.9	1000	—	1581.	830.	902.	916.

atom that strikes the filament escapes as an ion. Below T_c the ion emission is very small although it is sufficiently large to be measurable at temperatures as much as 100° below T_c.

Thermodynamic considerations place an upper limit to the fraction of the incident atoms that can be ionized, but with caesium vapor in contact with pure tungsten and with an accelerating field produced by more than −45 volts on the collector this theoretical limit is 0.9998 at 1200°K and 0.9977 at 1800°K.

The critical temperature increases with increasing caesium pressure. The data of Fig. 18 of the previous paper show breaks at the critical temperature T_c which can be expressed as a function of μ_a, the rate of arrival of Cs atoms (atoms·cm^{-2}·sec.$^{-1}$) at the filament, by

$$\log_{10} \mu_a = 27.791 - 14350/T_c. \qquad (6)$$

The temperatures calculated in this way, however, are those at which the filament goes over spontaneously to the emitting condition—it does not return to the nonemitting condition until a somewhat lower temperature is reached. Eq. (6) thus gives an upper limit to T_c.

To utilize this emission to measure μ_a we must know the area of the emitting part of the filament. The portions of the filament near the leads where the temperature is below T_c give no appreciable ion emission. This difficulty can be avoided by using a tube like that described in the previous paper[5] where the guard-ring principle was used to get the emission only from the central part of the filament. With such a tube it was found that an increase in voltage from 45 to 310 did not produce a change in ion emission as great as 0.05 percent. When the filament temperature was raised above 1400° the light from the filament liberated photoelectrons from the caesium film on the cylindrical conducting walls of the tube and increased the observed current.

An analysis of the data showed that these photoelectric currents i_e increased with the filament temperature according to the relation

$$\log_{10} (i_e) = A - 12270/T, \qquad (7)$$

where the constant A depended on the condition of the caesium film. After subtracting these photocurrents it was found that the ion emission was independent of temperature within the experimental error.

There is, however, a difficulty in using the tube of the previous experiments for accurate vapor pressure measurements. If the caesium vapor in such a tube is kept saturated, sufficient caesium deposits on the folds of glass which separate the three cylindrical sections to cause considerable conductivity between the sections and to decrease the accuracy of the measurements. Local heating coils on the glass folds were used in the experiments to prevent this conductivity, but these disturb the isothermal conditions desired in the vapor pressure measurements. Experiments with metallic cylinders (as early as 1923) had shown that at low pressures relatively large amounts of caesium are adsorbed on the cylinders and are very slowly given up as the cylinders become heated by radiation from the filaments. Under such conditions it is impossible to make sure of having equilibrium vapor pressure.

Our present knowledge of the heat conductivity of tungsten[12] and of the temperature distribution[13] along the filament near the leads has greatly decreased the need for guard rings to eliminate end effects. It was therefore decided to use a tube of very simple construction having a single hair-pin filament and a deposit of platinum on the inner surface of the bulb to serve as an ion-collecting electrode. The effective length of the emitting part of the filament was determined by calculating the distance from the leads to a point where the temperature is T_c. Visual observations were also made of the positions of the points where the filaments were just visibly incandescent (about 1050°K).

Description of Tube

The tube used in all the experiments recorded in this paper was made from a cylindrical glass bulb 5 cm in diameter and 15 cm long. Near its lower end a side tube 1 cm in diameter and 5 cm long was provided to contain the caesium. Through the walls of the tube two platinum wires were sealed to provide contact with the

[12] I. Langmuir and J. B. Taylor, Phys. Rev. **50**, 68 (1936).

[13] I. Langmuir, S. MacLane and K. B. Blodgett, Phys. Rev. **35**, 478 (1930).

platinum deposit. A platinum hairpin filament was mounted in the tube and vaporized in high vacuum until the resistance between the two platinum wires fell to 20 ohms.

The platinum filament was then removed and a pure tungsten hairpin filament of 0.00513 cm diameter and 18.90 cm total length was mounted in the bulb. This filament was of wire from the same spool as that used in the previous experiments.[5] The leads were of such heavy tungsten (20 times the filament diameter) that they were not appreciably heated by conduction from the filament. The leads were about 10 cm long and extended up through narrow glass tubes which extended above the bulb so that when desired their upper ends could be kept above the level of the insulating oil in which the rest of the tube was completely immersed during the experiment.

The caesium used in the experiments had been fractionally distilled in vacuum in several stages. About 1.5 cc of it was sealed into a thin-walled spherical bulb and this was placed in a side tube (attached to the appendix) in which there was also a heavy-walled sealed glass tube containing a piece of iron. The entire tube (except the side arm containing the Cs capsule, which was held at a somewhat lower temperature to avoid attack of the glass by the Cs) was then baked one hour at 410°, one hour at 350° and one hour at 300°C. The filament was aged at 2400°K and flashed at 2800°K. The Cs capsule was then broken by dropping upon it the glass-encased iron weight which had been lifted magnetically. About half of the Cs was then slowly distilled into the appendix and the side tube containing the capsule was sealed off; very little gas was evolved (only enough to raise the pressure about 0.001 mm). The filament was run at 2500°K for 15 minutes in presence of the Cs vapor and then the tube was sealed off from the pump. The melting point of the Cs in the appendix was measured and found to be 28.6°C, indicating freedom from other alkali metals since traces of these greatly lower the melting point.

Experiments to Determine the Vapor Pressure

The tube was completely immersed in oil in a large Dewar flask, holding about 6 liters, which was constantly stirred. The platinum deposit was used to collect the ions emitted by the filament. The current was measured by a galvanometer giving 2.32×10^{-11} amperes per mm deflection. The bath temperatures were not thermostatically controlled since it was found that the drift of temperature was imperceptible during the course of measurements at any given temperature. The temperatures were read to the nearest 0.1° by a calibrated thermometer. As a precaution against any changes in T_e which might conceivably result from contamination of the filament surface by oxygen sputtered from oxide on the walls by ion bombardment, the filament was momentarily flashed at 2600°K before each set of readings at a given bath temperature. No detectable changes in ion current resulted from this flashing.

Tables II and III give typical data. The reasonably satisfactory agreement between D(calc.) $(246+i_e)$ and D(corr.) shows that the increase

Table II. *Data taken with tube at −34.5°C. T_M, temperature at center of filament calculated from A/d^1 given in the Jones-Langmuir tables.* D, galvonometer deflection (proportional to ion current). ΔL, distance (cm) to point on filament at temperature T_e (Eq. (8)) where emission begins. $L=L_0-2\Delta L$, effective filament length. $D(\text{corr.})=DL_0/L$, calculated current if leads did not cool filament (should be independent of T_M, except for photoelectric emission). i_e, photoelectric emission calculated from Eq. (7). $D(\text{calc.})=246+i_e$. $T_e=788°K$; $V=-120$ volts; $A=10.277$; $D_0=246$; $I_p=1.874\times10^{-8}$ amp. cm^{-2}; $L_0=18.9$ cm.*

T_M	D	ΔL cm	L_0/L	D(corr.)	i_e	D(calc.)
1100	215	1.27	1.155	248	0.13	246
1200	224	0.92	1.108	248	1.1	247
1300	234	0.68	1.078	252	6.9	253
1400	262	0.45	1.050	275	33	279
1500	364	0.41	1.046	381	125	371
1600	630	0.33	1.037	653	405	651
1700	1310	0.27	1.030	1350	1140	1386
1800	2950	0.22	1.024	3020	2880	3126

* H. A. Jones and I. Langmuir, Gen. Elec. Rev. **30**, 310, 354, 408 (1927).

Table III. *Data taken with tube at +39.9°C. $T_e=1081°K$; $V=-80$ volts; $D_0=2.14\times10^4$; $I_p=1.630\times10^{-4}$ amp. cm^{-2}.*

T_M	$10^{-4}D$	ΔL cm	L_0/L	$10^{-4}D$ (corr.)
1100	130	2.99	1.46	190
1200	177	1.62	1.206	214
1300	188	1.11	1.134	213
1400	197	0.82	1.095	216
1500	200	0.63	1.071	214
1600	205	0.50	1.055	216
1700	208	0.40	1.044	217
1800	211	0.33	1.036	218

of D(corr.) with T_m is accounted for by the photoemission. The data of Table II thus give $D_0=246$ as the true ion current from the whole length of uncooled filament. Converting this to amperes and dividing by 0.3046, the total surface area of the filament, gives I_p, the positive ion current density.

In Table III at a higher bulb temperature the currents are more than 10,000 times greater and thus the photoelectric currents are negligible. It is seen that D(corr.) is satisfactorily constant, the marked variation of D with T_M being entirely accounted for by the cooling effect of the leads. The low value of D(corr.) at 1100 would be brought to normal by only a few degrees' change in T_c (which is only 19° less than T_M). The data confirm the accuracy of the choice of T_c.

Calculation of T_c

It has been pointed out that T_c given by Eq. (6) is an upper limit. A method of calculating the value of T_c at which the boundary between the emitting and nonemitting phases is stationary has been outlined in a previous paper.[14] Fig. 1 illustrates the calculations of T_c by this method. The ordinates represent $\nu_a+\nu_p$ as a function of θ. Here ν_a was calculated from columns 2 and 3 of Table I of reference 5, while ν_p is 7 times the value of ν_p given by columns 4 and 5 of this table. The factor 7 takes into account the effect of the field in increasing the ion emission as was shown on p. 445 of reference 5. Unpublished experiments[15] on the rate of movement of the boundary between the emitting and the nonemitting surface phases have furnished the experimental justification of the procedure we are now using to calculate T_c.

The two curves in Fig. 1 are calculated for $T=800°$ and $T=1111°$. The horizontal lines AA' and BB' are so drawn that the areas enclosed between this line and the upper and lower portions of the curve are equal. That is $\int(\nu_a+\nu_p-\mu_a)d\theta=0$, when the integration extends between the two outer intersections of the horizontal line with the curve (points A, A' or B and B'). From the location of these lines we find

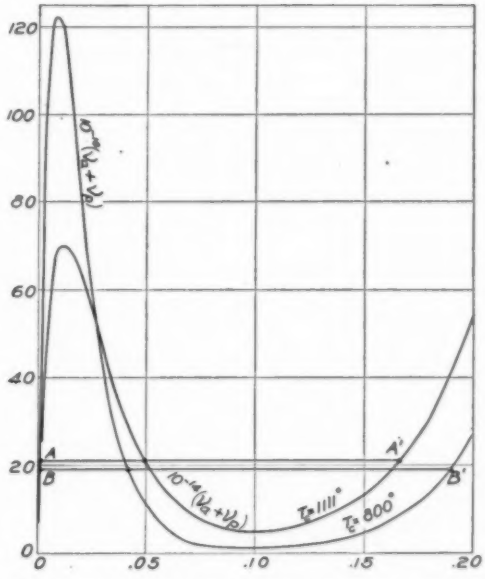

FIG. 1. Plot of $\nu_a+\nu_p$ as a function of θ, at two temperatures T_c to determine the value of μ_a at which the boundary between the emitting and nonemitting phases is stationary.

$$\text{at } T_c=800 \quad \mu_a=1.9\times10^{11},$$
$$\text{at } T_c=1111 \quad \mu_a=2.1\times10^{15}.$$

Plotting $\log\mu_a$ against $1/T$ as in Fig. 18 of reference 5 we find

$$\log_{10}\mu_a=25.66-11500/T_c \qquad (8)$$

for the relation between μ_a and the temperature T_c, which gives a stationary phase boundary. The values of μ_a vary with bulb temperature and can be calculated from p, the vapor pressure of Cs in Table IV by Eq. (10). The last column of Table IV contains values of T_c calculated in this way.

Calculation of ΔL

The value of $x-x_0$ was first calculated from the data of Table II of reference 13, taking the lead temperature to be 300°K. Then the heat flow Q into the lead was obtained by Eq. (37)[13]; this was used to calculate the correction Δx given by Eq. (75) which allows for the higher values of heat conductivity λ which were found for temperatures below 1500°K. The actual correc-

[14] I. Langmuir, J. Chem. Phys. 1, 1 (1933). See especially p. 7, also see reference 5, p. 441.
[15] I. Langmuir and J. B. Taylor, Phys. Rev. 40, 463 (1932).

TABLE IV. *Data for calculation of vapor pressure. Probable error in* $\log_{10} p = \pm 0.0043 = \pm 1.0$ *percent in* p. *Probable error in* t_B *(calc.) is* $\pm 0.10°$.

t_B	T	Accelerating Voltage	Lowest T_M Used	I_p amp. cm^{-2}	$\log_{10} p_{bar} + 10$	Diff. obs. minus calc. $\times 10^4$	Δt	T_c
−34.5°C	238.6	120	1100	1.874×10^{-8}	3.8973	− 29	−0.04°	788°K
−30.0	243.1	80	1000	3.85×10^{-8}	4.2146	+ 6	+ .01	805
−20.0	253.1	80	1000	1.736×10^{-7}	4.8772	+ 62	+ .10	844
0	273.1	5–80	1000	2.88×10^{-6}	6.0313	− 75	− .14	921
+ 3.6	276.7	160	1100	3.816×10^{-6}	6.2384	+ 76	+ .15	936
17.9	291.0	160	1200	1.904×10^{-5}	6.9475	+ 16	+ .03	992
19.8	292.9	80	1100	2.315×10^{-5}	7.0341	− 15	− .03	1000
25.4	298.5	40–160	1500	4.234×10^{-5}	7.3001	+ 68	+ .15	1025
30.2	303.3	30–125	1100	6.66×10^{-5}	7.5005	− 31	− .07	1042
38.2	311.3	45–160	1300	1.382×10^{-4}	7.8231	− 81	− .20	1072
39.9	313.0	80	1100	1.630×10^{-4}	7.8960	− 25	− .06	1081
46.2	319.3	300	1300	2.856×10^{-4}	8.1439	+ 23	+ .06	1106
67.8	340.9	320	1300	1.637×10^{-3}	8.9162	+111	+ .32	1193
72.7	345.8	320	1400	2.247×10^{-3}	9.0568	− 90	− .27	1208

tion used ranged from 75 to 95 percent of the value of Δx given by Eq. (75) since a study of possible transition curves between λ determined in reference 12 with that used in reference 13 showed that only for temperature T_c as high as 1500° should the full value of Δx be used. This is the most uncertain part of the determination of ΔL, but the possible error introduced into the calculation of L_0/L is not serious,[16] being of the order of 1 percent at $T_M = 1100$ and 0.5 percent at 1300°.

CALCULATION OF VAPOR PRESSURE

Data like those in Tables II and III were obtained at a series of other temperatures and the values of I_p, the ion current density, are recorded in column 5 of Table IV. In some of the experiments several negative voltages were used on the collector as shown in column 3. In every case within the ranges given there was no measurable change in current. At the higher bulb temperatures such as 46°C it became necessary to employ higher voltages to overcome the space charge of the ion current.

An attempt was made to use a bulb temperature of 88°C, but the current was limited by space charge even at 350 volts. Higher voltages seem undesirable because of possible gas evolution by ion bombardment.

In all cases except the measurement at 25.4°, T_M was varied from the value given in column 4 up to 1800°K. At 0°C the photocurrent was perceptible only above 1400°; at 30.2°C it was not observable even at 1800°. However, the observations above 1600° did not seem to be as accurate as those between 1400 and 1600°.

Dividing the I_p by 1.592×10^{-19}, the electron charge in coulombs, gives μ_a the number of atoms per sq. cm which strike the filament. This is related to the pressure p, in baryes, by the equation

$$p = (2\pi mKT)^{\frac{1}{2}}\mu, \tag{9}$$

from which we obtain for Cs ($M = 132.8$)

$$\log_{10} p = \log \mu_a + 0.5 \log_{10} T - 18.3621, \tag{10}$$

where T is now the bulb temperature.

The values of $\log_{10} p$ calculated in this way from I_F are given in column 6.

EQUATION FOR VAPOR PRESSURE

The data above the horizontal line in Table IV are for solid caesium, while the lower part contains data for liquid caesium. The latent heat of fusion must be taken into account in comparing these results. It should be noted that in the range covered by the experiments the pressure increases by a factor of about 140,000, which is about 43 per cent of the whole logarithmic range

[16] It was planned in these experiments to determine T_c by actual observation of the temperature T_M at which the emission suddenly increased and then after the filament was transferred to another bulb with clear walls to use an optical pyrometer to determine the points near the leads where the temperature is T_c with a series of values of T_M. In this way L_0/L could be determined with high accuracy. Dr. Taylor's untimely death interrupted these experiments and necessitates the more troublesome and less accurate calculations of L_0/L.

up to atmospheric pressure. Over any such wide range, especially if we are to extrapolate to higher temperatures, it is necessary to consider the temperature variation of the latent heat of vaporization, by taking into account the specific heats of the vapor and liquid.

Fortunately excellent calorimetric data are available from the work of Rengade.[17] He gives for the specific heats (at constant pressure)

$$\left.\begin{array}{l}\text{Solid Cs}\\ C_S=6.92+0.0036\,t \text{ cal. (g atom)}^{-1}\text{ deg.}^{-1},\\ \text{Liquid Cs}\\ C_L=8.00-0.0045\,t \text{ cal. (g atom)}^{-1}\text{ deg.}^{-1},\end{array}\right\} \quad (11)$$

where t is the temperature centigrade.

The vapor pressure curve can be put in the form

$$\log_{10} p=A+(2.5-C/R)\log_{10} T-B/T, \quad (12)$$

where the gas constant $R=1.986$.

The temperature coefficient of C_L was measured only between 28° and 100°C. It is certain that C_L at higher temperatures cannot fall below the Dulong and Petit value of a solid, 6.3, and thus the temperature coefficient of C_L at higher temperatures must decrease. We may therefore neglect the temperature coefficient of C_S and C_L if we use average values for the range of most interest. We chose for the coefficient $(2.5-C/R)$ the value -1.00 for solid and -1.35 for liquid Cs which correspond to $C_S=6.95$ (at $+6°$) and $C_L=7.65$ (at 78°C). The figures in parenthesis are the temperatures at which, by Eq. (11), C_S and C_L have the values chosen. These values should permit a wide extrapolation of the vapor pressure data.

Rengade gives 500.6 as the latent heat of fusion of Cs. For the alkali metals the values of L/T_F, where T_F is the temperature of fusion, are very nearly the same: -7.1 for Na; 7.1 for K; 7.0 for Rb and 6.95 for Cs. This is strong evidence that Rengade's value of L is accurate. The value of B for solid and liquid caesium should differ by $L/4.573$, so that we have

$$B_S=B_L+109. \quad (13)$$

The values of A_S, A_L, B_S and B_L for Eq. (12) have been chosen by the method of least squares to fit the data of Table IV, to satisfy exactly Eq. (13), and to give $p_S=p_L$ at $T=302$°K (the melting point).

The final equations which best represent the data are:

For solid caesium ($T<302°$), p in baryes

$$\log_{10} p_S=13.6710-1.00\log_{10} T-4150/T. \quad (14)$$

For liquid caesium ($T>302°$), p in baryes

$$\log_{10} p_L=14.1781-1.35\log_{10} T-4041/T. \quad (15)$$

To express the pressures in mm of Hg the equations are

$$\log_{10} p_S=10.5460-1.00\log_{10} T-4150/T, \quad (16)$$

$$\log_{10} p_L=11.0531-1.35\log_{10} T-4041/T. \quad (17)$$

Column 7 of Table IV gives the difference between $\log_{10} p$ in column 6 and the values of $\log_{10} p$ calculated by Eqs. (14) or (15), multiplied by 10^4. The "probable error" of the data for a single temperature is thus 1 percent in pressure.

Column 8 gives the amount by which t_B would have to be raised to give the observed pressure by Eqs. (14) or (15). The errors in pressure thus correspond to a "probable error" in temperature of 0.10°.

The change in slope of the $\log_{10} p$/*vs.* $1/T$ plot at the melting point is very apparent if the data in column 6 are plotted accurately. This may be better illustrated by applying Eq. (15), for liquid Cs, to calculate the pressure at $-34.5°$. We obtain a value of $\log_{10} p_L$ of 4.0320, whereas Eq. (14) gives $\log_{10} p_S=3.9002$. Thus p_L is 36 percent higher than p_S—a difference 36 times greater than the probable error.

The vapor pressures determined by this positive ion method are thus much more accurate than those obtained by other methods. They should also be particularly free from systematic errors. No attempt was made in these experiments to obtain greater accuracy than shown by these results. We believe that the method is capable of high precision if the cooling effects of the leads are properly determined by temperature measurements. Filaments of smaller diameter and greater length would also reduce the errors.

It is possible to extend the measurements of vapor pressure by the positive ion method to very

[17] Rengade, Comptes rendus **156**, 1897 (1913). See *International Critical Tables*, Vol. 2, 458 and Vol. 5, p. 93.

TABLE V. *Coefficients A and B in Eq. (18) which give the vapor pressure of Cs in mm within 0.5 percent for specified temperature ranges.*

T_N	Range °K	A	B
263°K	224– 302	7.6920	4036
355	302– 408	7.0223	3833
479	408– 551	6.8460	3760
647	551– 745	6.6706	3662
873	745–1000	6.4942	3529

much lower temperatures by using the accumulation method described in the previous paper.[5] For example, if the filament is flashed to clean it and is then allowed to remain in a lower pressure of caesium for a time sufficient to give 10^{10} ions per cm², these ions will give a ballistic kick on an electrometer (or vacuum tube) if the filament is again flashed. The difficulties due to photoelectric effect are also largely eliminated by this method. An accumulation time of ten hours and a sensitiveness of 10^{10} ions would correspond to a pressure of about 10^{-12} baryes or a temperature of about −70°C. With a good electrometer it is possible to detect ballistic kicks of 100 electrons which would be obtained in 10 hours by accumulation at a pressure of 10^{-20} baryes or an average of one atom per cubic meter. Of course, special means would then have to be adopted to avoid photoelectric effects. Dr. Kingdon in this laboratory detected the presence of caesium by galvanometer kicks at temperatures of about −70° but made no accurate measurements.

The pressures in mm of Hg by Eqs. (16) and (17) are given in the last column of Table I for comparison with the older data. The agreement with Eucken's equation from 500 to 1000°K is excellent. The greatest error is at low temperatures, Eucken's value being about 7 percent low at 300°.

The L-K equation between 250° and 330°K is the best single equation of this type that can represent the data. At 262° and at 314° the agreement is perfect. The greatest deviation between 250° and 330° is 4 percent at the melting point (302°K).

In calculating vapor pressures it is far more convenient to use an equation of the form

$$\log_{10} p = A - B/T \qquad (18)$$

than to use equations like (14) to (17) with a term containing log T. In the neighborhood of a selected temperature T_N it is always possible[18] to represent vapor pressure over a fairly wide range by Eq. (18) by proper choice of A and B.

The values of A and B to be used in specified ranges to get p_S or p_L within 0.5 percent are given in Table V.

Examination of Table I shows that the large discrepancies which troubled Rowe, de Boer, Dippel and v. Liempt are not real, but are due to their attempt to extrapolate over too wide a range of temperature by Eq. (18). Thus Kröner's data, as expressed by Eq. (2), agree exactly ($p=5.20$ mm) with our Eq. (17), or Table V, at 342°C, which is within the range 250 to 350°C covered by his experiments. At 250°C Kröner's data give 0.382 as compared to our 0.454 mm (or 16 percent too low). Hackspill's data are evidently not very accurate for they cannot be represented by Eq. (18). His measurement at the highest temperature (397°C), however, agrees exactly with our value of 15.9 mm at this temperature. His data at temperatures from 272° to 350°C are from 8 to 15 percent high, while a measurement at 244°C is 35 percent low.

We have thus experimental justification for using Eq. (17) up to the temperatures of about 700°K. The accuracy of the measurements of p indicated by the data of Table IV and the wide range of pressure covered by these data give reason for believing that no large error can arise even in extrapolating to 1000°K. Thus, if there is a 1 percent progressive error in p between −34.5°C and +72.7°C, this would entail an error of only 2.4 percent at 1000°. If we consider that the specific heat of liquid Cs above 600° begins to deviate from the value 7.65, which we have assumed and has an uncertainty of 0.5 unit at 1000°, the error in p at 1000° would be only 5 percent. It is therefore probable that Eq. (17) gives p correctly within 8 percent even at 1000°K.

[18] I. Langmuir, J. Am. Chem. Soc. **54**, 2798 (1932).

Electronic Energy Bands in Metallic Calcium

MILLARD F MANNING
Massachusetts Institute of Technology and University of Toledo
AND
HARRY M. KRUTTER*
Pennsylvania State College, State College, Pennsylvania
(Received February 1, 1937)

Theoretical studies of electronic energy bands in metallic calcium have been carried out by the Wigner-Seitz-Slater cellular method. The conductivity is found to be due to an overlap between the lowest "s" band and the "d" band. This overlap leaves a small number of vacant states near the points in the momentum cell whose coordinates are: 0, $\pi/\sqrt{2}R$, $\pi/2\sqrt{2}R$. In terms of the computed results, interpretations of the binding energy, pressure coefficient of resistance, and paramagnetic susceptibility are made. Predictions are made about the Hall coefficient and about optical properties.

THE Wigner-Seitz-Slater cellular method[1-4] of calculating energy bands in metals has so far been applied only to monovalent metals, for which there is little difficulty in understanding the fundamentals of the process of electrical conduction. For the case of a divalent metal some general conclusions have been drawn, but the authors believe that a more detailed study of a particular divalent metal is worthwhile. On account of the particular interest in the behavior of the first group of transition elements, and because Hartree's results for the calcium atom were available, metallic calcium has been chosen for this more detailed study.

The application of the cellular method to a face-centered lattice has been given in previous papers.[4, 5] Relations are given there which determine the energy of an electronic state in a metal as a function of the wave vector k. The relations between E and k can be handled easily only for particular directions. The special cases of propagation along 100, 110, and 111 directions were treated in detail in a previous paper.[4] Other special directions have been treated by Shockley.[5] The relations between E and k involve the values of the s, p, d, f functions and their derivatives at the half-distance between nearest neighbors. These values have been found by numerical integration, as in the Hartree method of finding the self-consistent field for an isolated atom. The potential used was found by taking Hartree's results[6] for the core and adding to this the potential of a valence electron of energy somewhat less than the eigenvalue and with the charge density normalized to the atomic volume.

For a particular interatomic distance, the lowest band will begin at the energy for which $s'=0$ at half of this distance. The next higher band will begin at the energy for which $d'=0$ at the same radius. For different interatomic distances, these conditions are fulfilled for different energies. In Fig. 1 a graph of the energies for which $s'=0$, $p'=0$, $d'=0$, $s=0$, $p=0$ are plotted as functions of the half-distance between neighbors.

The filled levels extend from $s'=0$ to about $d'=0$. As the interatomic distance is changed, the energy of the lowest filled levels depends upon the behavior of the $s'=0$ curve. The behavior of the upper filled levels depends upon the $d'=0$ curve. Since this curve is quite flat, most of the variation of energy with interatomic distance is due to the change of energy of the lower levels. This argument leads to the prediction that the actual interatomic distance would correspond to the minimum of the $s'=0$ curve. However, this argument neglects correlation effects. Qualitatively, correlation effects lead to the expecta-

* Work started at Purdue University.
[1] Wigner and Seitz, Phys. Rev. **43**, 804 (1933).
[2] Slater, Phys Rev. **45**, 794 (1934).
[3] Millman, Phys. Rev. **47**, 286 (1935).
[4] Krutter, Phys. Rev. **48**, 664 (1935).
[5] W. Shockley, Phys. Rev. **51**, 129 (1937). The authors wish to express their appreciation to Dr. Shockley for the privilege of seeing this paper in manuscript form, and for interesting discussions with him on the subject of electronic energy bands in solids.
[6] Hartree, Proc. Roy. Soc. **A149**, 210 (1935).

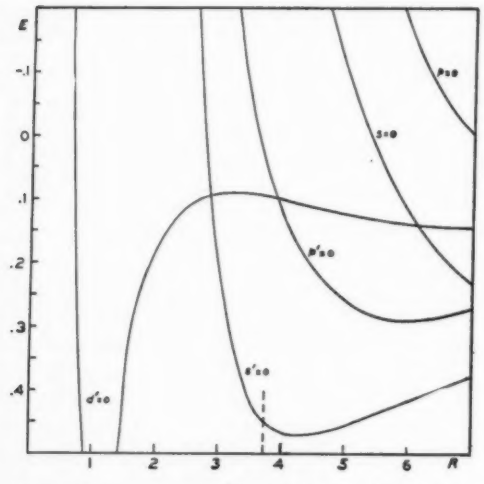

FIG. 1. Energy as a function of internuclear distance. The dashed vertical line indicates the observed interatomic distance of 3.72 Bohr units.

tion of a somewhat smaller interatomic distance than is predicted by the above argument.

In comparing the binding energy of calcium and potassium there are two chief differences to take into account. Since the effective potential for a valence electron in calcium is greater than in potassium, the minimum of the $s'=0$ curve comes at a lower energy and at a smaller value of the interatomic distance. Since there are two electrons per atom, there will be some electrons with energies greater than the eigenvalue. The fact that at a radius about half of the actual interatomic distance, $d'=0$ at an energy only a little above the $4s$ eigenvalue, shows that this effect will be small and the former effect will predominate to give calcium a greater binding energy than potassium. The actual values[7] are 0.085 and 0.13 atomic units per atom.

The values of E[8] as a function of k for the three principal directions are shown in Fig. 2. The notation is the same as in reference 4. Since the three principal directions gave no indication of overlapping of bands, the direction $k_z=0$, $k_x=\pi/\sqrt{2}R$ was investigated. The results for this line have been given by Shockley and will not be repeated here. The essential feature for the discussion of electrical conductivity is that the energy at the point $k_z=0, k_x=\pi/\sqrt{2}R, k_y=\pi/2\sqrt{2}R$ is determined by the condition that $(p'/p)+(d'/d)=0$. This will come above either $p'=0$ or $d'=0$. In calcium, for all radii less than 3.93, $d'=0$ will come for a lower energy than $(p'/p)+(d'/d)=0$, and hence there will be a certain number of vacant levels in the lower band and a corresponding number of filled levels in the next higher band. The number of these states will depend upon the energy overlap between the top of the first band and the bottom of the next higher band. The way that this energy overlap changes with interatomic distance is shown in Fig. 3. It should be pointed out that the approximations of this theory are such that this may not be a quantitatively correct representation of the behavior. The use of a more nearly correct

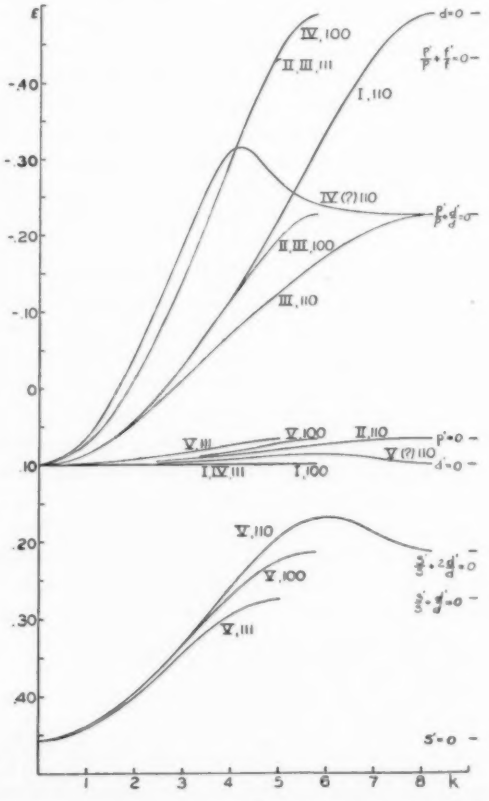

FIG. 2. Energy *versus* k for 100, 110, 111 directions. $R=3.80$.

[7] N. F. Mott and H. Jones, *The Theory of the Properties of Metals and Alloys* (Oxford University Press 1936) p. 23.

[8] The method of computing the potential leaves an arbitrary constant to be determined. If this arbitrary constant is chosen so that the x-ray term values are the same as for the free atom, the values of all energies quoted in this paper would be decreased by about 0.14.

potential and of a greater number of spherical harmonics in the expansion of the wave function, might make an appreciable difference in the magnitude of this energy overlap.[9] It seems less likely that its dependence upon interatomic distance should be in the opposite direction from that given in Fig. 3.

Fig. 4 shows approximate contours in the plane $k_z=0$. Similar contours were also drawn in the plane $k_y=k_x$. From these special planes, energy surfaces in k space were interpolated and by a combination of graphical and numerical methods, the volume in k space inclosed by a given energy surface was found. This volume is proportional to the number of states with energy less than the energy considered. From a plot of the volume in k space as a function of energy, the number of states between E and $E+dE$ was found by graphical differentiation. The results are shown in Fig. 5.

A better estimate of the shape of the $n(E)$ curve could be obtained by using more of the special directions which have been worked out by Shockley[5] and by obtaining an expansion of the large determinant which is valid in the region near 0, $\pi/\sqrt{2}R$, $\pi/2\sqrt{2}R$. The high density of states near the bottom of the d band seems to be real

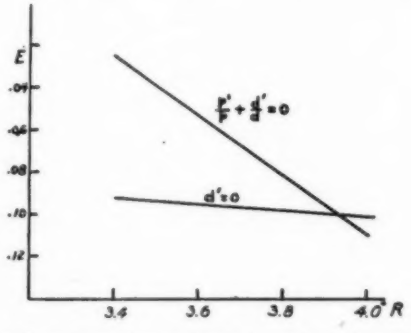

FIG. 3. Energy overlap at $k_z=0$, $k_x=\pi/\sqrt{2}R$, $k_y=\pi/2\sqrt{2}R$. $R=3.80$.

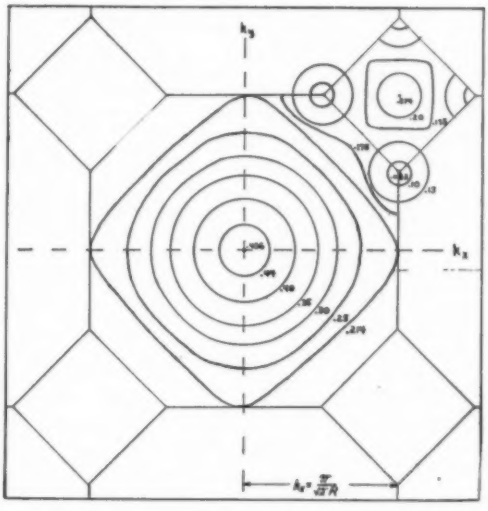

FIG. 4. Energy contours of lowest band in the $k_z=0$ plane for $R=3.80$.

and not the unfortunate consequence (as are *zero* width bands) of approximations in the theory. This point will be discussed in more detail in another paper.

In order to show the connection between these results and the electrical conductivity of metallic calcium, it is necessary to consider three important factors which effect the conductivity of a metal. They are:

1. Not all of the valence electrons can take part in the conduction process. Under the influence of the external field, some of the electrons in states near the top of the Fermi distribution will make transitions to other states of higher energy. These excited states are characterized by a mean momentum in the direction of the field, and hence by a current in that direction. For calcium at about the observed interatomic distance, all of the states, except those near 0, $\pi/\sqrt{2}R$, $\pi/2\sqrt{2}R$ and the twenty-three equivilant points, will be separated from vacant states by a finite energy gap, and hence only a small number can actually make transitions under the influence of the field.

2. The momentum which is imparted to the stream of electrons in a given length of time depends upon the spacing of the energy contours near the top of the Fermi distribution. For the highest states in the lower band the energy contours in momentum space will be much closer

[9] This pessimism is caused mostly by results obtained for the body-centered lattice. When fourteen boundary conditions are used instead of eight, a considerable change in the relations between E and k is found. (Manning and Chodorow, Phys. Rev. 50, 399 (1936), and unpublished work on potassium and tungsten.) However, the next state of improvement for the face-centered lattice would probably not involve such a drastic change. Shockley (Atlantic City Meeting, December, 1936) has attempted to justify Slater's method of fitting boundary conditions by showing that for the extreme case of a constant potential, the agreement within the lowest band is satisfactory.

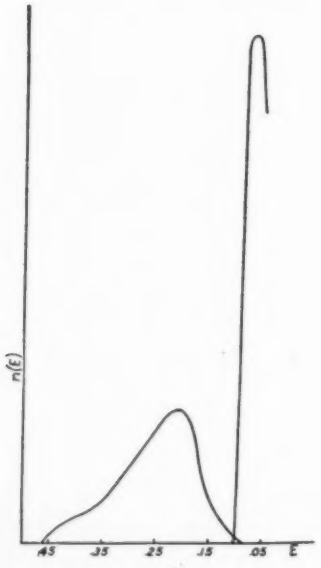

FIG. 5. $n(E)$ as a function of E. $n(E)dE$ is the number of states between E and $E+dE$. $R=3.80$.

together than for the states at the bottom of the upper band, and hence most of the conduction will be due to electrons in the lower band.

3. Electrons are scattered out of the beam by collision with ions. The probability of scattering will depend upon the amplitude of vibration of the scattering ions and upon the density of vacant states near the edge of the Fermi distribution. The first effect accounts for the ordinary change of resistance with temperature and has been discussed in detail by Mott and Jones.[10] Since the vacant d states are effective in scattering but not in conduction, the effect of the high density of d states just above the highest occupied level is to make the conductivity of calcium less than for an element where electrons in only one band need be considered. The effect of pressure on the conductivity can be understood by comparing Fig. 3 and Fig. 5. As the pressure is increased, the number of vacant d levels near the top of the Fermi distribution increases more rapidly than the number of vacant states in the lower band. This explains why the resistance of calcium increases with pressure.

The paramagnetic contribution to the susceptibility of a metal depends upon the number of vacant levels at the edge of the Fermi distribution. In calcium the density of vacant states is great enough so that the metal is paramagnetic. At higher pressures the number of vacant states is increased so much that it may be possible to detect experimentally a change of susceptibility with pressure.

As Mott and Jones[11] have pointed out, when the conduction is due to the holes in a nearly filled band, the Hall coefficient should be large and have the opposite sign from the case of free or nearly free electrons. No record has been found of an experimental determination of this coefficient.

There is a type of optical absorption by a metal which corresponds to a transition from an occupied state to a vacant state having the same coordinates in k space. From the E *vs.* k curves, it can be seen that when the end state is in one of the narrow bands near $d'=0$, the energy difference allowed by the selection rule can be equal to or less than 0.36 unit. This corresponds to an absorption of all wave-lengths greater than about 2500A. For wave-lengths less than this, there can be absorption to some of the other d bands. There may be a decreased absorption below 2500A but there does not seem to be any possibility of a transparent region between 4000A and 1000A.

The authors wish to thank Professor J. C. Slater and Professor N. H. Frank for helpful discussions about the subject matter of this paper.

[10] Reference 7, page 243.

[11] Reference 7, page 283.

On the Choice of the Action Function in the New Field Theory

B. HOFFMANN AND L. INFELD
The Institute for Advanced Study, Princeton, New Jersey

(Received January 4, 1937)

By the imposition of a regularity condition on the new field theory a new action function is found which is unique so far as the significant lower order terms of its expansion are concerned. The new action function leads to a theory in which the f_{kl} field is free from singularities, from which magnetic poles are automatically excluded, and in which the equations of motion can be deduced from the field equations without extra dynamical assumptions. When general relativity is taken into account the field of a particle is such that space-time is everywhere regular, and the theory leads to the identification of gravitational with electromagnetic mass.

INTRODUCTION

THE new field theory initiated by Born[1] introduces in the classical equations of the electromagnetic field a characteristic length r_0 representing the radius of the elementary particle through the relation

$$r_0=(e/b)^{\frac{1}{2}},$$

where e is the elementary charge and b the fundamental field strength entering the Lagrangian function.

The considerations of Heisenberg, Euler, and Kockel[2] on the scattering of light by light according to the theory of the positron, and Heisenberg's recent theory of cosmic-ray showers[3] indicate the importance of the introduction of a characteristic length in the early stages of the theory, i.e., in classical physics.

The question is still open as to which of the many conceivable action functions is to be used in the new field theory. It was originally thought that the Lagrangian and corresponding Hamiltonian

$$\mathfrak{L}=(1+F-G^2)^{\frac{1}{2}}, \quad \mathfrak{H}=(1+P-Q^2)^{\frac{1}{2}}, \quad (0.1)$$

where

$$F=\tfrac{1}{2}f_{kl}f^{kl}, \quad P=\tfrac{1}{2}p_{kl}{}^*p^{*kl}, \quad (0.2)$$

and

$$G=\tfrac{1}{4}f_{kl}f^{*kl}, \quad Q=\tfrac{1}{4}p_{kl}p^{*kl}, \quad (0.3)$$

was the simplest choice which would lead to a finite energy for an electric particle. This is, however, not the case. It is possible to find an infinite number[4] of quite different action functions, each giving simple algebraic relations between the f_{kl} and p_{kl} fields and each leading to a finite energy for an electric particle. This lack of uniqueness is not the only objection to the action function used up to now. For this action function gives complete symmetry between the electric and magnetic fields so that to the solution representing an electrical particle corresponds an exactly similar solution for a magnetic particle. Another serious objection to the theory is that the equations of motion are not a consequence of the field equations alone but require the introduction of a special hypothesis whose meaning is obscure.[5] This difficulty is connected with the existence of the singularity in the field of the elementary particle. Again, if the theory be treated within the framework of the general theory of relativity, the gravitational potentials are also not regular, with the result that space-time itself is singular at the "center" of the elementary particle.[6]

In the present paper we impose as a fundamental condition the requirement that only those solutions have physical significance for which the f_{kl} functions are everywhere regular. This condition, which we later generalize for the gravitational case, forms a criterion for the choice of the action function, and we show that the action function to which we are actually led

[1] Born, Proc. Roy. Soc. **A143**, 1410 (1934); Born and Infeld, Proc. Roy. Soc. **A144**, 425 (1934).
[2] Heisenberg and Euler, Zeits. f. Physik **98**, 714 (1936); Euler and Kockel, Naturwiss. **23**, 246 (1935).
[3] Heisenberg, Zeits. f. Physik **101**, 533 (1936).
[4] Infeld, Proc. Camb. Phil. Soc. **32**, 127 (1936), **33**, 70 (1937), hereinafter referred to, respectively, as I and II.
[5] Frenkel, Proc. Roy. Soc. **A146**, 933 (1934); Feenberg, Phys. Rev. **47**, 148 (1935); Born, Proc. Indian Acad. Sci. **3**, 8 (1936) and **3**, 85 (1936); Pryce, Proc. Roy. Soc. **A155**, 597 (1936).
[6] See § 5 of this paper.

avoids, at least partially, the various difficulties discussed above. Our action function is unique so far as terms of the significant lower orders are concerned, it leads to a regular f_{kl} field for the fundamental electric particle, it rejects the possibility of isolated magnetic poles, and it allows the derivation of the Lorentz law without extra hypothesis. Further, it leads to a regular gravitational field for the fundamental electric particle, and it shows that its gravitational mass and electromagnetic mass are essentially the same, thus showing that gravitational mass cannot be negative, a result which does not follow from the usual general theory of relativity. Moreover, the present theory preserves the general scheme of the earlier theory with all its inherent advantages.

We divide the paper into two parts. The first part contains all of the work which can be treated within the framework of the special theory of relativity, while the second part discusses those aspects of the work in which the explicit use of the gravitational potentials of the general theory of relativity is essential.

Part I

§1. The action function

We assume[7] that our action function T is a function of the two scalar invariants F, P defined by

$$\begin{aligned} F&=\tfrac{1}{2}f_{kl}f^{kl}=B^2-E^2;\\ P&=\tfrac{1}{2}p^*{}_{kl}p^{*kl}=D^2-H^2, \end{aligned} \tag{1.1}$$

where the star denotes the dual tensor and, in the Galilean case,

$$\begin{cases} f^{*14},\ f^{*24},\ f^{*34}\rightarrow f_{23},\ f_{31},\ f_{12}\rightarrow \mathbf{B},\\ f^{*23},\ f^{*31},\ f^{*12}\rightarrow f_{14},\ f_{24},\ f_{34}\rightarrow \mathbf{E},\\ \quad\begin{cases} p^{*14},\ p^{*24},\ p^{*34}\rightarrow p_{23},\ p_{31},\ p_{12}\rightarrow \mathbf{H},\\ p^{*23},\ p^{*31},\ p^{*12}\rightarrow p_{14},\ p_{24},\ p_{34}\rightarrow \mathbf{D}. \end{cases} \end{cases} \tag{1.2}$$

The f_{kl} and $p_{kl}{}^*$ are the four-dimensional curls of potential vectors φ_k, ψ_k, respectively, and must, therefore, satisfy the integrability conditions

$$(\partial f^{*kl}/\partial x^l)=0, \tag{1.3a}$$

$$(\partial p^{kl}/\partial x^l)=0. \tag{1.3b}$$

We assume that the f_{kl} and p^{kl} are canonically conjugate with respect to the action function, and that f^{*kl} and $p_{kl}{}^*$ are similarly conjugate. This means that

$$p^{kl}=(\partial T/\partial f_{kl})=2T_F f^{kl}, \tag{1.4a}$$

$$f^{*kl}=(\partial T/\partial p_{kl}{}^*)=2T_P p^{*kl}, \tag{1.4b}$$

where T_F, T_P denote partial derivatives of T with respect to F and P, respectively. With this assumption of conjugacy the field equations obtained from the action principle

$$\delta\int T dx^1dx^2dx^3dx^4=0 \tag{1.5}$$

by variation of the potentials φ_k and ψ_k are precisely the Eqs. (1.3a), (1.3b).

The Eqs. (1.4a), (1.4b) are twelve equations for determining the six quantities $p_{kl}{}^*$ as functions of the six quantities f_{kl}, or *vice versa*. They will thus, in general, not be consistent. It is easy to see that if they are to be consistent we must have

$$4T_F T_P=1. \tag{1.6}$$

Also, if we multiply (1.4a), (1.4b), respectively, by f_{kl} and $p_{kl}{}^*$ and add we get

$$T_F F+T_P P=0. \tag{1.7}$$

To satisfy (1.7) we take T to be a homogeneous function of F and P of degree zero. That is, we introduce

$$\epsilon=(-F/P)^{\frac{1}{2}} \tag{1.8}$$

and assume that T is a function of ϵ. From (1.7), by applying (1.6), we now obtain

$$2T_P\epsilon=1, \tag{1.9a}$$

$$2T_P\epsilon^{-1}=1, \tag{1.9b}$$

where the signs are determined by the convention that the f_{kl} and p_{kl} fields shall always have the same direction, in which case $2T_F$ and $2T_P$ must always be positive.

From (1.9a), (1.9b) and (1.8) we have

$$T_\epsilon=-P, \quad \text{or} \quad \epsilon^2 T_\epsilon=F, \tag{1.10}$$

giving F as a function of P, or *vice versa*.

[7] The general ideas underlying the variational method used in this paper will be found more fully developed in I and II.

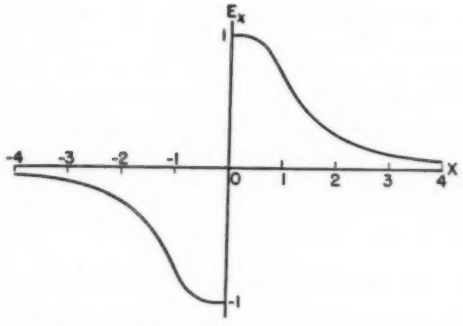

FIG. 1. E_x plotted against x for $E_r=1/(1+r^4)^{\frac{1}{2}}$.

Having summarized the general theory of the variational principle we use, we must now find a specific form for the T function which will give a field theory free from the difficulties formulated in the introduction.

We regard the f_{kl} field as fundamental and the p_{kl} components as functions of the f_{kl} components in accordance with (1.10). Since P is thus a function of F we may write

$$p^{kl}=\lambda f^{kl}, \tag{1.11}$$

where λ depends on the scalar F only.

The field equations (1.3a), (1.3b) may now be written in the form

$$(\partial f^{*kl}/\partial x^l)=0, \quad (\partial f^{kl}/\partial x^l)=4\pi\rho^k, \tag{1.12}$$

where ρ^k is the charge and current density vector and has the form,

$$4\pi\rho^k=-(\partial \log \lambda/\partial x^l)f^{kl}. \tag{1.13}$$

The Eqs. (1.12) are formally the same as those of the Lorentz theory. The difference lies in the fact that the ρ^k are functions of the f_{kl} field. The conservation law of the current density vector follows at once from (1.12) because of the antisymmetric character of f^{kl}:

$$4\pi(\partial\rho^k/\partial x^k)=(\partial^2 f^{kl}/\partial x^l\partial x^k)=0. \tag{1.14}$$

In a pure field theory the field equations must be well defined for every point of space-time since whenever the field equations are undefined extra conditions must be introduced to take the place of the defaulting equations in the singular domain.

We are thus led to the following *regularity condition* for the present case:

Only those solutions of (1.12) may have physical meaning for which the functions f_{kl} and their first derivatives exist everywhere.

We shall now show that this regularity condition restricts the possibilities for the action function T and allows us ultimately to determine the essential terms in its expansion uniquely, thus removing the arbitrariness in the choice of the action function which has hitherto existed.

In order to find the action function we must discuss the character of a spherically symmetric electrostatic solution. In the previous theory f_{kl} was not everywhere continuous, for in that theory we had[8] for this case, in natural units,

$$D_r=1/r^2; \quad E_r=1/(1+r^4)^{\frac{1}{2}}; \tag{1.15}$$

thus E_x changes from $(+1)$ to (-1) on passing through the "center" of the particle, $r=0$, as shown in Fig. 1. It is evident that any finite value for E_r at $r=0$ will lead to a discontinuity of this type. Therefore it is essential that in the spherically symmetric electrostatic case E_r shall vanish for $r=0$:

$$\text{For } r\to 0; \quad E_r\to 0\sim r^n; \quad \epsilon\equiv E_r/D_r\to r^{2+n}, \quad n>0. \tag{1.16}$$

The condition (1.16), which is an expression of the regularity condition, concerns the behavior of the field as $r\to 0$. We impose the further condition that for large r the field shall become Maxwellian. This gives, by (1.10)

$$\text{For } r\to\infty; \quad D_r\to E_r\to r^{-2}\to 0; \quad \epsilon\to 1; \quad T_\epsilon\to 0; \quad T\to 0.^9 \tag{1.17}$$

From (1.16) we have

$$\text{For } r\to 0; \quad P\to r^{-4}; \quad 1/\epsilon\to r^{-(2+n)}, \quad n>0.$$

Thus if T_ϵ can be expanded in a power series in ϵ it follows from (1.10) that the lowest term must contain $(1/\epsilon)$. We therefore assume

$$-P=T_\epsilon=-1/\epsilon+\alpha+\cdots, \tag{1.18}$$

where α is a constant. On integrating we find

$$T=k+\alpha\epsilon-\log\epsilon+\cdots, \tag{1.19}$$

where k is a constant of integration.

[8] Born, Infeld, reference 1, §6.

[9] For this last see I, p. 132, § 6. This result can also be obtained from Eq. (3.7) of this paper since in the Maxwell case T_s^s is known to be zero.

The values of α and k can be determined from the application of (1.17) to (1.18) and (1.19) if we neglect the higher order terms in ϵ:

$$\alpha=1, \quad k=-1.$$

Thus, if we consider only the lower order terms of the expansion of T we may take

$$T=\epsilon-\log\epsilon+1. \tag{1.20}$$

This is the form we shall use for the action function in the present work. Although we have neglected expressions of order ϵ^2 in (1.19) we see that every field theory avoiding discontinuities must have essentially the same features as the one here formulated.[10]

From (1.10) and (1.20) we find, as the connection between F and P,

$$(-P/F)^{\frac{1}{2}}=1+P, \tag{1.21}$$

$$-P/(1+P)^2=F, \tag{1.22}$$

and thus, because of (1.11),

$$f_{kl}=p_{kl}/(1+P), \tag{1.23}$$

$$p_{kl}=\frac{-1\pm(1+4F)^{\frac{1}{2}}}{2F}f_{kl}. \tag{1.24}$$

The sign to be used in (1.24) is determined from the following considerations:

For $F<0$ and $f_{kl}\to 0$ we have

$p_{kl}\to\infty$ if the minus sign is taken before the square root,

$p_{kl}\to 0$ if the plus sign is taken before the square root.

For $F>0$ only the plus sign may be taken since only in this case will f_{kl} and p_{kl} have the same direction. For $f_{kl}\to 0$ we always have $p_{kl}\to 0$ in this case.

From (1.24), since p_{kl} is real, it is seen that the smallest value for F is given by

$$1+4F=0, \quad \text{or} \quad F=-\tfrac{1}{4}. \tag{1.25}$$

The Eq. (1.25) defines a surface, in general. If real charges exist, i.e., if (1.3b) breaks down at certain points, the minus sign must be taken inside the surface and the plus sign outside. On the surface itself, of course, the square root vanishes. The existence of regions in which the minus sign has to be taken before the square root is directly connected with the existence of charges. The extrema for F exist whenever there are charged particles. This is a general consequence of the fact that F must be zero both at the center of the particle, where $P\to\infty$, and at large distances, where $P\to 0$.

[10] This case is exactly that of $j=0$ in II if we interchange the electric and magnetic fields. The Hamiltonian has the simple form

$$\mathfrak{H}=\tfrac{1}{2}\log(1+P).$$

§2. The spherically symmetric electrostatic case

In the spherically symmetric electrostatic case we have $\mathbf{B}=\mathbf{H}=0$, and the field equations take the form

$$\operatorname{curl}\mathbf{E}=0, \tag{2.1}$$

$$\operatorname{div}\mathbf{D}=0. \tag{2.2}$$

We have to replace $\mathbf{D}$ in (2.2) by its value as a function of $\mathbf{E}$. Eqs. (1.23) and (1.24) give as the relation between the radial components of $\mathbf{E}$ and $\mathbf{D}$,

$$E_r=D_r/(1+D_r^2), \tag{2.3}$$

$$D_r=\frac{-1\pm(1-4E_r^2)^{\frac{1}{2}}}{2E_r^2}E_r=\lambda E_r, \tag{2.4}$$

where the minus sign must be used inside the sphere $E_r=\frac{1}{2}$ and the plus sign outside.

Eqs. (2.1) are identically fulfilled since E_r is a function of r alone.

Eq. (2.2) can be written as

$$\operatorname{div}\mathbf{E}=-\frac{\partial\log\lambda}{\partial r}E_r=4\pi\rho, \tag{2.5}$$

where ρ is the free charge density, defined as a function of E_r. The solution of (2.5) is

$$E_r=r^2/(1+r^4), \tag{2.6}$$

as we can easily deduce by inserting for D_r in (2.3) its value r^{-2}. Thus the field strength vanishes for $r=0$ as shown in Fig. 2, and its derivative of the first order exists everywhere. It has a maximum where $r=1$, exactly corresponding to the sphere given by $(1+4F)^{\frac{1}{2}}=0$. From (2.6) and (2.5) we find that the free charge density is given by

$$\rho=\frac{1}{\pi}\frac{r}{(1+r^4)^2}; \tag{2.7}$$

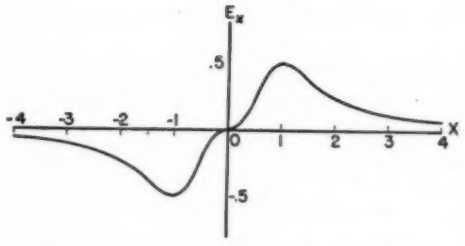

FIG. 2. E_x plotted against x for $E_r=r^2/(1+r^4)$.

it vanishes for $r=0$ and decreases for large r like r^{-7}.

The total charge is defined by

$$e=\int \rho dv=1/4\pi \int \operatorname{div} \mathbf{E} dv, \tag{2.8}$$

and in the special case here considered it turns out that $e=1$ since we have used natural units.

The potential function $\varphi(r)$ belonging to E_r can be at once calculated since

$$E_r=-d\varphi/dr. \tag{2.9}$$

This gives

$$\varphi(r)=\int_r^\infty \frac{r^2dr}{1+r^4}=\frac{\sqrt{2}}{8}\left\{\log\frac{1+\sqrt{2}r+r^2}{1-\sqrt{2}r+r^2} -2\tan^{-1}\frac{\sqrt{2}r}{1-r^2}\right\}. \tag{2.10}$$

The potential is finite for $r=0$:

$$\varphi(0)=\sqrt{2}\pi/4. \tag{2.11}$$

The energy density is measured by $T_4{}^4$ and the total energy is given by

$$W=\int T_4{}^4 dv$$

integrated over all space. Since the total energy in the spherically symmetric electrostatic case, independently of the choice of the action function, is[11] $\frac{2}{3}\varphi(0)$, we have

$$W=2\phi(0)/3=\sqrt{2}\pi/6. \tag{2.12}$$

It can easily be shown that a magnetic solution of this kind does not exist. For both B_r and H_r are discontinuous at $r=0$ in the spherically symmetric magnetostatic case and the regularity condition is thus not fulfilled.

[11] II, §5.

§3. The energy momentum tensor and the laws of motion

We go back now to the general case and calculate the energy-momentum tensor. For the sake of simplicity we shall use both the tensors f_{kl} and p_{kl}.

The field equations (1.3a), (1.3b) can be written in the form

$$\frac{\partial f_{lm}}{\partial x^k}+\frac{\partial f_{mk}}{\partial x^l}+\frac{\partial f_{kl}}{\partial x^m}=0, \tag{3.1}$$

$$\frac{\partial p_{lm}{}^*}{\partial x^k}+\frac{\partial p_{mk}{}^*}{\partial x^l}+\frac{\partial p_{kl}{}^*}{\partial x^m}=0. \tag{3.2}$$

Multiplying (3.1) by $\frac{1}{2}p^{lm}$, (3.2) by $\frac{1}{2}f^{*lm}$ and adding, we get

$$\frac{1}{2}\left[p^{lm}\frac{\partial f_{lm}}{\partial x^k}+f^{*lm}\frac{\partial p^*{}_{lm}}{\partial x^k}\right] +\frac{1}{2}\frac{\partial}{\partial x^l}[p^{lm}f_{mk}+f^{*lm}p^*{}_{mk}]=0. \tag{3.3}$$

By (1.3a) and (1.3b) the terms in the first brackets are merely the derivative of T with respect to x^l. So if we introduce

$$T_k{}^l=\tfrac{1}{2}\{T\delta_k{}^l+(p^{lm}f_{mk}+f^{*lm}p^*{}_{mk})\}, \tag{3.4}$$

Eq. (3.3) becomes

$$\partial T_k{}^l/\partial x^l=0. \tag{3.5}$$

Thus $T_k{}^l$ is the energy momentum tensor for the present theory. The $\frac{1}{2}$ factor is inserted in order to obtain the Maxwellian expression for the limiting case. This is clearly seen in the case of $T_4{}^1$, for instance:

$$T_4{}^1=E_yH_z-H_yE_z, \tag{3.6}$$

which, for weak fields, goes over into the Maxwellian expression for the x component of the Poynting vector.

From (3.4) we find

$$T_s{}^s=2T, \tag{3.7}$$

showing that our action function is half the trace of the energy momentum tensor.

It was shown by Feenberg[5] that in the earlier form of the new field theory the equations of

motion are not consequences of the field equations but constitute an extra dynamical condition. We shall show now that in the present form of the theory, in the first approximation, the Lorentz equations of motion follow from the field equations without further assumption. The absence of singularities in the f_{kl} field is essential for this result.

One of the equations expressing the conservation of energy and momentum is

$$\frac{\partial T_{34}}{\partial t}=\frac{\partial T_{31}}{\partial x}+\frac{\partial T_{32}}{\partial y}+\frac{\partial T_{33}}{\partial z}, \tag{3.8}$$

or, in space notation,

$$\partial S_z/\partial t+\operatorname{div} Z=0, \tag{3.9}$$

where $-S_z\sim T_{34}$, $Z\sim T_{31}$, T_{32}, T_{33}.

We may integrate (3 9) over some volume and transform the integral on the right-hand side into a surface integral. For simplicity we assume, though this is not essential, that S_z, Z are functions of f_{kl} and p_{kl} according to (3.4). We should exclude those points at which Z can become infinite, which can only occur where $P\to\infty$. We thus have, assuming for simplicity that only one such point is in question,

$$\frac{\partial}{\partial t}\int_\Omega S_z dv=\int_{\Sigma'} Z_n d\sigma-\int_\Sigma Z_n d\sigma, \tag{3.10}$$

where Σ' is a small surface enclosing the space point at which $P\to\infty$, Σ is an arbitrary surface enclosing Σ', and Ω is the volume between Σ and Σ'.

Now it follows from (2.6) and the fact that $D_r=1/r^2$, that the $p^{lm}f_{mk}$ and $f^{*lm}p_{mk}{}^*$ terms in $T_k{}^l$ will be at most of the order of 1. Further the part of $T_k{}^l$ involving the action function T can only give a contribution to the surface integral over Σ' of the order of $r^2\log r$. Thus in the limit when Σ' shrinks to a point the whole integral over Σ' vanishes, and we have left

$$\frac{\partial}{\partial t}\int_\Omega S_z dv=-\int_\Sigma Z_n d\sigma. \tag{3.11}$$

The vanishing of the integral

$$\int_{\Sigma'} Z_n d\sigma$$

in the limit, together with the similar vanishing of the corresponding integrals for the x and y directions, is here a consequence of the regularity condition and of the special form of the action function. But this vanishing constitutes the dynamical condition which leads to the Lorentz laws of motion[12] under the usual conditions concerning the possibility of separating the whole field into a spherically symmetric field and a weak uniform external field.

PART II

§4. Action function and field equations

The field equations of the general theory of relativity are of the form

$$R_{kl}-\tfrac{1}{2}g_{kl}R=-8\pi\gamma T_{kl}, \tag{4.1}$$

where R_{kl} is the Ricci tensor formed out of the metrical tensor g_{kl}, R its contraction, T_{kl} the material energy momentum tensor, and γ the relativistic gravitational constant. Though the precise form of T_{kl} is not specified by the general theory of relativity, its physical significance must definitely be that of an energy momentum tensor and we shall accordingly use here for T_{kl} the energy momentum tensor corresponding to the theory described in the first part of this paper.

Since, in the general theory of relativity, the g_{kl} may not be assumed to be Galilean, we must define the scalars F, P so as to show explicitly their dependence on the g_{kl}:

$$\begin{cases} F=\tfrac{1}{2}g^{kl}g^{mn}f_{km}f_{ln}; & f_{km}=\left(\dfrac{\partial\varphi_m}{\partial x^k}-\dfrac{\partial\varphi_k}{\partial x^m}\right); \\ P=\tfrac{1}{2}g^{kl}g^{mn}p_{km}{}^*p_{ln}{}^*; & p^*{}_{km}=\left(\dfrac{\partial\psi_m}{\partial x^k}-\dfrac{\partial\psi_k}{\partial x^m}\right). \end{cases} \tag{4.2}$$

Further we shall need to know the relationship between a six-vector and its dual. The general formula leads to

$$\begin{cases} f^{*23}=\dfrac{1}{\sqrt{(-g)}}f_{14}, \text{ etc.}; & f^{*14}=\dfrac{1}{\sqrt{(-g)}}f_{23}, \text{ etc.}; \\ f^*{}_{23}=-\sqrt{(-g)}f^{14}, \text{etc.}; & f^*{}_{14}=-\sqrt{(-g)}f^{23}. \text{etc.}, \end{cases} \tag{4.3}$$

with, of course, analogous relations holding for the p's.

[12] Pryce, reference 5, §9.

The correct action principle for the general theory is

$$\delta\int\left(\frac{1}{8\pi\gamma}R-T(\epsilon)\right)\sqrt{(-g)}dx^1dx^2dx^3dx^4=0, \quad (4.4)$$

where $T(\epsilon)$ is the function defined in (1.20) and variation is with respect to g_{kl}, φ_k and ψ_k, respectively.

The variation with respect to g_{kl} gives the conditions[13]

$$\sqrt{(-g)}\{(R_{kl}-\tfrac{1}{2}g_{kl}R)+8\pi\gamma T_{kl}\}=0, \quad (4.5)$$

with $$T_{kl}=\tfrac{1}{2}g_{kl}T-\partial T/\partial g^{kl}. \quad (4.6)$$

This T_{kl} reduces to the T_{kl} of (3.4) in the flat case.

Since T is homogeneous of degree zero in g_{kl}, as follows from (4.2), we have

$$g^{kl}\partial T/\partial g_{kl}\equiv 0. \quad (4.7)$$

Thus, on contracting (4.6) we find at once that

$$T_s{}^s=2T, \quad (4.8)$$

a result already obtained for the Galilean case in §3. Further, the variations with respect to φ_k and ψ_k give field equations equivalent to (4.2):

$$\frac{\partial}{\partial x^k}(p^{kl}\sqrt{(-g)})=0, \quad (4.9)$$

$$\frac{\partial}{\partial x^k}(f^{*kl}\sqrt{(-g)})=0, \quad (4.10)$$

where use has been made of the "constitutive" equations

$$p^{kl}=\partial T/\partial f_{kl}, \quad f^{*kl}=\partial T/\partial p_{kl}{}^*. \quad (4.11)$$

§5. The regularity condition

We have already seen that the condition of regularity of the field gives the restriction that in the spherically symmetric electrostatic case $E_r=0$ for $r=0$.

In the general theory we apply the regularity condition not only to the f_{kl} field but also to the g_{kl} field. The regularity condition for the general theory is that:

Only those solutions of the field equations may have physical meaning for which space-time is everywhere regular and for which the f_{kl} and g_{kl} fields and those of their derivatives which enter the field equations and the conservation laws exist everywhere.

The most general spherically symmetric static line element may always be brought to the form

$$ds^2=e^\nu dt^2-e^\lambda dr^2-r^2(d\theta^2+\sin^2\theta d\varphi^2), \quad (5.1)$$

where λ and ν are functions of r alone.

In the general theory of relativity the spherically symmetric solution of the purely gravitational field equations is given by the Schwarzschild line element

$$ds^2=Adt^2-A^{-1}dr^2-r^2(d\theta^2+\sin^2\theta d\varphi^2), \quad (5.2)$$

$$A=1-2m\gamma/r, \quad (5.3)$$

where $(-2m\gamma)$ is a constant of integration, m having the significance of the gravitational mass of the body producing the field and γ being the gravitational constant. This line element has an essential singularity at $r=0$ and does not satisfy the regularity condition.

In the general relativity form of the original Born theory the requirement that there be no infinities in the g_{kl} forces the identification of gravitational with electromagnetic mass[14] and leads to the line element (5.2) with

$$A=1-\frac{8\pi\gamma}{r}\int_0^r\{(r^4+1)^{\frac{1}{2}}-r^2\}dr. \quad (5.4)$$

This line element approximates the Schwarzschild form for r greater than the electronic radius but avoids the infinities of that line element for $r=0$. However, there is still a singularity at the pole.[15] For, when $r\to 0$, (5.4) gives

$$A\to(1-8\pi\gamma)=\beta \text{ (say)}$$

so that (5.2) becomes

$$ds^2\to\beta dt^2-(1/\beta)dr^2-r^2(d\theta^2+\sin^2\theta d\varphi^2). \quad (5.5)$$

Thus the ratio of the circumference to the radius of a small circle having its center at the pole is, in

[13] It has been pointed out to us by H. P. Robertson that we use two different conventions in the variational process. For variations of f_{kl} etc. we assume $\delta f_{kl}=-\delta f_{lk}$, but for variations of g_{kl} we assume δg_{kl} to be independent of δg_{lk}. Since no confusion is likely to arise from this usage we employ the present convention in order to agree with previous work in this field.

[14] Hoffmann, Phys. Rev. **47**, 877 (1935). This paper includes a detailed discussion of the difficulties connected with the Schwarzschild line element and of the physical principles underlying the argument of this and the next section. For the sake of brevity much of this discussion is not repeated here.

[15] This was kindly pointed out by Einstein and Rosen.

the limit, $2\pi\beta$ and not 2π. Therefore the pole is a conical point and not regular. No coordinate system can be introduced which will be non-singular at $r=0$ and derivatives are actually undefined at this point.

Thus the regularity condition applied to (5.1) requires that

$$\lim_{r\to 0}(e^{\lambda})=1 \tag{5.6}$$

and that certain derivatives shall exist. We shall consider this matter in more detail later.

§6. The general spherically symmetric electrostatic case

The solution of the general spherically symmetric electrostatic case can be very largely reduced to that of the corresponding Galilean case treated in Part I because of a result we shall now prove.

The energy tensor (4.6) can be written as

$$\begin{aligned}T_{kl}&=-\frac{1}{2}g_{kl}T-\frac{\partial T}{\partial \epsilon}\frac{\partial \epsilon}{\partial g^{kl}}\\&=-\frac{1}{2}g_{kl}T-\frac{1}{2}\frac{\partial T}{\partial \epsilon}\left\{\frac{1}{(-FP)^{\frac{1}{2}}}g^{mn}f_{km}f_{ln}\right.\\&\qquad\left.-\left(-\frac{F}{P^3}\right)^{\frac{1}{2}}g^{mn}p^*{}_{km}p^*{}_{ln}\right\}.\end{aligned} \tag{6.1}$$

For the line element and coordinate system defined by (5.1) the only non-zero components of f_{kl} and $p_{kl}{}^*$ are, in the present case, $f_{14}=-f_{41}$ and $p_{23}{}^*=-p_{32}{}^*$, respectively. Thus, since g^{kl} vanishes if $k\neq l$, the tensors

$$F_{kl}=g^{mn}f_{km}f_{ln} \quad\text{and}\quad P_{kl}=g^{mn}p_{km}{}^*p_{ln}{}^* \tag{6.2}$$

are easily seen to be such that

$$F_1{}^1=F_4{}^4; \quad P_1{}^1=P_4{}^4(=0). \tag{6.3}$$

Since, further

$$g_1{}^1=g_4{}^4(=1),$$

it follows from (6.1) and (6.3) that

$$T_1{}^1=T_4{}^4. \tag{6.4}$$

Thus the field equations (4.5) imply that

$$\sqrt{(-g)}\{R_1{}^1-\tfrac{1}{2}g_1{}^1R\}=\sqrt{(-g)}\{R_4{}^4-\tfrac{1}{2}g_4{}^4R\}. \tag{6.5}$$

These equations at once give[16]

$$\lambda'+\nu'=0$$

and since e^{λ} and e^{ν} must each approach unity as $r\to\infty$, we obtain the result that

$$\lambda+\nu=0 \tag{6.6}$$

or
$$g_{11}g_{44}=1/(g^{11}g^{44})=-e^{\lambda+\nu}=-1. \tag{6.7}$$

This result shows that the values of $\sqrt{(-g)}$, F, P, T, and $T_k{}^l$,[17] for the present case, take the same form as in the Galilean case for polar coordinates and we may thus use results obtained in Part I which are valid for the more general case considered here.

We have, therefore, at once,

$$p_{14}=D_r=1/r^2; \quad f_{14}=E_r=r^2/(1+r^4) \tag{1.15}$$

and it turns out that the only equations which remain to be satisfied are the $(1-1)$ and $(2-2)$ equations of the set (4.5). Without making use of (6.6) we may write these in the form

$$e^{-\lambda}(\nu'r+1)-1=-8\pi\gamma r^2T_1{}^1=-8\pi\gamma r^2T_4{}^4, \tag{6.8}$$

$$\begin{aligned}&r^2e^{-\lambda}\{\tfrac{1}{2}\nu''-\tfrac{1}{4}\lambda'\nu'+\tfrac{1}{4}\nu'^2+(1/2r)(\nu'-\lambda')\}\\&\qquad=-8\pi\gamma r^2T_2{}^2,\end{aligned} \tag{6.9}$$

these being the same as

$$e^{-\lambda-\nu}\frac{d}{dr}(re^{\nu})-1=-8\pi\gamma r^2T_4{}^4, \tag{6.8a}$$

$$\begin{aligned}&e^{-\lambda-\frac{1}{2}\nu}r\frac{d}{dr}\left\{r\frac{d}{dr}(e^{\frac{1}{2}\nu})\right\}\\&\quad-e^{-\lambda}r^2\{\tfrac{1}{4}\lambda'\nu'+(1/2r)\lambda'\}=-8\pi\gamma r^2T_2{}^2.\end{aligned} \tag{6.9a}$$

The values of the components $T_4{}^4$, $T_2{}^2$ may be calculated directly from (6.1) or from the value (3.4) of the first part, with the help of (6.7), (4.2), (4.3), (1.20) and (1.15). The values are found to be

$$T_4{}^4=-\log\left(\frac{r^4}{1+r^4}\right), \tag{6.10}$$

$$T_2{}^2=-\log\left(\frac{r^4}{1+r^4}\right)-\frac{2}{1+r^4}. \tag{6.11}$$

[16] See the values of $(R_1{}^1-\frac{1}{2}g_1{}^1R)$ and $(R_4{}^4-\frac{1}{2}g_4{}^4R)$ given in Eddington, *Mathematical Theory of Relativity*, second edition, p. 104, Eqs. (46.9).

[17] This last can best be seen from (6.1) with the help of (4.2), (4.3) and the fact that only $f_{14}=-f_{41}$, $p_{14}=-p_{41}$, and $f_{23}{}^*=-f_{32}{}^*$, $p_{23}{}^*=-p_{32}{}^*$ of the covariant components are different from zero in the present case.

If we use (6.7) to simplify the left-hand sides of (6.8), (6.9) we now obtain

$$e^{\nu}(\nu' r+1)-1=\frac{d}{dr}(e^{\nu} r)-1=-8\pi\gamma r^2 T_4^4$$

$$=8\pi\gamma r^2 \log\frac{r^4}{1+r^4}, \quad (6.12)$$

$$r^2 e^{\nu}(\nu''+\nu'^2+\nu'/r)=-16\pi\gamma r^2 T_2^2$$

$$=16\pi\gamma r^2\left\{\log\left(\frac{r^4}{1+r^4}\right)-\frac{2}{1+r^4}\right\}. \quad (6.13)$$

The solution of (6.12) is seen to be

$$e^{\nu}=1-\frac{k}{r}-\frac{8\pi\gamma}{r}\int_0^r r^2 T_4^4 dr$$

$$=1-\frac{k}{r}+\frac{8\pi\gamma}{r}\int_0^r r^2 \log\frac{r^4}{1+r^4}dr, \quad (6.14)$$

where k is a constant of integration corresponding to the $(-2m\gamma)$ of the Schwarzschild line element (5.2), (5.3). The Eq. (6.13) is essentially the derivative of (6.12) with respect to r so that a solution of (6.12) whose appropriate derivatives exist will automatically be a solution also of (6.13).

The regularity condition shows that we must take $k=0$ in (6.14) since otherwise we shall have an essential singularity at $r=0$. But if $k=0$ we must regard the quantity $4\pi\gamma\int_0^r r^2 T_4^4 dr$ as the gravitational mass causing the field at coordinate distance r from the pole. This quantity, however, is precisely

$$\gamma\int\int\int T_4^4 r^2 \sin\theta dr d\theta d\varphi \quad (6.15)$$

taken over the sphere having its center at $r=0$ and coordinate radius r and is thus the measure, in gravitational units, of the total *electromagnetic* mass within this sphere. For r appreciably greater than the electronic radius this line element closely approximates the Schwarzschild form. Thus the regularity condition shows that electromagnetic and gravitational mass are the same and it is seen that, as in the Newtonian theory, we now have the result that the attraction due to a uniform spherical shell of matter is zero at any point inside the shell. A further result of this identification of gravitational with electromagnetic mass is the fact that the gravitational mass (6.15) is necessarily positive, which was not the case in the Schwarzschild line element.

It remains to show that the regularity conditions are completely fulfilled by our solution

$$\begin{cases} ds^2=A dt^2-A^{-1}dr^2-r^2(d\theta^2+\sin^2\theta d\varphi^2), \\ A=1+\dfrac{8\pi\gamma}{r}\displaystyle\int_0^r r^2 \log\frac{r^4}{1+r^4}dr, \\ E_r=r^2/(1+r^4). \end{cases} \quad (6.16)$$

In the limit $r\to 0$ we have $A\to 1$ so that we avoid a singularity of space-time at $r=0$. Also, since γ is very small, A will not change sign. Finally all the derivatives entering (6.8a), (6.9a) are seen to exist and the derivative of (6.8a) with respect to r, the only part of the divergence relations which involves further derivatives with respect to r, also exists. The regularity of the f_{kl} field was discussed in §2 and that discussion remains valid for the present case.

We have thus found a solution of the general spherically symmetric electrostatic case which fulfills the demands of the regularity condition and which carries over to gravitational theory the general ideas of the first part.

Since the g_{44} of (6.16) has the value unity at $r=0$ and at $r=\infty$ it follows that its derivative must change sign. In the usual gravitational theory of general relativity the derivative of g_{44} is proportional to the gravitational force which would act on a test particle in the Newtonian approximation. In the present theory, then, it is interesting to note that although this force is an inverse square attraction for ordinary distances, it is actually a repulsion for very small r.

LETTERS TO THE EDITOR

Prompt publication of brief reports of important discoveries in physics may be secured by addressing them to this department. Closing dates for this department are, for the first issue of the month, the eighteenth of the preceding month, for the second issue, the third of the month. Because of the late closing dates for the section no proof can be shown to authors. The Board of Editors does not hold itself responsible for the opinions expressed by the correspondents.

Communications should not in general exceed 600 words in length.

The Magnetic Anisotropy of Four-Coordinated Co^{++} Ions in Crystals

In a recent communication[1] we described some magnetic measurements on single crystals of the blue cobalt salt $Cs_2[CoCl_4]$. In marked contrast with the ordinary (pink) cobalt salts like the hydrated sulphates and selenates, which are strongly anisotropic, the crystal of $Cs_2[CoCl_4]$ is only feebly so; $\Delta x/x$ is of the order of 20 percent to 40 percent for the former salts, whereas for $Cs_2[CoCl_4]$ it is only 5 percent. This striking difference in the magnetic behavior of the hydrated sulphates and selenates of cobalt on the one hand, and $Cs_2[CoCl_4]$ on the other, is indeed to be expected in view of the different dispositions of negative charges around the Co^{++} ions in the two types of crystals. Whereas in the former salts the cobalt ion is six-coordinated and is surrounded by six negative charges, which occupy the corners of an octahedron with the Co^{++} at the center, in the crystal of $Cs_2[CoCl_4]$, on the other hand, the Co^{++} ion is surrounded by four negative charges, which form a tetrahedron. Though for both the above distributions of charges about Co^{++} the electric fields acting on it will be predominantly cubic in symmetry, and the Stark patterns of Co^{++} produced by the two fields will be very similar, it is found theoretically[2] that the pattern should be inverted as we pass from the octohedral type of distribution to the tetrahedral. Since one extreme level of the Stark pattern is single while the other is triply degenerate, this inversion of the pattern will make a great difference to the magnetic anisotropy, as the latter depends on the degree of degeneracy of the *lowest* level. When the distribution is octohedral the threefold level is lowest, and will therefore lead to a large anisotropy, while with the tetrahedral distribution, such as obtains in $Cs_2[CoCl_4]$, the single level is lowest and the crystal will be almost isotropic.

We have now measured the magnetic susceptibilities of single crystals of another compound of cobalt in which the Co^{++} ion is four-coordinated, namely, $Cs_3[CoCl_4]Cl$. The crystals are tetragonal, and their structure has recently been analyzed by x-ray methods by Powell and Wells.[3] They find that each Co^{++} ion is closely associated with four (negatively charged) chlorine atoms, which form a tetrahedron about it, the fifth chlorine atom standing apart at a much greater distance from it. We should therefore expect the anisotropy of this crystal also to be very feeble. This is actually so, as will be seen from the following results of our magnetic measurements. Denoting the gram molecular susceptibilities of the crystal along its tetragonal axis and along perpendicular directions by $x_{\parallel}$ and $x_{\perp}$, respectively, we find that, at 30°C, $x_{\parallel}-x_{\perp}=650\times10^{-6}$, and the mean susceptibility $x=(x_{\parallel}+2x_{\perp})/3=9930\times10^{-6}$, both in c.g.s. e.m.u. The anisotropy is thus quite small, $\Delta x/x$ (=650/9930) being only 6½ percent.

K. S. KRISHNAN
ASUTOSH MOOKHERJI

Indian Association for the Cultivation of Science,
210 Bowbazar Street,
Calcutta, India,
March, 1937.

[1] Phys. Rev. **51**, 528 (1937).
[2] See Van Vleck, Phys. Rev. **41**, 208 (1932), and Gorter, Phys. Rev. **42**, 437 (1932).
[3] Powell and Wells, J. Chem. Soc. London 359 (1935).

Width of Iodine Resonance Neutron Band

Preiswerk and von Halban[1] have reported experiments showing that the absorption of iodine resonance neutrons in iodine is changed markedly if the neutrons are first filtered through iodine layers. Stating that the absorption coefficient in boron of such filtered neutrons is identical with that for those unfiltered, they conclude that the phenomenon involved in their experiments is the "self-reversal of the nuclear line."

The authors have measured the boron absorption coefficients of the iodine filtered neutrons for different filter thicknesses. The results, given in Table I, though

TABLE I. *Boron absorption coefficient for iodine filtered iodine resonance neutrons.*

Percent of Activity, due to Resonance Neutrons, Absorbed by Iodine Filter	Filter Thickness (g of iodine/cm²)	Boron Absorption Coefficient (cm²/g)
0	0	0.35±0.07
40	0.30	0.10±0.06
55	0.75	0.05±0.04

rough, indicate that the absorption probably first removes the lower energy section of a wide band or group of narrow bands leaving residual neutrons of considerably higher energy. These results are in agreement with the considerations of Bethe and Placzek.[2]

SAMUEL RUBEN
W. F. LIBBY

Department of Chemistry,
University of California,
Berkeley, California,
April 14, 1937.

[1] Preiswerk and von Halban, Nature **138**, 163 (1936).
[2] Bethe and Placzek, Phys. Rev. **51**, 450(1937).

The Scattering of Neutrons by Ortho- and Parahydrogen

The observed binding energy of the deuteron yields information concerning the interaction of neutrons and protons with parallel spins, but permits nothing to be deduced about the neutron-proton interaction with antiparallel spins. It has been pointed out by Wigner[1] that the large slow neutron scattering by free protons provides evidence for an antiparallel spin interaction between neutrons and protons which is weaker than the interaction with parallel spins. The numerical value of the slow neutron cross section,[2] $\sigma = 13 \times 10^{-24}$ cm², can be explained by either a stable or a virtual singlet state about 2 Mev higher than the ground state of the deuteron. It is the purpose of this note to indicate that experiments on the scattering of neutrons by ortho- and parahydrogen would enable one to determine the sign of the singlet state energy and the range of the neutron-proton interaction, in addition to providing direct information concerning the spin dependence of the neutron-proton interaction.

A dependence of the neutron-proton interaction upon the relative spin orientation of the particles will manifest itself in a marked difference between the slow neutron scattering cross sections of orthohydrogen (parallel proton spins) and parahydrogen (antiparallel proton spins). Neutrons with energy less than 0.068 ev, incident upon para-H_2 in its ground state ($J=0$, $v=0$, $S=0$), may be either elastically scattered, or inelastically scattered with excitation of the molecule to the ground state of the ortho-system ($J=1$, $v=0$, $S=1$). This latter process, requiring 0.023 ev, occurs only if the neutron-proton interaction is spin dependent. Provided the neutron energy is less than 0.045 ev, the cross section for the scattering of neutrons by ortho-H_2 in its ground state will be the sum of the elastic scattering cross section and the cross section for the inelastic process in which the molecule is converted to a para-H_2 molecule in its ground state, with the neutron taking up the excess energy.

Accepting Wigner's explanation of the large slow neutron scattering by free protons, the cross sections of these four processes have been calculated with the assumption of an interaction range of 2×10^{-13} cm and a virtual singlet state of the deuteron.[3] For liquid-air temperature neutrons ($3kT/2 = 0.012$ ev) $\sigma_{\text{para}}(0.012) = 0.21 \times 10^{-24}$ cm², while $\sigma_{\text{ortho}}(0.012) = 65 \times 10^{-24}$ cm². The cross sections for neutrons at ordinary temperatures ($3kT/2 = 0.037$ ev), however, are $\sigma_{\text{para}}(0.037) = 19 \times 10^{-24}$ cm² and $\sigma_{\text{ortho}}(0.037) = 50 \times 10^{-24}$ cm². Therefore, if the present concept of the neutron-proton interaction is valid, one would expect the following results: (a) The orthoscattering cross section for liquid-air neutrons should be about 300 times the corresponding parascattering cross section. (b) The parascattering cross section for ordinary thermal neutrons should be roughly 100 times the parascattering cross section for liquid-air neutrons. For a real singlet state, however, these ratios are of the order of one.

The elastic parascattering cross section is quite sensitive to the value of the range of interaction if the singlet state is virtual. For example, the paraelastic scattering cross section at liquid-air neutron temperatures with zero range of interaction is 1.75×10^{-24} cm², as compared with 0.26×10^{-24} cm² for an interaction range of 2×10^{-13} cm. Hence, from a measurement of the paraelastic scattering cross section for homogeneous neutrons at some energy less than 0.023 ev, the range of interaction may be inferred with some degree of accuracy.

A more detailed discussion will be published shortly in the *Physical Review*.

JULIAN SCHWINGER
E. TELLER

Columbia University,
New York City.

George Washington University,
Washington, D. C.,
April 13, 1937.

[1] H. A. Bethe and R. F. Bacher, Rev. Mod. Phys. **8**, 82 (1936).
[2] E. Amaldi and E. Fermi, Phys. Rev. **50**, 899 (1936).
[3] Experiments on the magnetic capture of neutrons by protons seem to indicate the existence of a virtual singlet state of the deuteron. Cf. reference 2.

Proton-Induced Radioactivity in Heavy Nuclei

The elements $_{14}$Si, $_{20}$Ca, $_{24}$Cr, $_{25}$Mn, $_{27}$Co, $_{28}$Ni, $_{30}$Zn, $_{33}$As, $_{34}$Se, $_{42}$Mo, $_{48}$Cd, $_{49}$In, $_{50}$Sn and $_{51}$Sb become radioactive under the bombardment of protons of about 3.6 Mev from the cyclotron. $_{12}$Mg, $_{13}$Al, $_{16}$S, $_{17}$Cl, $_{26}$Fe, $_{29}$Cu, $_{47}$Ag, $_{78}$Pt and $_{82}$Pb appear to show no signs of radioactivity under the same conditions. The relative activities of the first group as measured with an ionization chamber after a 15-minute bombardment with a beam of 1 microampere are as follows: 6, 21, 5, 27, 6, 21, 40, 13, 2000, 10, 20, 3, 2, 1.

Practically none of these radioactivities have been previously reported. Mn, Co and As are of particular interest because they cannot form radioactive nuclei by the usual proton capture reaction or by the proton capture alpha-particle emission reaction. Presumably the reaction here is proton capture with either deuteron or neutron emission. For Mn this unusual type of reaction has been shown to take place by a chemical separation which proved that the active substance was an isotope of Mn. The following reaction is therefore considered to be the one taking place:

$$_{25}\text{Mn}^{55} + {}_{1}\text{H}^{1} \rightarrow {}_{25}\text{Mn}^{54} + {}_{1}\text{H}^{2}.$$

The chemical separation with Se showed active material in the As precipitate, thus indicating one of the usual types of reaction:

$$_{34}\text{Se} + {}_{1}\text{H}^{1} \rightarrow {}_{33}\text{As} + {}_{2}\text{He}^{4}.$$

Further chemical separations are being made.

The Se period (approximately 17 min.) is of the same order as the short periods in the above elements. Excluding the possibility of a large contribution from accompanying gamma-rays, the high relative activity in Se indicates a large cross section for the proton reaction. A study of the yield as a function of the proton energy showed a very slow rise from 2.2 Mev to 3.1 Mev, at which energy the yield rises almost vertically.

S. W. BARNES
L. A. DUBRIDGE
E. O. WIIG
J. H. BUCK
C. V. STRAIN

Department of Physics,
University of Rochester,
Rochester, New York,
March 29, 1937.

Photoelectric Investigation of the "Allison Magneto-Optic Effect"

The continued controversy over the existence of the "Fred Allison Magneto-Optic Effect" has justified further investigation of the phenomena produced in the apparatus. The author is herewith reporting the results of an extended study as to the existence of the minima by means of photo-electric technique of greater sensitivity than previously reported.

The optical system of the Allison apparatus[1] has been modified to permit the use of an auxiliary beam from the same light source as a comparator. Collimated light from the source was incident upon the apex of a 45° prism whose faces had been aluminized. The two beams so formed, were again reflected by plane mirrors so as to travel in parallel beams, the one through the usual coils and the other serving as an auxiliary or comparison beam. The auxiliary path was made as optically identical as possible with the main path, which contained the magnetic field coils, by placing similar polarizing and analyzing Nicols, cells, liquids, and lenses in each. The emergent light from the analyzing Nicols was focused by lenses upon two similar vacuum type photo-cells. The two photo-cell currents were fed in opposition into an FP-54 balanced amplifier of the DuBridge-Brown type. The photo-cells and amplifier tube were housed in an evacuated chamber to insure greater electrical stability at the low d.c. current levels used. Variations of the plate current of the amplifier as observed by a sensitive galvanometer were directly proportional to the difference in the two photo-cell currents.

It was found possible by this method to balance out the troublesome fluctuations produced in the light source itself, so that one could be assured that any variations of the amplified currents were due to changes in the light beam which occurred differently in the two paths. With the capillary mercury arc which was generally used as light source, fluctuations of the arc were balanced out to 0.2 of one percent of the light intensity incident on the photo-cell. This then was the lower limit of sensitivity of the apparatus. With a magnesium spark as light source, this limit was 1 percent of the light intensity. The light from the mercury arc was filtered to permit either the 4358A or 5461A line to be used as the source; with the spark source the 4481A line of magnesium was used.

The electrical circuit and trolley system of Allison's apparatus has been duplicated with the exception of the replacement of the bar trolley contactors by strong springs giving more positive contacts with the trolley wires. Measurements with a wave meter have shown strong damped oscillations of from 250 to 1000 kilocycles in frequency always present at the coils and along the trolley wires. Decrements of less than 0.2 indicate that the oscillatory currents are long wave trains of an effective length of thirty or more oscillations. Electric circuit analyses of the oscillatory circuit using measured high frequency values of the various resistances, capacitances, and inductances involved were in complete agreement with the observations in respect to frequency, damping constants, and effective value of the currents in the coils. In general the peaks of the oscillatory current in one coil were shown to be slightly out of phase with those in the other due primarily to the difference in inductances of the two parts of the trolley system. No evidence was found for the existence of types of current surges so prominently discussed in Allison's papers. The "initial transient surge" is nothing more than the first peak of the oscillatory train. With the addition of 230 ohms or more of noninductive resistance into the spark circuit, the oscillatory currents may be damped out to single aperiodic current pulses. The measured value of the critical damping resistance and the effective value of the aperiodic currents are in agreement with those calculated by theory. It appears, then, that no mysteries exist concerning the nature of the currents in the coils.

The usual method of searching for the minima by slowly moving the trolley over their reported positions has been used. A variety of solutions were tested: namely, (1) CS_2 in both cells; (2) CS_2 in one cell and, in the other, either (a) dilute solution of HCl (1 part in 10^3) or (b) more concentrated solution of HCl (1 part in 10^2) or (c) a mixture of $CoCl_2$, $NiCl_2$ and $CuCl_2$ (1 part in 10^4).

Attempts to observe the sharp minima were made using several arrangements of the apparatus for which minima have been reported: (1) Nicols crossed and the magnetic fields of the coils in opposition, (2) Nicols parallel and the magnetic fields assisting, (3) Nicols at 45°, the magnetic fields assisting. Observations were made both with the normal condition of damped oscillatory currents and with aperiodically damped currents, thus reproducing the electrical conditions of Ball[2] and the recent work from Allison's laboratory by Hughes.[3] During these observations many variations were made in the capacity of the condenser, high voltage across it, width of spark, length of leads from spark to trolley system, etc.

At no time, under any of these conditions, has a reproducible "sharp" minimum corresponding to a change of intensity of greater than 0.2 of one percent been observed when the steady mercury arc source was used nor greater than 1 percent when the spark was used as light source.

Small changes of the intensity of the main beam for short periods of time, comparable with the time required for the trolley to pass over a minimum position, were made by passing through it thin sheets of glass and Cellophane. These tests have convinced the author of the ability of the photo-cell system to detect any changes in the total intensity of the main beam greater than the above limits of sensitivity no matter what the cause of such changes may be, whether they be rotations of the plane of polarization, double refraction, or absorption. These limits of sensitivity are well below the least perceptible intensity differences which the eye can detect at the light intensity levels used in the experiments, particularly in the case of the mercury arc. There remains the possibility that a change in the distribution of the intensity of the light beam over its area, caused by some phenomena such as scattering, might be observable by the eye, although not by the photo-cell system, since, as used, this measured only the total intensity of the beam. The possibility that the eye does not integrate these high frequency, small intensities of light as does the photo-cell has been investigated (Talbot's law) and is considered exceedingly remote.

In our experiments there have thus appeared no minima of the type reported by Allison which are attributable to changes of the total intensity of the light. The author wishes to thank Professor J. Barton Hoag for his continued guidance in this work.

GEORGE C. COMSTOCK

Ryerson Physical Laboratory,
University of Chicago,
April 5, 1937.

[1] J. Beams and F. Allison, Phys. Rev. **29**, 161 (1927).
[2] S. S. Cooper and T. R. Ball, J. Chem. Ed. **13**, 210, 278, 326 (1936).
[3] G. Hughes, J. Am. Chem. Soc. **58**, 1924 (1936).

On the Saturation Property of Nuclear Forces

The symmetrical interaction operator[1]

$$V=\sum_{i<j}\{(1-g-g_1-g_2)P_{ij}+gP_{ij}Q_{ij}+g_1 1+g_2 Q_{ij}\}J(r_{ij}) \quad (1)$$

possesses the saturation property if the several different types of exchange forces are present in proportions satisfying the inequality[1]

$$G=1+g-5g_1-3g_2\geqq 0. \quad (2)$$

Recent calculations by Inglis[2] on the binding energy of Li^6 show that the most satisfactory theory based on Eq. (1) is obtained by requiring that the saturation parameter G vanish. The artificial appearance of the condition $G=0$ is only apparent. It is the purpose of this note to point out that there exists an alternative formulation of the theory in which the vanishing of the saturation parameter G is an entirely natural restriction without any trace of artificiality.

In terms of the Pauli spin matrices,[3] $\sigma=(\sigma_x, \sigma_y, \sigma_z)$, and the isotopic spin matrices,[4] $\tau=(\tau_\xi, \tau_\eta, \tau_\zeta)$, the exchange operators in Eq. (1) can be expressed in the form[5]

$$\begin{aligned} Q_{ij}&=\tfrac{1}{2}(1+\sigma_i\cdot\sigma_j),\\ P_{ij}Q_{ij}&=-\tfrac{1}{2}(1+\tau_i\cdot\tau_j),\\ P_{ij}&=-\tfrac{1}{4}(1+\sigma_i\cdot\sigma_j)(1+\tau_i\cdot\tau_j). \end{aligned} \quad (3)$$

The operator V now contains terms linear in $\sigma_i\cdot\sigma_j$, $\tau_i\cdot\tau_j$, $\sigma_i\cdot\sigma_j\tau_i\cdot\tau_j$ and also the term $G\,\Sigma J(r_{ij})$. If this last term is dropped by setting $G=0$ there remains an interaction operator which is a linear function of the three operators

$$\Sigma\sigma_i\cdot\sigma_j J(r_{ij}), \quad \Sigma\tau_i\cdot\tau_j J(r_{ij}), \quad \Sigma\sigma_i\cdot\sigma_j\tau_i\cdot\tau_j J(r_{ij}), \quad (4)$$

each of which separately possesses the saturation property. The omission of the term which does not involve the spin and isotopic spin matrices is quite natural here because there is no need to balance carefully terms of different types which have the saturation property only when combined in the correct proportions.

The two formulations which are connected by Eq. (3) are equivalent only because the nuclear wave functions are antisymmetric with respect to the interchange of the Cartesian, spin and isotopic spin coordinates of any two heavy particles.[5, 6] For this reason arguments purporting to show that *symmetrical* interactions of the Majorana exchange type cannot be obtained from any form of the neutrino-electron field theory are not conclusive against the formulation in terms of the spin and isotopic spin matrices.[7] However, interaction terms of the form $\tau_i\cdot\tau_j$, $\sigma_i\cdot\sigma_j\tau_i\cdot\tau_j$ between two heavy particles can be obtained from a field theory only if the description of the field includes an "isotopic spin" variable in addition to the ordinary spin variable which is usually ascribed to the light particles making up the field.

To obtain a good fit with the experimental binding energies and cross sections it may be necessary to associate different potential functions $J(r)$ in (4) with each of the different modes of dependence on the spin and isotopic spin matrices. For actual calculations an interaction operator based on (4) is most conveniently expressed as a linear combination of the three saturation type operators

$$\begin{aligned} V_a&=\tfrac{1}{2}\sum_{i<j}(4P_{ij}+1)J_a(r_{ij}),\\ V_b&=\tfrac{1}{2}\sum_{i<j}(P_{ij}Q_{ij}+Q_{ij})J_b(r_{ij}),\\ V_c&=\tfrac{1}{2}\sum_{i<j}(1-P_{ij})(4-5Q_{ij})J_c(r_{ij}). \end{aligned} \quad (5)$$

Each of these is a special case under Eq. (1) satisfying the condition $G=0$. The most important term is V_a which determines the binding energy and the excitation energies of the low terms in the light stable nuclei belonging to the mass series $4n$, $4n+1$, $4n+3$; the effective depth and range of the potential function $J_a(r)$ are known from calculations on the binding energies of the three- and four-particle systems.[8] The singlet-triplet splitting in nuclei of the $4n+2$ type determines V_b; the effective range of $J_b(r)$ must differ from that of $J_a(r)$ according to the calculations of Present and Rarita[9] who have shown that the model in which the two ranges are equal cannot account for the observed properties of the two-, three- and four-particle systems within the limits of experimental error. The remaining term V_c enters into the p scattering of fast neutrons and protons in hydrogen and also is involved in the order of the singlet and triplet levels[10] in Li^8 and B^{12} and in the capture of fast neutrons in hydrogen.

In addition to explaining the essentially linear dependence of binding energy on the number of particles a model of nuclear forces must also account for the strong dependence of binding energy on the symmetry properties of the space and spin wave functions.[10, 11] The latter requirement would seem to rule out the nuclear model in which the forces are all of the ordinary type with the saturation property resulting from strong forces of repulsion between particles when they approach closely.

EUGENE FEENBERG

Institute for Advanced Study,
Princeton, New Jersey,
April 7, 1937.

[1] G. Breit and E. Feenberg, Phys. Rev. **50**, 850 (1936). The operators P and Q exchange Cartesian and spin coordinates, respectively.
[2] D. R. Inglis, Phys. Rev. **51**, 531 (1937).
[3] P. A. M. Dirac, *Quantum Mechanics* (Oxford, 1935), pp. 69 and 225.
[4] These operators are formally identical with the spin matrices, but operate on the variables which determine whether the particle is a neutron or a proton (first introduced by W. Heisenberg, Zeits. f. Physik **77**, 1 (1932)).
[5] B. Cassen and E. U. Condon, Phys. Rev. **50**, 846 (1936).
[6] J. H. Bartlett, Phys. Rev. **49**, 102 (1936).
[7] G. Gamow and E. Teller, Phys. Rev. **51**, 289 (1937).
[8] E. Feenberg and S. S. Share, Phys. Rev. **50**, 253 (1936).
[9] R. D. Present and W. Rarita, to appear in Phys. Rev.
[10] E. Feenberg and M. Phillips, Phys. Rev. **51**, 597 (1937).
[11] E. Wigner, Phys. Rev. **51**, 106 (1937).

Paramagnetism at Radiofrequencies

With the heterodyne beat method small changes in the inductivity of a coil at radiofrequencies can be detected with good accuracy. This has been used in order to study the magnetic susceptibility at radiofrequencies of a paramagnetic specimen inserted into the coil. It has been found that this susceptibility in some cases decreases considerably if simultaneously a strong constant magnetic field is applied in the direction of the alternating field.

Preliminary experiments have been performed with several paramagnetic alums at temperatures of 77°K, with frequencies of about 2 megacycles and constant magnetic fields up to 4 kilo-oersteds. The magnetic susceptibility of iron alum for the high frequency field decreases in strong fields to about 25 percent of its normal value. Chromic alum shows a similar behavior. Vanadium alum on the contrary retains at least 80 percent of its normal susceptibility. These figures are in a first approximation independent of the frequency.

The explanation of this phenomenon is not difficult. In previous experiments[1] the relaxation time of the magnetic moment in these alums has been shown to be of the order of 10^{-10} seconds in the absence of a constant field. According to the theory[2] this relaxation time is determined primarily by the interaction energy ΔE between the magnetic ions, which is of course of the order of $(h/2\pi)10^{-10}$. If, however, the Zeeman separations introduced by the constant magnetic field are larger than ΔE, changes in the distribution over the Zeeman levels cannot be "paid" out of the interaction energy. Such changes only can result from the feeble coupling between the magnetic moments and the heat motion of the crystal lattice. The experiments thus demonstrate that this coupling involves a relaxation time of more than 10^{-7} seconds.[3]

The different behavior of V alum indicates that the main part of its susceptibility is due to nondiagonal elements of the magnetic moment,[4] which is connected with the fact that the number of electrons is even.

Further experimental data as well as a theoretical discussion will appear in *Physica*.

C. J. GORTER

Natuurkundig Laboratorium der Rijks-Universiteit te Groningen
Holland,
March 22, 1937.

[1] C. J. Gorter, Physica **2**, 503 (1936) and 1006 (1936).
[2] I. Waller, Zeits. f. Physik **79**, 370 (1932); C. J. Gorter and R. de L. Kronig, Physica **3**, 1009 (1936).
[3] In agreement with: W. Heitler and E. Teller, Proc. Roy. Soc. **A155**, 629 (1936).
[4] J. H. Van Vleck, *Electric and Magnetic Susceptibilities*, Chapter VI.

Approximately Relativistic Equations for Nuclear Particles. Addendum. Proof of Approximate Invariance

Possible forms of approximate relativistic equations have been discussed in a recent paper.[1] The following points should be noted in connection with the proof of approximate invariance of Eq. (16.1) with Q given by Eq. (16.3).

Variational integrals [Eq. (15)] are used. The time t is the same for every particle. The integral in K extends over a region of space time corresponding to $t_i < t < t_f$. This region differs from any similar region $t_i' < t' < t_f'$ in K'. In order to avoid dealing with different regions, the published calculation was made by keeping fixed the portion of space time corresponding to particle 1. The points x_2', y_2', z_2', $t' = B$ covered in the integral used in K' are contained between t_i' and t_f'. The region of space time covered by them does not coincide with the region covered by the points A which were used for the integration in K. It is thus natural to expect the difference of the integrals in K and K' to be an unsymmetrical expression in 1 and 2, as is seen in the second line of Eq. (16.7).

The variational integral can be used by supposing χ to be known and varying φ. This is analogous to fixing the motion of 2 and looking for the equations of motion of 1 in the classical theory. The integrals over V_2 are just like potentials determining the forces acting on 1. The region of integration for 1 is not contained between two planes corresponding to fixed values of t. This does not prevent one from using the variational integral in determining φ because for a single particle the variational integral can be used for any portion of space time. For Dirac's electron subjected to external forces the integral is invariant.

The calculation leading to Eq. (16.5) shows that in the present case the integral is not invariant. The extra term is equivalent to the addition of a four potential to the field acting on 1. To within a constant factor, which is of no interest, the four potential, in Dirac's notation, is

$$A_0 = -\int(\varphi^*\boldsymbol{\alpha}_2\varphi)\frac{\partial(\mathbf{r}J)}{\partial x}dV_2, \quad \mathbf{A} = \int(\varphi^*\varphi)\frac{\partial(\mathbf{r}J)}{\partial x}dV_2.$$

This can be expressed as:

$$A_0 = -\frac{\partial G}{c\partial t}, \quad A_x = \frac{\partial G}{\partial x_1};$$

$$G = -\int(\varphi^*\varphi)\frac{\partial K}{\partial x}dV_2; \quad K = \int J(r)rdr.$$

Being derivable from the gauge G, it can be removed by a suitable transformation of ψ. The extra term may be thus disregarded and the last line of Eq. (16.7) follows. It would have been better to use a new letter instead of ψ in the last line in order to indicate the function obtained by the gauge transformation. The need of it in this argument is analogous to the presence of a term in $d[(\mathbf{rv})J]/dt$ [Eq. (13″)] in the classical Lagrangian. The formal analogy is more striking if the transformation is performed in the configuration space of the two particles by setting

$$\psi = S\psi^{(1)}; \quad S = 1 + ivxJ/(2c^2\hbar).$$

The addition to $\mathfrak{L}$ required by the transformation is then

$$\mathfrak{L}^{(1)} - \mathfrak{L} = S^{-1}(\mathfrak{L}S - S\mathfrak{L}) \cong \mathfrak{L}S - S\mathfrak{L}$$

and this compensates the extra term. The transformation S leaves the density, current expressions invariant. The physical conditions are clearer, however, using G. This discussion does not prove that the equation is invariant for arbitrarily large J. It only shows that there is no need of terms linear in J in addition to those included.

G. BREIT

Department of Physics,
University of Wisconsin,
Madison, Wisconsin,
April, 1937.

[1] G. Breit, Phys. Rev. **51**, 248 (1937).

Note on the Reaction of Deuterium on Deuterium

The hypothesis that the specific nuclear forces between elementary nuclear constituents (i.e., proton-proton, proton-neutron and neutron-neutron forces) are identical both as to magnitude and spin dependence has been inferred[1] from scattering experiments with protons and neutrons and has proven sufficient for an understanding of the binding energy of light nuclei.[2] The purpose of the present note is to suggest further testing this hypothesis by a study of a certain class of nuclear transmutations.

Let a nucleus containing n protons and k neutrons be designated by (n, k) and by $(n, k)'$ if it is an intermediary product in a nuclear reaction. The atomic number is then n and the mass number k. The class of reactions referred to is

$$\text{Reactants}\rightarrow(n, n)'\rightarrow(n-1, n)+(1\,0) \qquad (1)$$

$$\rightarrow(n, n-1)+(0\,1) \qquad (2)$$

$$\rightarrow\text{Other products.}$$

It is characterized by an intermediate product which is here definitely assumed to exist,[3] which has equal numbers of protons and neutrons. From thence it may proceed according to (1) or (2) whose products are obtained from each other by interchanging the number of protons and neutrons. The two reactions are clearly equivalent so far as the fundamental statistics satisfied by the proton and neutron are concerned. If the electrical forces are negligible, the reactions (1) and (2) are completely equivalent dynamically if, and only if the hypothesis of the equality of all specifically nuclear forces is correct. It is to be expected that the small mass difference between proton and neutron will have a very slight effect in differentiating the structure of the nuclei $(n-1, n)$ and $(n, n-1)$ although it is of importance for their comparative stability with respect to positron or electron emission. Therefore a detailed study of this class should greatly assist in establishing the hypothesis of equal specific nuclear forces on a more comprehensive experimental basis as well as verifying the assumed mechanism of the intermediate product $(n, n)'$ in the reaction.

The lowest member of the class $(n=1)$ is unsuitable because the reactions (1) and (2) are indistinguishable. The next member $(n=2)$ is the familiar deuterium reaction

$$_1D^2+{}_1D^2\rightarrow({}_2He^4)^1\rightarrow{}_1H^3+{}_1H^1$$

$$\rightarrow{}_2He^3+{}_0n^1.$$

The principal influence of the electrical forces on the transition to (1) or (2) is on the proton which escapes with an energy of about 3 Mev (deuterium bombarding energy =0.2 Mev). A simple estimate shows that this should decrease the probability of the first reaction by about 15 percent. The difference in structure between $_1H^3$ and $_2He^3$ due to the Coulomb force should be slight so the kinetic energy of the neutron in (2) should be nearly equal to the kinetic energy of the proton in (1).[4]

If the supposition as to the mechanism of the reaction and the hypothesis of equal specific nuclear forces are correct, a comparative study of the protons and neutrons should show the same yield for both particles at all angles and for all bombarding energies of the deuterium. (The factor 15 percent would be changed to 10 percent if the bombarding energy is increased to 1 Mev.) The small amount of experimental data available appears to bear out this conclusion.

Higher members of this class of reactions are also known experimentally. Though similar comparative studies would undoubtedly be useful, the influence of the electrical forces becomes more pronounced. They are therefore not as suitable from point of view of simplicity as is the deuterium reaction.

M. H. Johnson, Jr.

New York University,
New York, N. Y.
April 1, 1937.

[1] Breit, Condon and Present, Phys. Rev. **50**, 825 (1936).
[2] For a summary see Bethe and Bacher, Rev. Mod. Phys. **8**, 134–149 (1936).
[3] H. Bohr, Nature **137**, 344 (1936). The presence of this intermediate product should also show itself on the elastic scattering of the reactants, as deviations from the Rutherford formula, if the reactants carry charges.
[4] See Bethe and Bacher, reference 2, p. 147.

Erratum: Heights of Reflection of Radio Waves in the Ionosphere

The formulae for the index of refraction of an ionized medium used in a recent paper[1] contain factors introduced by the assumption of a Lorentz correction for local polarization. This correction should be omitted in the problem considered; the following analysis is submitted as an exposition of the fundamental reasons for its omission.[2]

From an examination of all the contributions to the periodic electric force E at a point which result from the motion of a positive or negative ion in a periodic field, including those due to the retardation,[3] it can be seen that r^2E is bounded if r, the distance from the ion, is small. Let F_V be the sum of the forces exerted by all of the ions interior to a cylindrical section V whose center is the origin. If the ion concentration is bounded near the origin, F_V is finite and can be shown to approach zero with the volume of V, whether the radius of a cross section or the height of the cylinder first approaches zero. Hence the "pipe force" is equal to the "crack force," as these are defined by Fowler. The result is that no true polarization of the ionized medium can exist if only forces between ions of this type (r^2E bounded for small r) are present.

Instead of Eq. (7)[1] equivalent to the equation $N=1.86\times10^{-8}f^2$, there results the equation $N=1.24\times10^{-8}f^2$ between the electron concentration N and the frequency f at the reflection level. In addition, the heights h' calculated from Eqs. (11) or (12) are reduced by approximately 15 percent. This affects the total heights as shown in Figs. 8, 9 by a reduction of at most 8 percent.

The expressions defining k_1, k_2 on page 336 should each be divided by 10^6.

F. H. Murray

Ryerson Physical Laboratory,
University of Chicago,
Chicago, Illinois,
April 10, 1937.

[1] Murray and Hoag, Phys. Rev. **51**, 333 (1937).
[2] Darwin, Proc. Roy. Soc. **A146**, 17 (1934); **151**, 572 (1935); R. H. Fowler, *Statistical Mechanics*, second edition (1936), 437–447.
[3] Riemann-Webers, *Differentialgleichungen der Physik*, II (1927), p. 419, 420.

Isotope Shifts in Li I

The Li I emission line $2P$–$2S$ (6708A) has been examined with a Fabry-Perot interferometer and a glass spectrograph for isotope shift. The displacement was found to be 0.330 cm^{-1} in agreement with the measurements of Hughes.[1] The h.p.f. pattern has been resolved and the error can definitely be set at less than ± 0.010 cm^{-1}. Since the level splittings calculated from the theoretical work of Hughes and Eckart[2] and Eckart[3] give a shift of 0.272 $cm^{-1} \pm 0.007$ the present experimental result can only mean that an effect other than the simple "mass effect" of Hughes and Eckart is contributing to the displacement. This conclusion is further confirmed by work on $3S$–$2P$. Other lines are being investigated and a complete report will be published shortly.

DOMINIC D'EUSTACHIO

Physics Department,
Washington Square College,
New York University,
April 8, 1937.

[1] D. S. Hughes, Phys. Rev. **38**, 857 (1931).
[2] D. S. Hughes and C. Eckart, Phys. Rev. **36**, 694 (1930).
[3] C. Eckart, Phys. Rev. **36**, 878 (1930).

Remanence in Single Crystals

The magnetization curve of ferromagnetic single crystals has in almost all cases been measured for short, straight specimens.[1] Their demagnetizing factor is not accurately known and a determination of the true value of remanence is thus impossible. A single crystal ring, on the other hand, magnetized in the direction of its circumference, has no demagnetizing field in the usual sense; the field, however, changes its direction with respect to the crystal axes from place to place. It could be expected that, in spite of the latter disadvantage, the ring experiment would decide whether the remanence in single crystals approaches zero, or whether it has the value $I_s/l+m+n$ found by Kaya[2] for the induction at the sharp bend in the magnetization curve.

A ring of 2.78 cm outer diameter, 0.28 cm width, and 0.046 cm thickness was cut from a single crystal of iron containing 2.8 percent silicon and annealed at 1100° in pure dry hydrogen. The direction of the cubic axes with respect to a line on the surface of the original disk was, in polar coordinates: [001]: $\varphi = 110°$, $\vartheta = 72°$; [010]: $\varphi = 307°$, $\vartheta = 17°$; [100]: $\varphi = 215°$, $\vartheta = 5°$. Magnetizing and search coil having 145 and 280 turns, respectively, were wound uniformly along the circumference. H_{max} was 100 oe.

Fig. 1 shows the magnetization curve. A sharp break occurs at 0.02 oe, slightly below zero field, and the remanence is 860 e.m.u. The fact that the break did not occur exactly at zero field may have been due to the presence of a slight strain. This assumption was made quite probable by an induction measurement while the ring was compressed elastically in the direction of a diameter by a weight of 150 g. The dashed curve in Fig. 1 gives the hysteresis loop in this case.

An extension of the flat part of the magnetization curve to the I axis intersects the latter at 940 e.m.u., whereas the value of I_s, according to Kaya's formula, varies along the circumference between 1560/1.09 and 1560/1.65, or 1430 and 950 e.m.u. While the ring experiment thus does not admit a direct confirmation of the formula, as applied to true remanence, without making further assumptions about the magnetization process in a ring, it gives results consistent with the formula. The experiment indicates definitely that true remanence in single crystals is not zero.

The irregularities in the two loops near zero induction suggest the occurrence of reversal processes requiring different values of coercive force, such as 90- and 180-degree changes from one to another of the six directions of easy magnetization in a cubic crystal.

K. J. SIXTUS

Research Laboratory,
General Electric Company,
Schenectady, New York,
March 19, 1937.

[1] For references see L. W. McKeehan, Met. Techn. T. P. 554 (1934).
[2] Kaya, Zeits. f. Physik **84**, 705 (1933); theoretical derivation by C. J. Gorter, Nature **132**, 517 (1933). l, m and n are the direction cosines of field with respect to the crystal axes.

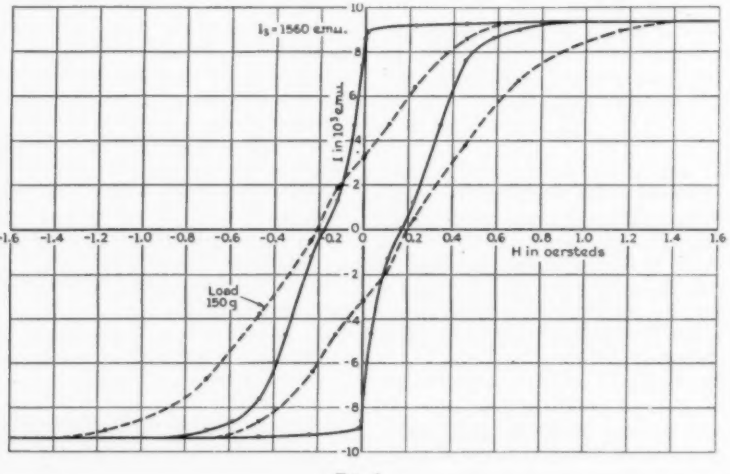

FIG. 1.

Remarks on the Paper by E. B. Baker and H. A. Boltz, "Thermionic Emission into Dielectric Liquids"[1]

It is natural to presume that the electronic work function of a metal in a dielectric of dielectric constant D is smaller than the normal work function in vacuum. As yet it has not, however, been possible to demonstrate this effect by simple experiment. Because of the equality of the thermionic and photoelectric work functions one would expect a displacement of the long wave-length limit toward the red end of the spectrum. If the currents observed in insulating fluids are assumed to be electronic, one would expect long wave-length limits in the visible and infrared regions. Experiments of the author[2] show, however, that the photoelectric effects with and without fluid are practically identical. For this reason an electronic mechanism (thermal, or as the author called it, cold electron emission) is inadequate to explain the currents in insulating fluids.

A more plausible explanation of the effect of increase in conductivity with the field is given by the "potential-dissociation-effect"[3] of Wien and Schiele. This theory also correctly gives the qualitative influence of the dielectric constant by the formula:

$$J = J_0 \cdot \exp\left[(e^3 \cdot F/D)^{\frac{1}{2}}/kT\right] \quad F \text{ large} \qquad (1)$$

whereas Baker and Boltz give

$$J = J_0 \cdot \exp\left[e \cdot (e \cdot F \cdot D)^{\frac{1}{2}}/kT\right]. \qquad (2)$$

The existing experimental measurements with different values of D corroborate formula (1) rather than formula (2).

To explain the observed dependence of the conductivity upon temperature it is not necessary to assume that electrons are the carriers of the current since a slow dissociation of the molecules would also give an exponential temperature dependence.[4]

We may conclude that the experiments indicate an electrolytic process rather than an electronic current in the fluids. This does not in any way minimize the importance of the very careful experiments of Baker and Boltz.

KARL HANS REISS

Elektrophysischen Laboratorium,
Elektrotechnischen Institutes der Technischen Hochschule,
München, Germany,
March 10, 1937.

[1] Baker and Boltz, Phys. Rev. **51**, 275 (1937).
[2] K. H. Reiss, Ann. d. Physik **28**, 325 (1937).
[3] Lars Onsager, J. Chem. Phys. **2**, 599 (1934).
[4] K. H. Reiss, Zeits. f. physik. Chemie **178**, 37 (1936).

Superconductivity

In a recent paper by Slater[1] an attempt is made to give a theoretical interpretation of the supraconductive state in connection with which the following points seem to be of interest: (a) We have very recently determined the entropy difference between the normal and the supraconductive state by magnetic experiments on Sn, Hg, Pb, Ta and Nb.[2] The values obtained allow us to fix a lower limit for the electronic specific heat of these metals in the normal state which according to Sommerfeld is $c = AT$. In Table I we give our values for A for the supraconductors, together with values for Ag, Cu, Ni, Pb and Pd (all non-supraconductive) obtained by various authors from direct determination of the specific heat.

TABLE I. *Values of the constant A in Sommerfeld's formula.*

	Transition point (°K)	$A \times 10^4$ (cal./mole degree)		$A \times 10^4$ (cal./mole degree)
Sn	3.7	3.5	Ag	1.6
Hg	4.1	4.1	Cu	1.78
Pb	7.2	6.3	Ni	16.6
Ta	4.4	19.	Pt	16.07
Nb	8.4	40.	Pd	31.

Slater concludes that (Ni, Pd, etc.) will not, or only at very low temperatures, become supraconductive on account of their high A. It is evident, however, from our results that Ta and Nb have even higher A values and nevertheless become supraconductive at comparatively high temperatures (4.4° and 8.4°K).

This result is not surprising because for the thermodynamical description of supraconductivity at least two parameters are needed (even if we assume that the equilibrium curve in the H, T diagram is the same function for all supraconductors). We can therefore not expect the transition temperature to depend only on A.

So far the experiments seem even to indicate that metals with high electronic entropies become supraconductive more easily and the difficulty seems to be to explain why the metals of group VIII do not show supraconductivity *although* they have high A values. We are inclined to think that it is here the high internal magnetic field which prevents supraconductivity in the same way as an external magnetic field in an ordinary supraconductor.

A detailed discussion of these questions will be given as soon as more experimental results are available.

(b) I have pointed out previously[3] that the magnetic effects at the transition in an external field cannot be explained by persistent currents. Such an explanation only holds for the transition from the supraconductive to the normal state but not for the inverse. The reversible change to zero induction is an absolutely independent phenomenon which cannot be derived electrodynamically from the fact that the resistance becomes zero, and which any theory of supraconductivity will have to explain.

(c) Magnesium, on which Slater has illustrated his theory has been found to be nonsupraconductive even down to extremely low temperatures (0.05°K).[4]

KURT MENDELSSOHN

The Clarendon Laboratory,
Oxford, England,
February 25, 1937.

[1] J. C. Slater, Phys. Rev. **51**, 195 (1937).
[2] J. G. Daunt and K. Mendelssohn, Proc. Roy. Soc. A. in print.
[3] K. Mendelssohn, Proc. Roy. Soc. **A152**, 34 (1935).
[4] N. Kurti and F. Simon, Proc. Roy. Soc. **A151**, 610 (1935).

Production of X-Rays by High Speed Argon Ions

Argon ions of energies up to 450 kev were obtained by the method of multiple linear accelerator of Sloan-Lawrence, and the x-rays produced when each one of the elements: Li, Be, C, Mg, Al, Si, Ni, Cu, Zn, Mo, Pd, Ag, Cd, Sn, Pt, Au, and Pb was bombarded by these ions were investigated by Geiger counter.

From the measurements of the absorption of the x-rays, by thin starch films (medical wafer $(C_6H_{10}O_5)_x$), these radiations were determined to be the characteristic K in the case

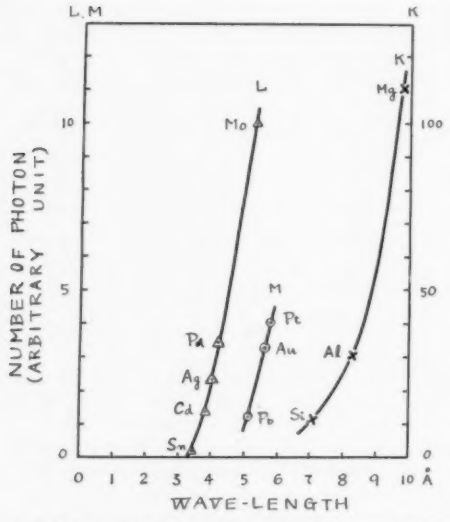

FIG. 1. Relative number of photons produced in several elements.

of Mg, Al and Si; the characteristic L in the case of Mo, Pd, Ag, Cd and Sn; and the characteristic M in the case of Pt, Au and Pb. The relative number of photons of these characteristic radiations when thick targets are bombarded by ions of 440 kev are given in Fig. 1 and in Table I, where the absorption of radiations by windows and the sensitivity of the counter are corrected.

In all cases, no other radiations than those mentioned above were detected except a low intensity radiation of wave-length about 5.2A. By careful measurements, it was ascertained that this faint radiation which accompanies in every case was produced by the ions and not by electrons.

TABLE I. *Relative number of photons produced by 440 kev ions (thick target).*

ATOMIC NUMBER	ELEMENT	WAVE-LENGTH OF CHAR. RAD. IN A (weighted mean)		RELATIVE NUMBER OF PHOTONS
12	Mg	K	9.8	111
13	Al	K	8.3	30.4
14	Si	K	7.1	11.6
42	Mo	L	5.3	10.1
46	Pd	L	4.2	3.46
47	Ag	L	4.0	2.35
48	Cd	L	3.8	1.38
50	Sn	L	3.45	0.21
78	Pt	M	5.8	4.02
79	Au	M	5.6	3.32
82	Pb	M	5.1	1.23

Also this radiation is not the characteristic radiation of argon, as the weighted mean wave-length of argon is 4.2A. This faint radiation is thought to be due to contamination of lead from the soldered parts of the apparatus or of sulphur from Apieson oil or other materials, as the wave-length of the characteristic radiations of lead and sulphur are about 5.2A.

The absolute yield is very uncertain, but by rough calculations it was shown that about 5×10^{-4} photons are produced per ion in the case of Al K radiation and about 4×10^{-5} photons in the case of Ag L radiation.

The intensity of each characteristic radiation was found to increase very rapidly with the energy of the ions, and also it was found to be proportional to $W^{3.7}$ in the case of Ag L radiation, where W is the energy of ions.

Detailed report will soon be found in the *Proceedings of the Physico-Mathematical Society of Japan.*

The Research Laboratory of the
Tokyo Electric Company,
Kawasaki, Kanagawa-Ken, Japan,
March 29, 1937.

M. TANAKA
I. NONAKA